Doctoral Dissertation (Censored)
博士論文（要約）

Development of Nitrogen-Doped Carbon Supported Heterogeneous Catalysts towards Electrochemical Organic Transformations

(電気化学的有機変換を指向した窒素ドープカーボン担持不均一系触媒の開発)

A Dissertation Submitted for the Degree of Doctor of Science

December　2022

令和４年１２月博士（理学）申請

Department of Chemistry, Graduate School of Science,

The University of Tokyo

東京大学大学院理学系研究科

化学専攻

Ryusuke Masuda

増田　隆介

論文の内容の要旨

Development of Nitrogen-Doped Carbon Supported Heterogeneous Catalysts towards Electrochemical Organic Transformations

（電気化学的有機変換を指向した窒素ドープカーボン担持不均一系触媒の開発）

増田　隆介

Introduction

Heterogeneous catalysts have great advantages over homogeneous catalysts due to their reusability, easy separation from products and reducing wastes significantly. Especially, continuous-flow reactions using heterogeneous catalysts can provide efficient synthetic methods of organic compounds in terms of environmental compatibility, efficiency and safety. Nitrogen-doped carbon (NDC) is attractive support for metal nanoparticles or single-atom catalysts to stabilize metal species by strong metal-nitrogen interactions.[1] Our laboratory has recently developed nitrogen-doped carbon incarcerated metal nanoparticle catalysts (NCI-M) prepared from poly(4-vinylpyridine) through a polymer-incarceration method, in which metal nanoparticles are encapsulated and stabilized by NDC layers.[2] Although NCI-M catalysts have enabled several organic transformations, development of more general and challenging organic reactions using NCI-M is desired.

Development of nitrogen-doped carbon incarcerated rhodium nanoparticle catalysts for asymmetric insertion reactions

I have developed NCI-Rh catalyst for asymmetric insertion of α-diazoesters into N−H bonds in the presence of chiral phosphoric acids in my master course studies. With the optimized catalytic system in hand, substrate generality was investigated. Various chiral α-amino acid derivatives were synthesized in high yields with high enantioselectivities, and NCI-Rh could be reused in seven runs

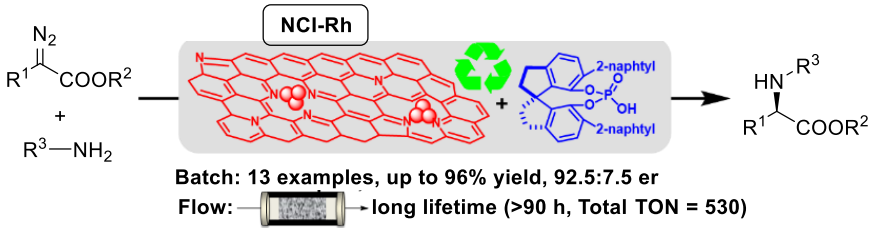

Scheme 1. NCI-Rh catalyzed asymmetric insertion reactions

without Rh leaching under batch reactions. The corresponding continuous-flow reactions using a column packed with NCI-Rh were also successfully demonstrated. The desired products were obtained efficiently over 90 h through the reactivation of NCI-Rh (Scheme 1). The chiral phosphoric acid was recovered by trapping with a basic resin. Furthermore, it was found that the reaction proceeded in a heterogeneous manner. These results exhibited robustness of NDC supported catalysts to inhibit metal leaching even after the carbenoid formation in the presence of chiral activators.

Development of nitrogen-doped carbon incarcerated zinc nanoparticle catalysts for electrochemical allylations of carbonyl compounds

Organometallic reagents hold a special place in organic synthesis because they have widespread synthetic applications based on carbon-carbon bond formation. Conventionally, stoichiometric amounts of metal reagents are required in such transformations and large amounts of metallic wastes are generated, which hindered applications to continuous-flow systems. Therefore, catalytic carbon-carbon bond forming reactions without metallic wastes are required significantly. I envisioned an electrochemical approach in which metal catalysts on cathode are involved in reactions with organometallic reagents and metal(0) species can be electro-reductively regenerated (Scheme 2). Inspired by the robustness of NCI-M catalysts, I reasoned that they would be suitable materials for electrodes that could be used without causing metal leaching. NDC materials have been employed as electrodes extensively in the field of electrochemistry. However, their applications to electrochemical organic transformation, especially C−C bond-formation reactions remain challenging.

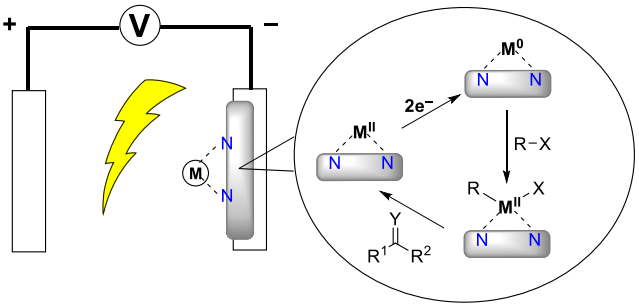

Scheme 2.
Electrochemical approach with heterogeneous catalyst electrode

Allylation reactions using organometallics have been developed extensively and zinc has been demonstrated to be a particularly good reagent to mediate Barbier-type reaction. Recently, electrochemical allylation of carbonyls in water using a zinc electrode has been developed with a catalytic amount of zinc consumed from the electrode.[3] Nevertheless, a large amount (ca. 25 mol%) of zinc still leached out and an excess amount of zinc was used in terms of a substrate amount. Moreover, the system required a divided cell and substrate scope was limited.

First, I prepared NCI-Zn from a 5:1 (w/w) ratio of poly(4-vinylpyridine) and conductive carbon black XC-72, that have a relatively high density. Treatment of NCI-Zn with hydrochloric acid to remove aggregated zinc species afforded NCI-Zn/HCl. After NCI-Zn/HCl was mixed with a Nafion™ solution at 0 °C under sonication for 1 h and was put on a carbon cloth, the composite was dried at 50 °C for 1 h (Scheme 3). The carbon cloth was fixed on a graphite electrode with carbon tape and used as an electrode. When several kinds of NCI-Zn were evaluated for electrochemical allylation of benzaldehyde, additional nitrogen dopants were

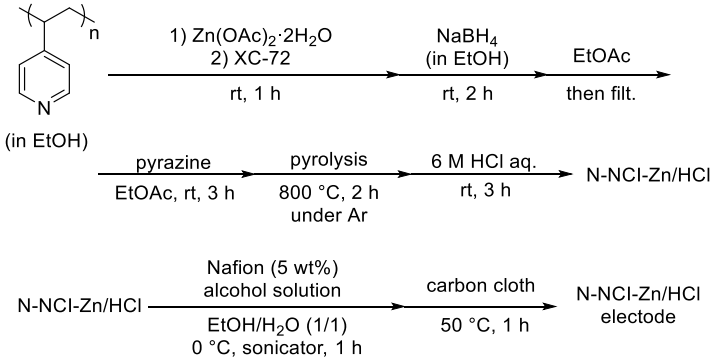

Scheme 3. Preparation of N-NCI-Zn/HCl and it's electrode

found to have positive effects on suppression of zinc leaching with keeping high activity (N-NCI-Zn/HCl) (Scheme 3). The optimized reaction system efficiently produced a range of homoallylic alcohols in high yields with <10 mol% zinc leaching (Scheme 4). NDC-stabilized zinc nanoparticle species showed advantages in terms of scope of heteroaromatic substrates compared with bulk zinc electrodes and enabled the reactions in an undivided cell. Hot filtration tests indicated that the reaction was mediated by zinc species on the surface of the cathode. On the other hand, the amount of leached zinc was still not ignorable and turnover number (TON) was limited (nearly 1). They were problematic for applications to continuous-flow systems.

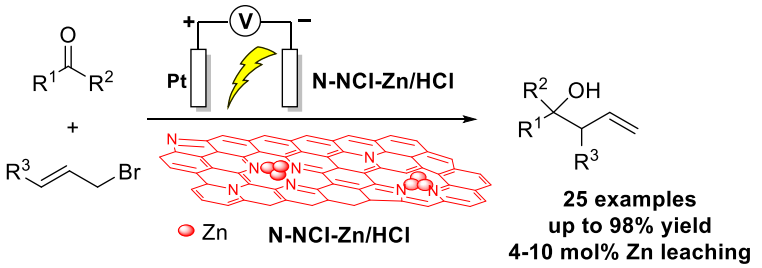

Scheme 4. NCI-Zn catalyzed electrochemical allylation of carbonyls

Conclusion

In my doctoral course studies, I have developed NDC supported metal nanoparticles and single-atom catalysts toward efficient and clean organic transformations. In the asymmetric insertion reactions, NDC worked as a solid ligand to support the metals and realize the asymmetric reaction catalyzed by metal nanoparticles. Furthermore, NDC supported single-atom zinc catalyst was successfully employed in electrochemical allylation reactions and enabled catalytic C−C bond forming reaction with minimum amount of metallic waste. This work highlights the potential of NDC supported heterogeneous metal catalysts toward fine chemical synthesis.

References

[1] M. Beller, *et al*., *Angew. Chem. Int. Ed*. **2016**, *55*, 12582. [2] S. Kobayashi *et al*., *Org. Lett.* **2018**, *20*, 5172. [3] J. M. Huang, *et al*., *Chem. Commun*. **2010**, *46*, 2286.

Table of Contents

Chapter 1: General Introduction

The environment is the foundation of our daily lives and realizing a sustainable society is the greatest concern all over the world. Japan aims to cut greenhouse gases to zero by 2050 and realize a carbon-neutral society. Under this circumstance, the focus on green chemistry is one of the important missions of scientists. In order to create a sustainable society, from the view-point of synthetic organic chemistry, we should design organic reactions that do not produce much waste and use clean energy.

Catalysts are indispensable in modern organic chemistry including industrial processes. In chemical reactions, catalysts can promote a reaction by lowering the activation energy of the transition state without changing themselves before and after the reaction. Today, around 90% of all modern processes in the chemical industry uses catalysts that can control the rate of a given reaction.[1] Despite significant efforts toward sustainable chemistry in the past century, the development of novel catalyst systems remains important not only for limited applications such as energy-related catalysis and bulk chemistry, but also for a wide range of applications in fine chemical synthesis.

Catalysts are generally classified into two major categories: homogeneous catalysts and heterogeneous catalysts (Scheme 1). Homogeneous catalysts completely dissolve in a reaction mixture and exist in the same phase as the reactants. In contrast, heterogeneous catalysts exist in a different phase from reactants. The major advantage of homogeneous catalysis is high activity and selectivity. Furthermore, the catalysts can be easily modified to achieve the desired molecular properties by tuning electronic and steric states of metals with ligands. Therefore, metal catalysts for organic synthesis have been long-established in homogeneous manners. However, when metals are used as homogeneous catalysts, these catalysts should be eliminated from products due to their toxicity, especially for medicines that are sent in human bodies. Usually, scavengers are used to remove these metal catalysts from products, which makes the reuse of the catalysts practically impossible. In terms of reusability and easy separation from products, heterogeneous catalysts have great advantages over homogeneous catalysts and are more suitable for large-scale synthesis of fine chemicals such as pharmaceuticals.

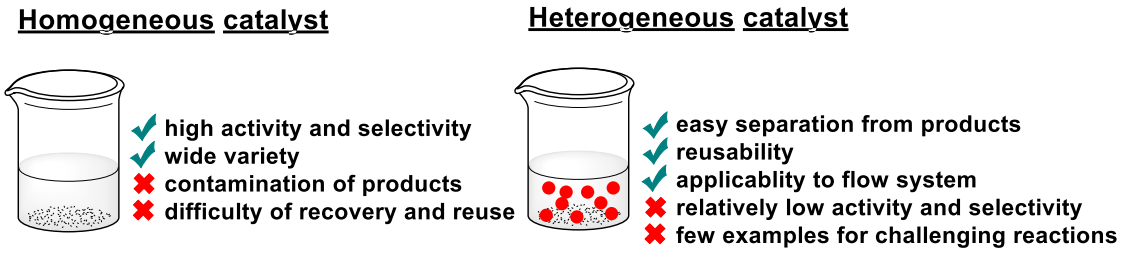

Scheme 1. Homogeneous catalysts and heterogeneous catalysts

Another major advantage of heterogeneous catalysts is their applicability to continuous-flow systems. Chemical reactions are carried out mainly by either batch methods or flow methods (Scheme 2).[2] In the batch methods, reactions are performed by adding all reactants, solvents, and so on to reactors such as flasks, and after the reaction is completed, a post-treatment such as purification should be carried out to obtain the desired product. On the other hand, in the flow methods utilizing heterogeneous catalysts, a raw material is continuously passed through the containers filled with heterogeneous catalysts, and the target products can be continuously obtained. It is used for large-scale reactions of gaseous molecules, such as the synthesis of ammonia by the Harbor-Bosch process. At present, the batch method is the mainstream in the synthesis of organic compounds including fine chemicals such as chiral molecules, presumably because the development of heterogeneous catalysts is challenging and limiting for sophisticated reactions. However, the flow methods utilizing heterogeneous catalysts have great advantages in terms of environmental compatibility, efficiency, and safety, and are expected to be applied to the synthesis of fine chemicals. In 2015, our laboratory achieved flow fine synthesis of Rolipram by connecting four columns packed with different heterogeneous catalysts (Scheme 3).[3] However, such applications for drug synthesis are very limited; in particular, heterogeneous catalysts with high activity and enantioselectivity and long lifetime for asymmetric reactions are very few at present.

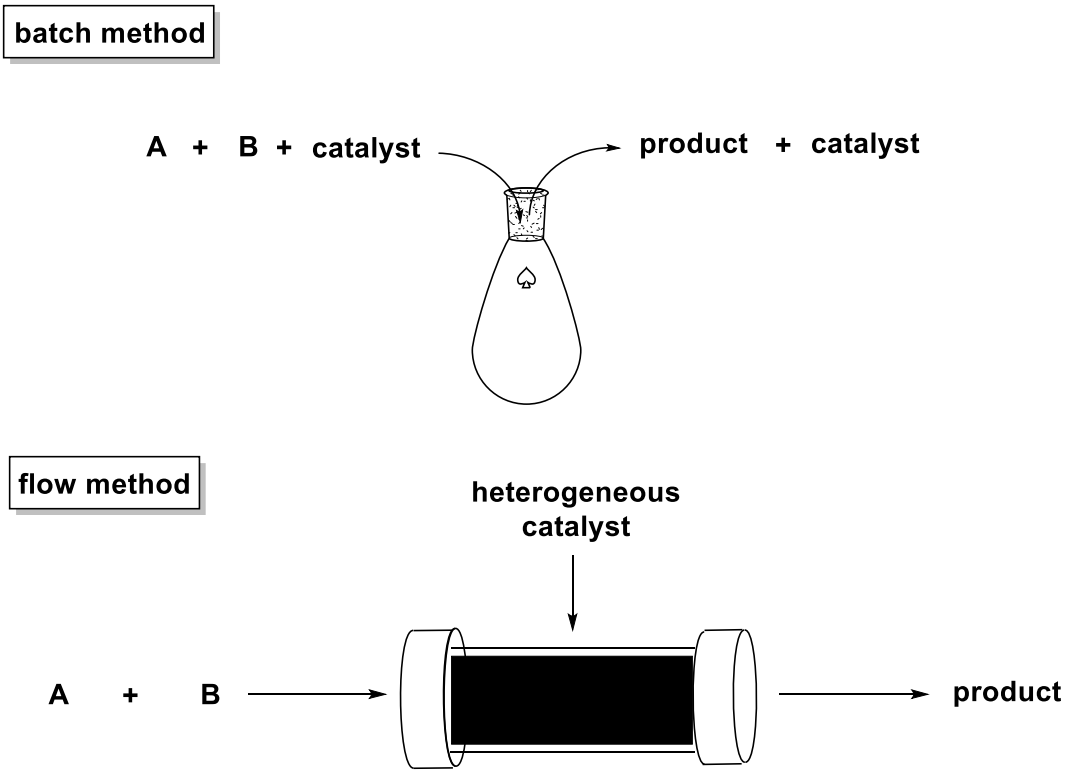

Scheme 2. Batch methods vs flow methods

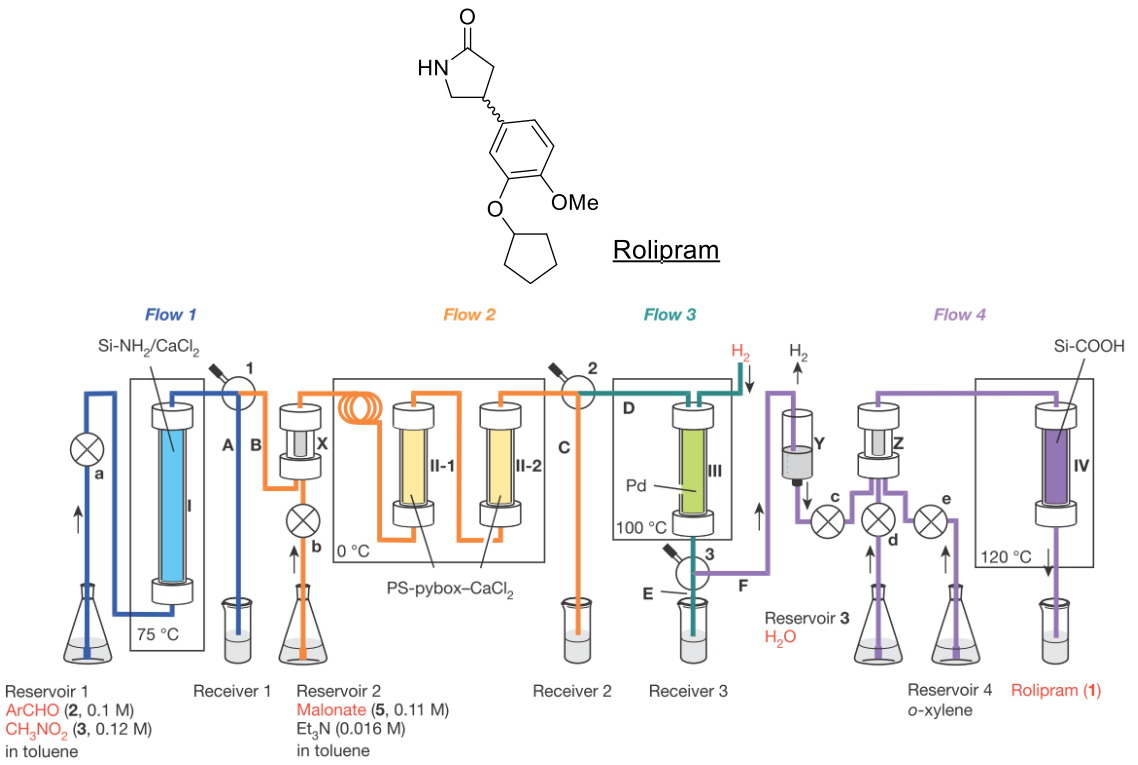

The figure was quoted from ref.3.

Scheme 3. Synthesis of Rolipram in flow systems

Although inert inorganic materials such as Al_2O_3 and SiO_2 are ubiquitous supports for heterogenous catalysts,[4] carbon-based supports have wide applications due to their attractive characteristics such as high electrical conductivity and micropore structure.[5] In addition, a slight modification of the carbon surface can effectively change the properties of the designed catalyst systems. In this context, heteroatom doping of carbon matrix enables tuning of the reactivity of the active metal sites,[6] and nitrogen-doped carbon, especially, has been intensively studied as an attractive material. Indeed, nitrogen-doped carbon or nitrogen-doped carbon-supported metal species are known to be good electrocatalysts in the field of electrochemistry.[7-9]

Despite the extensive investigations in electrocatalysts, the applications of nitrogen-doped carbon-supported heterogeneous catalysts to organic reactions are still less explored.[10] A representative example is nitrogen-doped carbon-supported cobalt nanoparticle catalysts, which are successfully utilized for several organic transformations, such as oxidative esterification,[11-14] oxidation of hydrocarbons,[15,16] and hydrogenation reactions[17-22] (Scheme 4). However, the examples are mostly restricted to redox reactions, and applications to general organic reactions such as bond-forming reactions are desirable.

Oxidative esterification

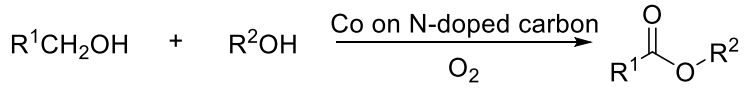

R^1 = aryl, heteroaryl or alkyl; R^2 = alkyl

Hydrogenation

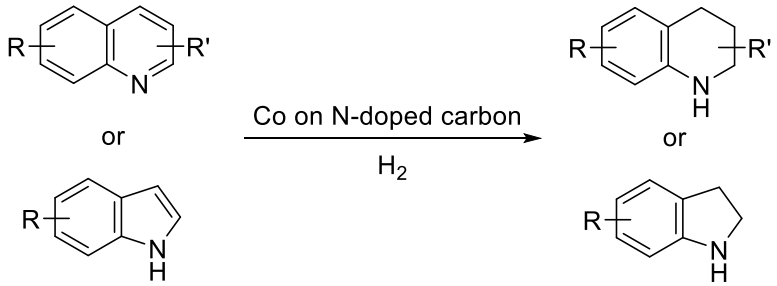

Scheme 4. Examples of organic reactions using nitrogen-doped carbon supported cobalt catalysts

In recent years, our laboratory developed nitrogen-doped carbon incarcerated metal nanoparticle catalysts (NCI-M) based on a polymer-incarceration strategy (Scheme 5).[23] The process included nanoparticle formation by reduction of metal salts in the presence of poly(4-vinylpyridine) as a nitrogen source and microencapsulation of nanoparticles by polymer before pyrolysis, expecting stabilization of metal nanoparticles through multiple interactions with nitrogen-doped carbon layers. Using these catalysts, a variety of organic reactions have been achieved. NCI-Co catalyzed esterification[23] and oxygenation[24] were developed (Scheme 6). NCI catalysts were also applicable for several C−C bond forming reactions such as Friedel-Crafts reactions catalyzed by TfOH-treated NCI catalysts (NCI-Ti-TfOH) (Scheme 7)[25,26] and olefination catalyzed by NCI-Co.[27] Remarkably, several reactions were not catalyzed by the corresponding dopant-free carbon-supported catalysts. Furthermore, NCI-M exhibited robustness for suppression of leaching of metal species.

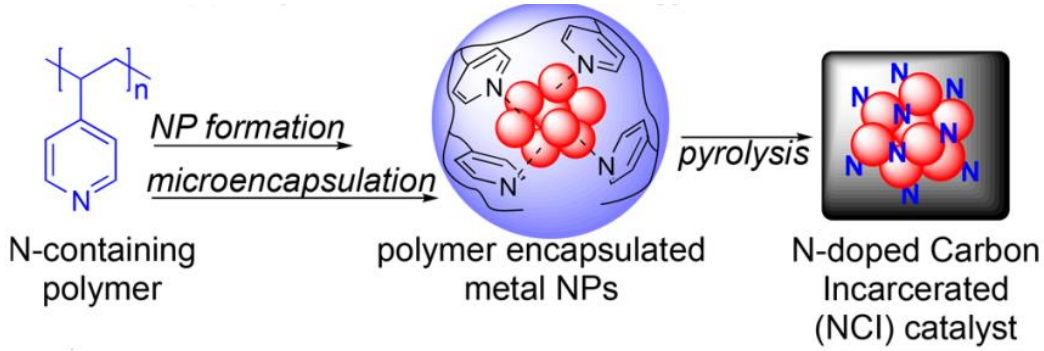

The figure was quoted from ref.23.

Scheme 5. Concept of nitrogen-doped carbon incarcerated metal nanoparticle catalysts (NCI-M)

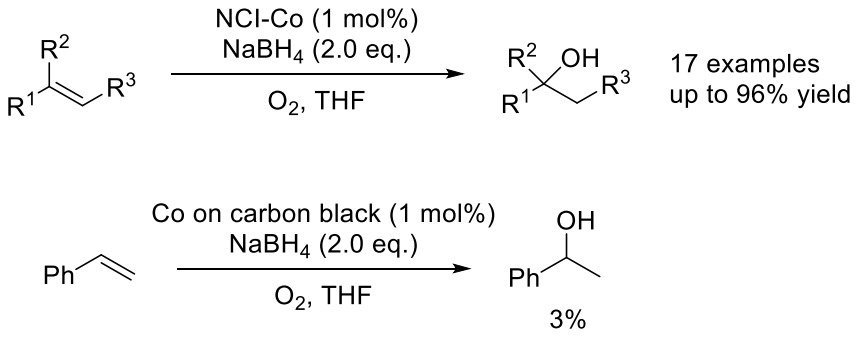

Scheme 6. Oxygenation of styrenes catalyzed by NCI-Co

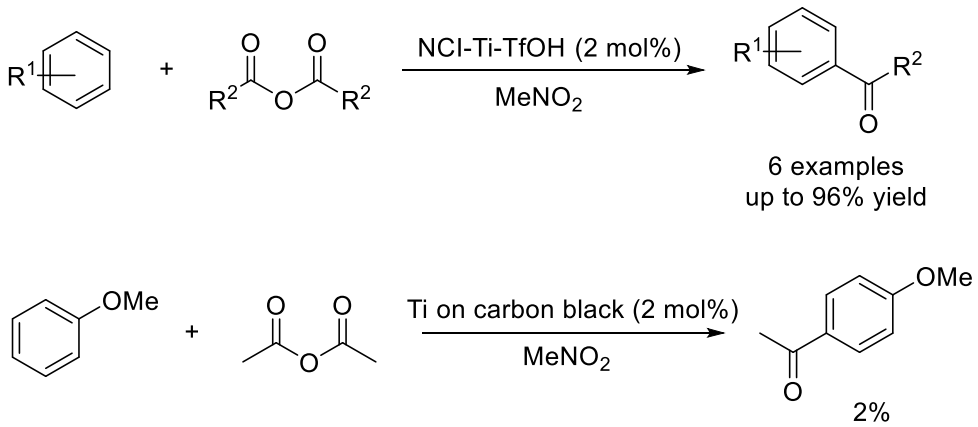

Scheme 7. Friedel-Crafts acylation catalyzed by NCI-Ti-TfOH

While NCI-M showed unique catalytic activity in these organic transformations, I believed that there was still room for the development of more challenging organic reactions using nitrogen-doped carbon-supported heterogeneous catalysts. In this thesis, I have developed nitrogen-doped carbon-supported heterogeneous catalysts especially for

asymmetric reactions and electrochemical reactions.

Chapter 2: Development of Nitrogen-Doped Carbon Incarcerated Rhodium Nanoparticle Catalysts for Asymmetric Insertion Reactions

2-1. Introduction

The efficient construction of chiral molecules is one of the most important targets in organic synthesis. In the synthesis of fine chemicals such as pharmaceuticals and agrochemicals, asymmetric reactions to introduce chirality are often regarded as key steps. Nowadays, such asymmetric reactions rely exclusively on homogeneous chiral catalysts, and the development of heterogeneous chiral catalysts lags far behind that of homogeneous ones.[28,29]

Immobilization of chiral ligands on solid supports is one of the most common methods to prepare heterogeneous chiral metal complexes (Scheme 8).[30,31] This method can be applied to various types of ligands, but additional synthetic steps are necessary to functionalize the ligands, and the lifetime of the catalyst depends on the lifetime of the metal complexes.

Scheme 8. Immobilized chiral ligand with metal salt

In contrast, heterogeneous metal nanoparticle catalysts have gained attention because of their unique activity and robustness.[32,33] Metal nanoparticles can be easily immobilized and stabilized on solid supports, and such catalysts are usually used for bulk chemical synthesis because they are easy to prepare and have high physical stability considering that they form at very high temperatures. Based on these properties, heterogeneous chiral metal nanoparticle catalysts are expected to realize robust chiral catalyst systems with long lifetimes. In fact, metal nanoparticles with chiral ligands can be applied to asymmetric catalysis;[34-36] however, there are still very limited examples of achieving high enantioselectivity for a wide variety of substrates (Scheme 9).[37-45] One of the major difficulties of metal nanoparticles for asymmetric reactions is the reduced flexibility in tuning the electronic properties of active metal species and the suppression of metal leaching. Although several ligands enable the modification of the reactivity of metal nanoparticles,[46-49] the available ligands are limited because strong interactions between metals and ligands often cause metal leaching.[44,50,51]

Scheme 9. Immobilized metal nanoparticle with chiral ligand

In order to overcome these issues, I thought that nitrogen-doped carbon would be suitable as a support because interactions from nitrogen-doped carbon were expected to both activate and stabilize metal nanoparticles.[10] Especially in our laboratory's previous work, nitrogen-doped carbon incarcerated metal nanoparticle catalysts (NCI-M) activated metal species efficiently and suppressed metal leaching.[23,24] Inspired by these findings, I envisioned that NCI-M could be employed with an appropriate chiral source to realize asymmetric reactions (Scheme 10). To the best of my knowledge, there is no example of asymmetric catalysis using heteroatom-doped carbon supported catalysts. Additionally, cooperative catalytic systems with metal nanoparticles and chiral sources would be beneficial, since rate acceleration by chiral co-catalysts can avoid undesirable racemic pathways. However, such catalytic systems were also poorly studied.[36]

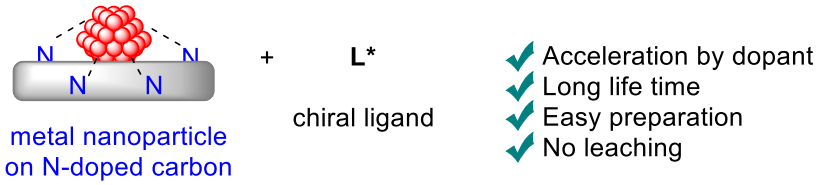

Scheme 10. Cooperative catalytic system with activated metal nanoparticle

α-Amino acids are essential building blocks of peptides, proteins, and many other bioactive compounds, and the development of efficient and enantioselective synthetic methods has been a long-standing goal of synthetic chemistry (Scheme 11).[52,53]

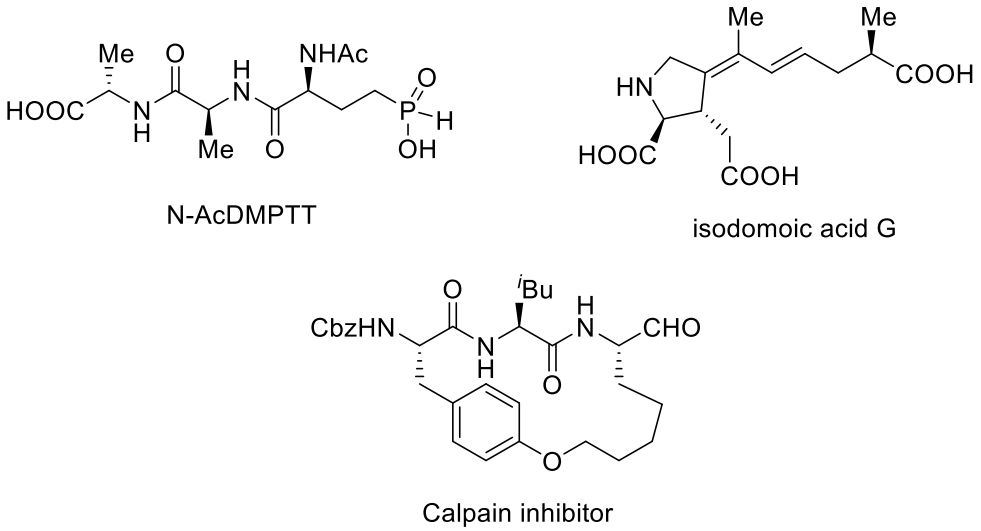

Scheme 11. Selected bioactive compounds containing chiral α-amino acids derived structures

Among the synthetic methods of α-amino acids, asymmetric insertions of carbene derived from diazoesters into N−H bonds is one of the most attractive methods to construct carbon-nitrogen bonds containing chirality.[54,55] It has long been challenging to obtain high enantioselectivity for these reactions until several catalytic systems using copper with chiral ligands were developed (Scheme 12).[56-58] Although progress on copper-catalyzed asymmetric N−H insertions has been substantial, they had limitations. For instance, high catalyst loading (more than 5 mol%) was required for satisfactory yields and enantioselectivities.

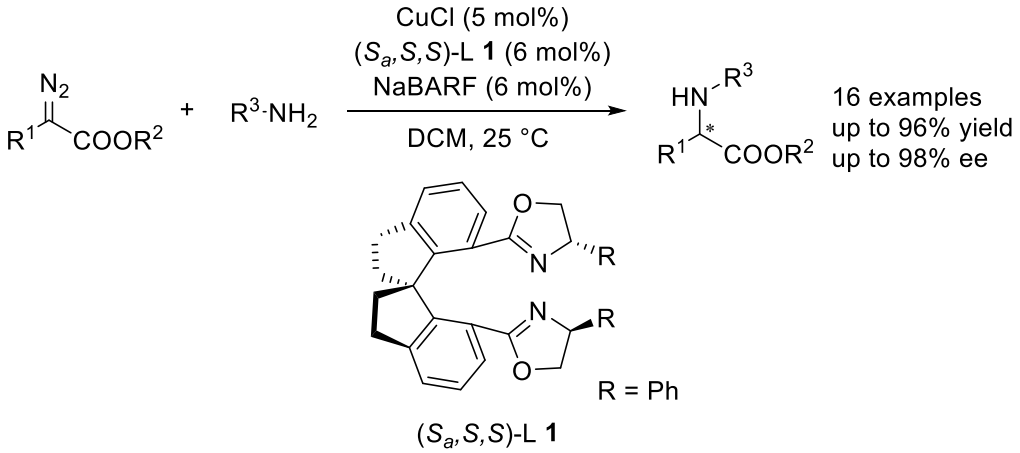

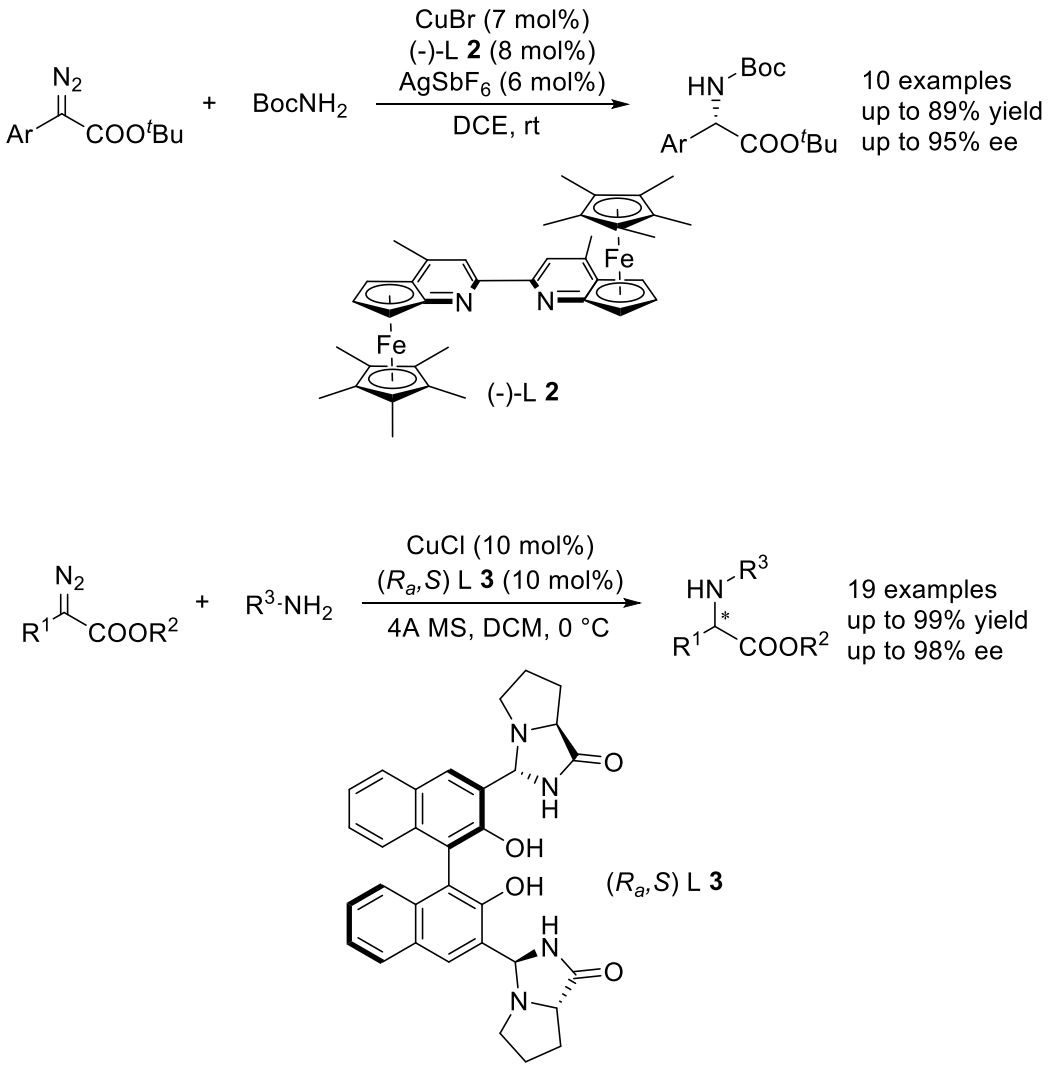

Scheme 12. Copper catalyzed asymmetric carbene insertions into N−H bonds

Because the activity of dirhodium(II) catalysts was usually superior to that of copper catalysts in non-enantioselective N−H insertion reactions, the possibility of dirhodium catalysts achieving highly enantioselective N−H insertion reactions gained attention (Scheme 13). In 2010, Miyairi's group reported that dirhodium(II) carboxylates and cinchona alkaloids cooperatively catalyze the asymmetric N−H insertion reactions of α-diazo-α-arylacetates with anilines.[59]

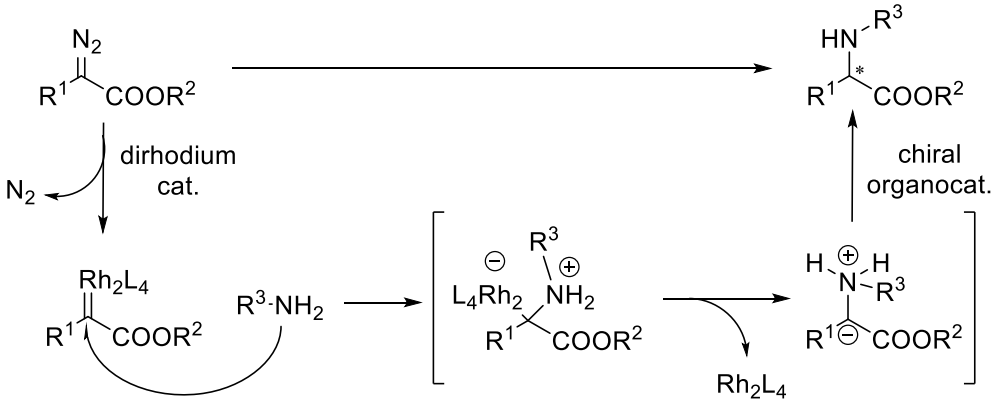

Scheme 13. An ideal mechanism of asymmetric N-H insertion catalyzed cooperative catalytic systems

As remarkable advances in this field, Zhou's group has developed several highly enantioselective N−H insertion reactions by the cooperative catalytic systems of dirhodium complexes and chiral Brønsted acids, especially chiral phosphoric acids (Scheme 14).[60-62] In these catalytic systems, chiral phosphoric acids catalyzed the final proton transfer step to realize high enantioselectivities.

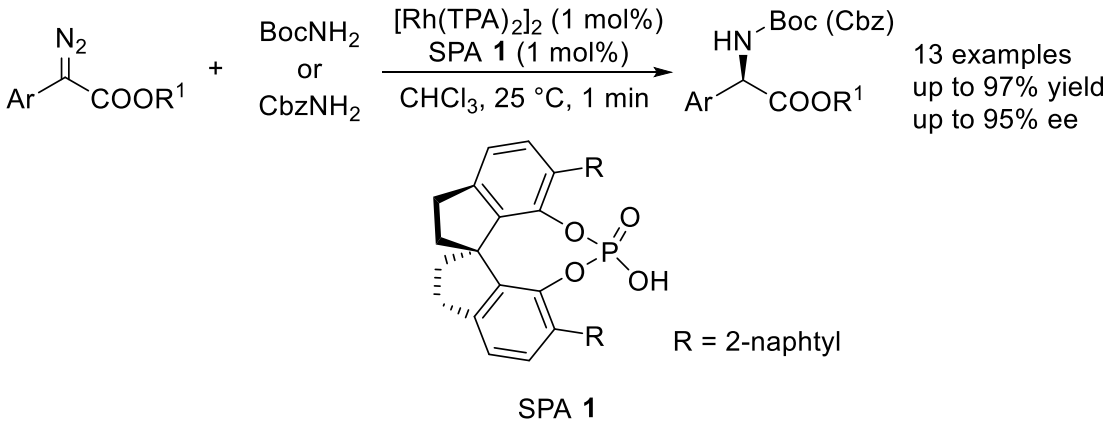

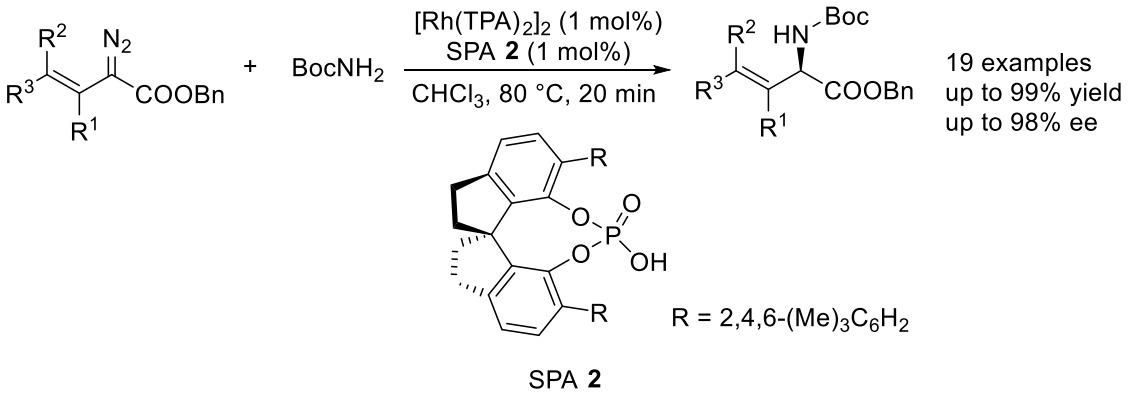

Scheme 14. The asymmetric cooperative catalytic systems of dirhodium complexes and chiral phosphoric acids

One of the advantages of the asymmetric insertions of carbenoids into N−H bonds is that only nitrogen gas is generated as a byproduct, and the reaction seems to be suitable for continuous-flow systems. However, effective heterogeneous catalyst systems have not been reported.

From these backgrounds, based on the cooperative systems with Rh catalysts and chiral phosphoric acids, I began the development of nitrogen-doped carbon supported Rh nanoparticle catalysts for the asymmetric insertions of diazoesters into N−H bonds toward the efficient and continuous synthesis of chiral α-amino acids.

2-2. Synthetic utilities and applications to continuous-flow systems

In my master course studies, I have developed nitrogen-doped carbon incarcerated Rh nanoparticle catalysts (NCI-Rh) for asymmetric insertion of α-diazoesters into N−H bonds in the presence of chiral phosphoric acids (CPA) (Scheme 15). NCI-Rh was prepared from a 5:1 (w/w) ratio of poly(4-vinylpyridine) (PVP) and ketjen black (CB). In the presence of PVP and CB, Rh nanoparticles were formed by the reduction of Rh salt. A poor solvent was then added to form polymer encapsulated nanoparticles as precipitates, which were further pyrolyzed to afford NCI-Rh.

I examined several kinds of heterogeneous Rh nanoparticle catalysts for the model reaction of methyl phenyldiazoacetate (**1a**) with *p*-anisidine (**2a**) using 3,3'-bis(2,4,6-triisopropylphenyl)-1,1'-binaphthyl-2,2'-diylhydrogenphosphates (TRIP) as CPA (Table 1). NCI-Rh gave the desired product **3a** quantitatively with low enantioselectivity (entry 1), although other Rh nanoparticle catalysts supported on polystyrene-copolymer/carbon black (PI/CB-Rh)[44] or polysilane/alumina (PSi/Al_2O_3-Rh)[63] gave almost no desired product **3a** (entries 2,3). Commercially available Rh/C did not work well (entry 4), and CB-Rh prepared without PVP in the same method as NCI-Rh gave almost no product (entry 5). These results indicate that nitrogen dopants play an important role in catalytic activity. Finally, I found that spirobiindane diol (SPINOL)-derived CPA (SCPA) improved enantioselectivity to 83% ee (entry 6). This result was comparable to that using a homogeneous Rh catalyst (entry 7).

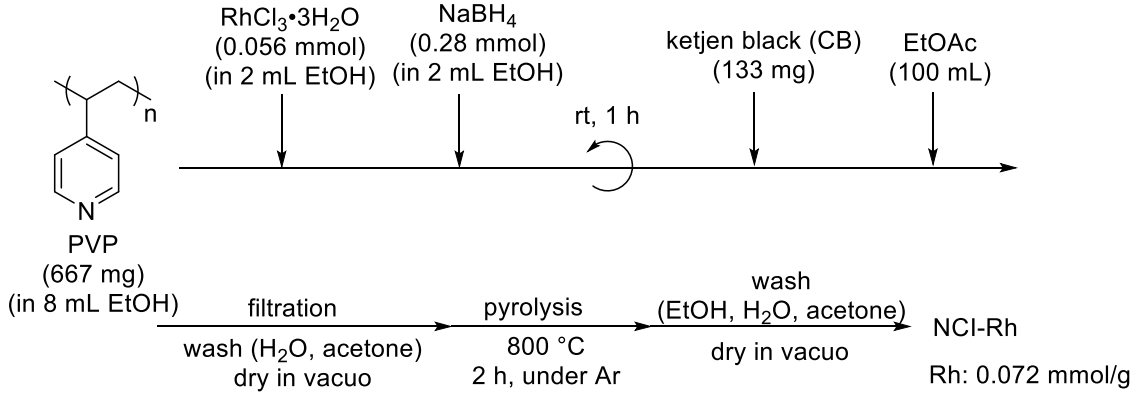

Scheme 15. Preparation of NCI-Rh

Table 1. Screening of Rh catalysts and chiral phosphoric acid catalysts

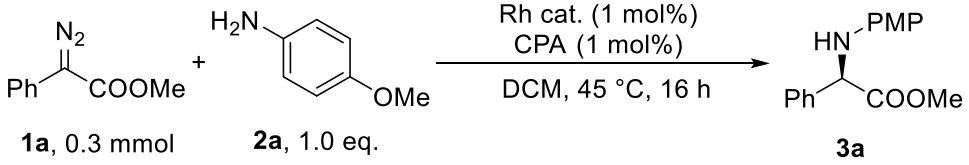

1a, 0.3 mmol **2a**, 1.0 eq. **3a**

entry	Rh cat.	CPA	yield (%)[a]	ee (%)[b]
1	NCI-Rh	TRIP	quant. (95)	17
2	PI/CB-Rh	TRIP	3	-
3	PSi/Al_2O_3-Rh	TRIP	1	-
4	Rh/C (Wako)	TRIP	N.R.	-
5	CB-Rh	TRIP	3	-
6	NCI-Rh	SCPA	93(91)	83
7	$[Rh(OAc)_2]_2$	SCPA	95	84

a: Determined by ^{1}H NMR analysis; isolated yield given in parentheses.,

b: Determined by HPLC analysis.

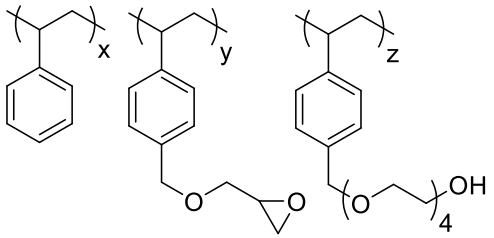

PI
(Polymer-incarcerated)

PSi
(Polydimethylsilane)

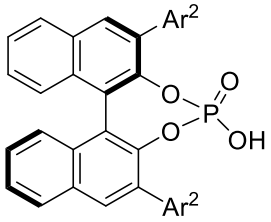

TRIP

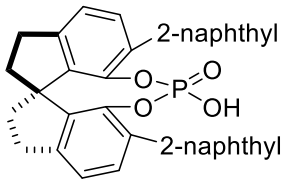

SCPA

Ar^2 = 2,4,6-(^{i}Pr)$_3$C$_6$H$_2$

With the optimized catalyst system in hand, I examined the substrate scope (Scheme 16). A wide variety of protected amines, *p*-anisidine, *o*-anisidine, $BocNH_2$, $FmocNH_2$, and $CbzNH_2$, afforded the corresponding protected products **3a**-**3e** smoothly. Diazo compounds with ethyl or isopropyl ester gave a little lower yield and enantioselectivity than methyl ester (**3f**, **3g**).

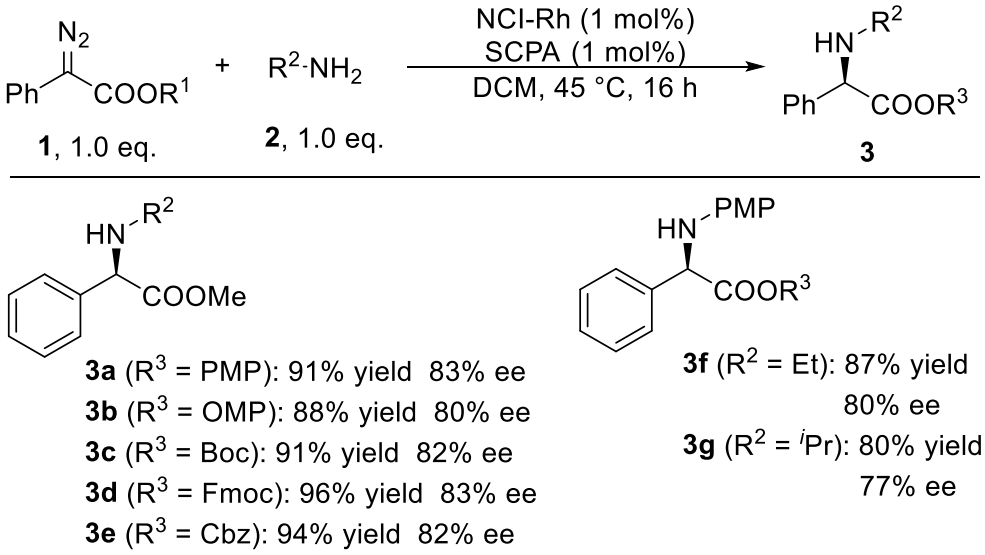

Scheme 16. Substrate scope (1)

I then explored other diazo compounds bearing a substituent on the aryl ring (Scheme 17). Irrespective of electrocnic effects or positions of substitutions, the reaction proceeded smoothly to afford desired products **3h**-**3l** in high yields with high enantioselectivities. 2-Naphthyl-substituted diazoester also worked well in this system (**3m**).

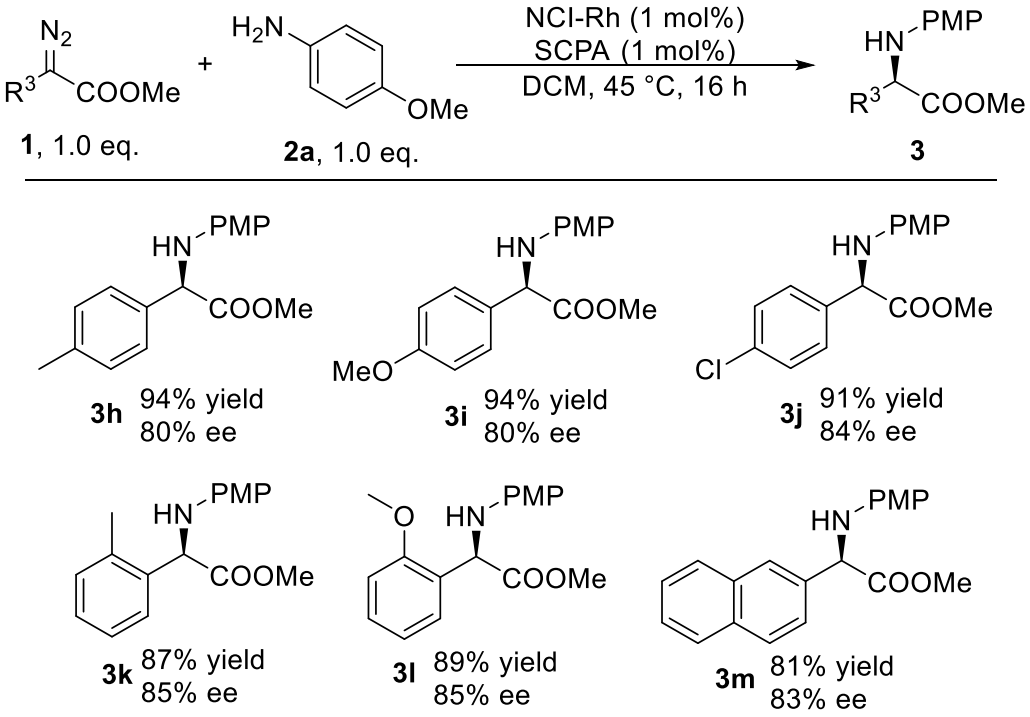

Scheme 17. Substrate scope (2)

The recovery and reuse of NCI-Rh were investigated (Table 2). After the reaction, NCI-Rh was collected and washed by centrifugation, dried in vacuo, and used for the next trial. NCI-Rh was successfully reused seven times without losing activity and enantioselectivity. After deactivation in the eighth run, I attempted to reactivate the recovered NCI-Rh by heating. Unfortunately, heating at 200 ℃ or 800 ℃ did not reactivate the recovered NCI-Rh. This suggested that the decrease in catalytic activity was not due to the attachment of organic compounds. Furthermore, since Rh loading did not change after eight reuses, deactivation due to the leaching of Rh was also unlikely.

Table 2. Recovery and reuse of NCI-Rh

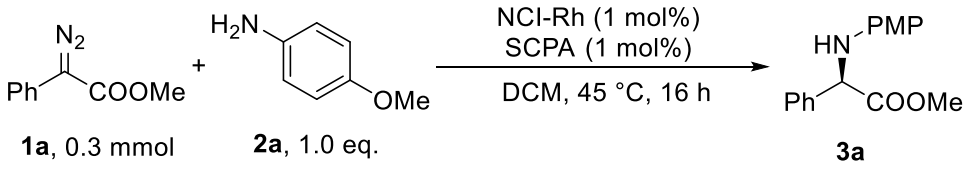

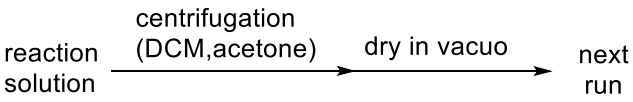

run	yield[a] (%)	ee[b] (%)	Rh loading (mmol/g)
1	92	83	0.072
2	94	82	
3	90	83	
4	90	82	
5	93	82	
6	89	81	
7	91	82	
8	49	81	0.074

a: Isolated yield., b: Determined by HPLC analysis.

run	yield[a] (%)	ee[b] (%)	comment
9	32	81	heated at 200 ℃ under Ar after 8th run
10	41	79	heated at 800 ℃ under Ar after 9th run

a: Isolated yield., b: Determined by HPLC analysis.

The PMP group of chiral product **3a** was successfully deprotected without losing the chiral information by oxidation with cerium ammonium nitrate (CAN) (Scheme 18). The ee of chiral free amine **4a** was enhanced to 91% by crystallization with EtOH after the formation of hydrogen chloride salts.

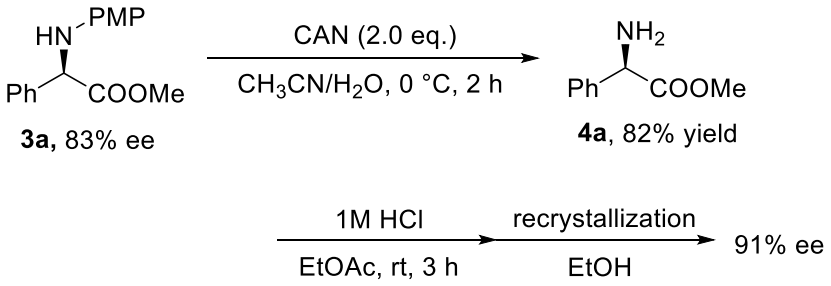

Scheme 18. Deprotection of PMP group and enhancement of the ee

NCI-Rh was applied to the continuous-flow system (Table 3). Based on the results of the batch reactions, an initial study of the continous-flow reactio was carried out under the condition that the reaction proceeded smoothly when the turnover frequency (TOF) was 6-7 h^{-1}. Specifically, 0.1 M of the reaction solution was flowed through a column packed with 930 mg of NCI-Rh (Rh: 0.067 mmol) at a flow rate of about 0.1 ml/min. The reaction system was stable for 2 hours and the desired product **3a** was obained in about 60% yield continuously for 20 hours. As for enantioselectivity, almost the same ee as the batch reaction was obtained. The calculated TOF was 4.5~4.8 h^{-1}.

Table 3. Preliminary trial for continuous-flow system

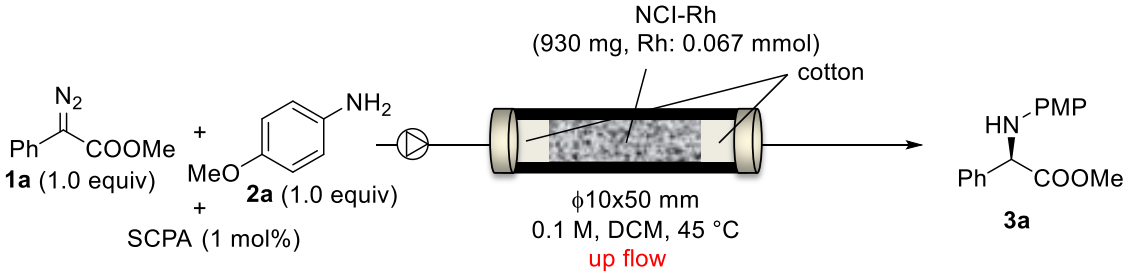

time (min)	flow rate (ml/min)	yield (%)[a]	ee (%)[b]	TOF (h^{-1})
73-129	0.09	21	82	1.6
129-330	0.08	59	82	4.7
330-446	0.08	58	82	4.5
446-577	0.08	55	82	4.5
577-1372	0.08	64	82	4.8

a: Isolated yield., b: Determined by HPLC analysis.

Based on the TOF obtained above, the reaction conditions under the continous-flow system were modified (Scheme 19). The length of a column for NCI-Rh was changed to 10 cm, and the amount of NCI was increased to 1500 mg (Rh: 0.108 mmol). Additionally,

a column packed with basic resin for recovery of SCPA was connected. The product **3a** was obtained in high yields with high enantioselectivity from 4 h after starting the system, which could work for over 65 h without siginificant loss of catalytic activity. The turnover number (TON) was 366, and the highest TOF was 5.7 h^{-1}.

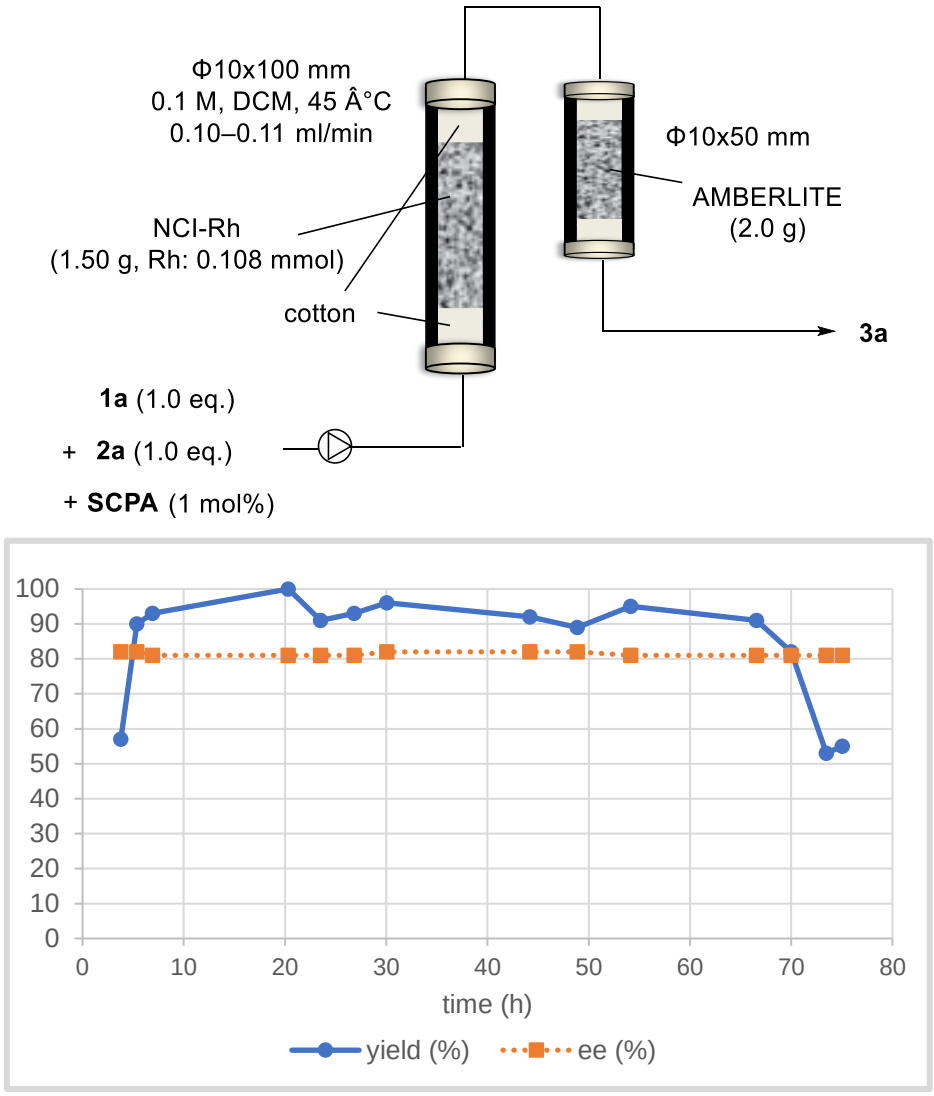

Scheme 19. Continuous-flow system

I then attempted to reactivate NCI-Rh used in the above flow reaction by heating. When the recovered NCI-Rh was treated at 800 °C for 2 h under Ar, the reactivity was restored. This was probably because some attached molecules causing the deactivation of NCI-Rh were removed by heating. A second run of the continuous flow system was performed using the reactivated NCI-Rh (Scheme 20). The system gave products in high yields with high enantioselectivity over 25 h. The TON was 164, and the highest TOF was 6.0 h^{-1}. Through two trials of the flow system, a total TON of 530 was achieved, and 15.3 g of

product was produced. These results exhibited the efficiency of the continuous flow system and the robustness of the metal nanoparticle catalyst.

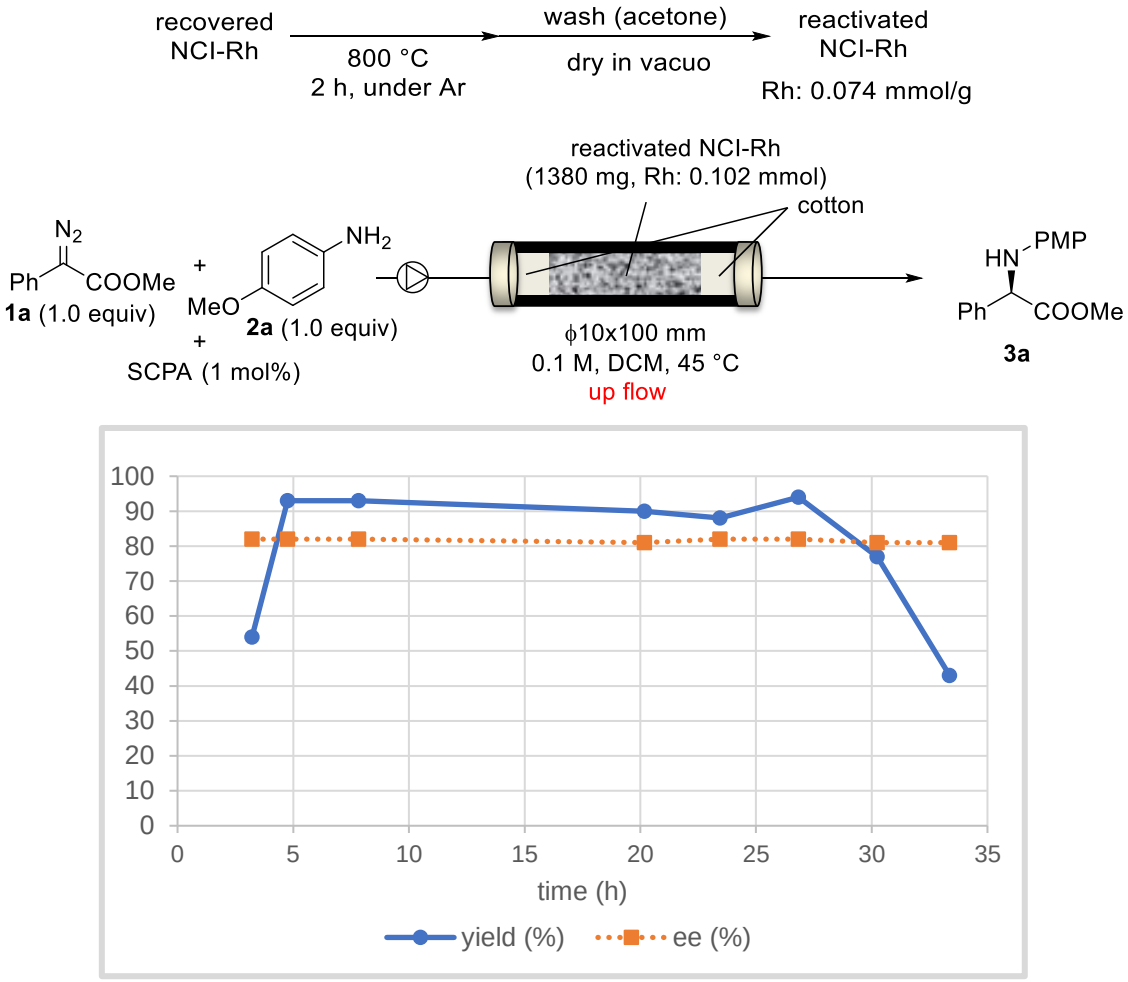

Scheme 20. Continuous-flow system using reactivated NCI-Rh

The recovery and reuse of chiral phosphoric acid SCPA trapped by basic resins in continuous-flow reactions were investigated (Table 4). The recovered basic resin was treated with hydrogen chloride and the aqueous phase was extracted with toluene to recover SCPA **1**. When the recovered SCPA **1** was used for the batch reaction, ee was lower than that using the fresh SCPA (entry 1). Therefore, SCPA **1** was purified by column chromatography and used again for the batch reaction to obtain the original high activity and enantioselectivity (entry 2).

Table 4. Recovery and reuse of SCPA

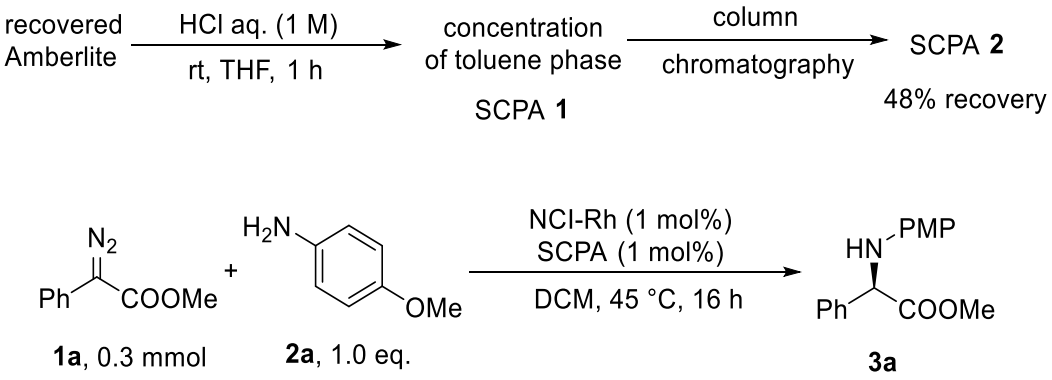

entry	SCPA	yield (%)[a]	ee (%)[b]
1	SCPA **1**	89	70
2	SCPA **2**	91	82

a: Isolated yield., b: Determined by HPLC analysis.

2-3. Characterizations of catalysts and mechanistic studies

To get insight into the effect of nitrogen dopants, I conducted several analyses of NCI-Rh and CB-Rh. Scanning transmission electron microscopy (STEM) analysis and energy dispersive X-ray spectroscopy (EDS) mapping showed that nitrogen dopants contributed to the high dispersion of Rh nanoparticles on nitrogen-doped carbon (Figure 1). The average size of the particles on NCI-Rh was determined to be 3.0 ± 0.7 nm. On the other hand, it was difficult to determine the average particle size on CB-Rh because of aggregation.

NCI-Rh

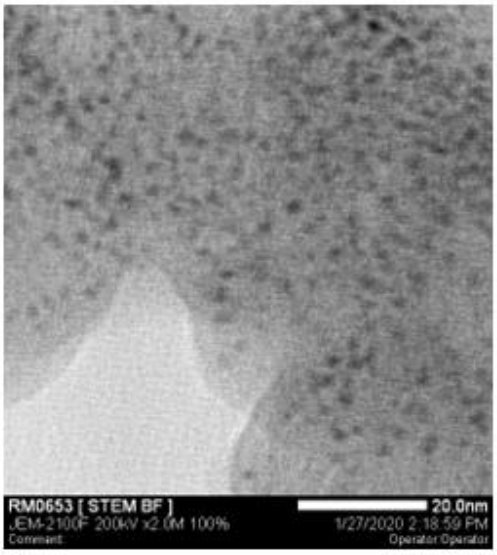

CB-Rh

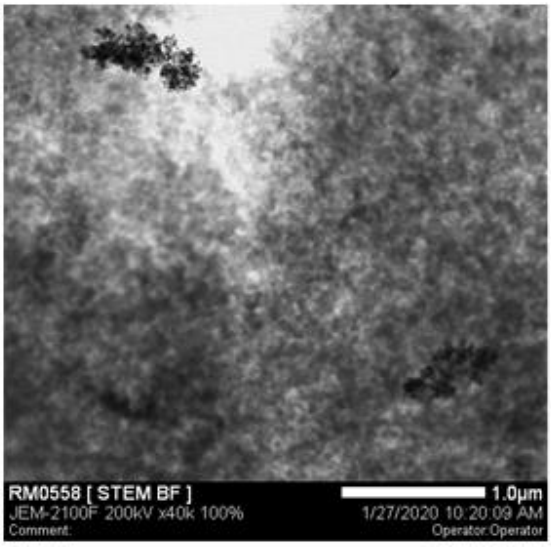

NCI-Rh

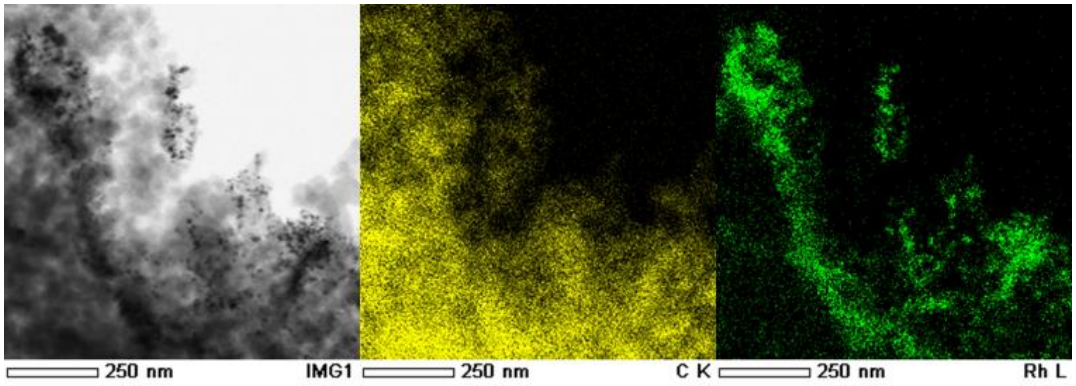

CB-Rh

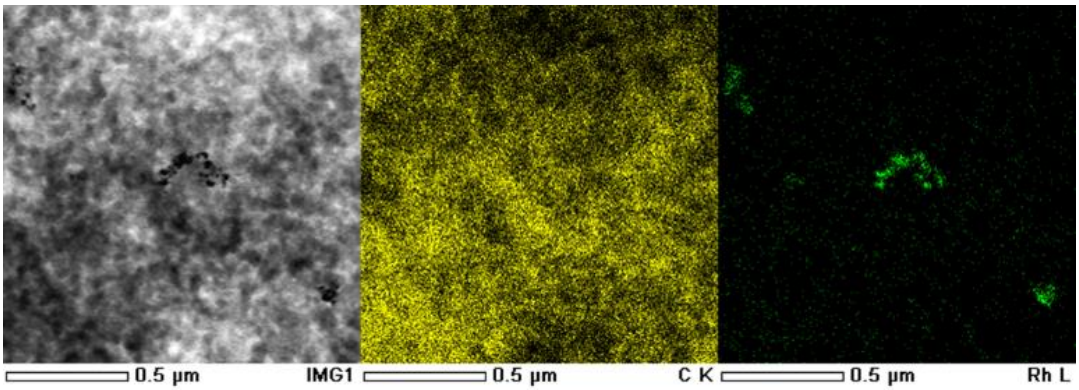

Figure 1. STEM analysis and EDS mapping of NCI-Rh and CB-Rh

I then performed X-ray photoelectron spectroscopy (XPS) analysis of NCI-Rh and CB-Rh (Figure 2). The binding energy of Rh $3p_{3/2}$ of NCI-Rh became higher than CB-Rh. The binding energy of N 1s of NCI-Rh revealed the presence of both pyrrolic and pyridinic nitrogen, the latter being the dominant species. Since both nitrogen species were suggested to act as an electron acceptor,[64-66] these results indicate that electron transfer from Rh to nitrogen dopants took place, and that electron-deficient Rh species could easily form metal carbenoid intermediates by facilitating the attack of diazo compounds.

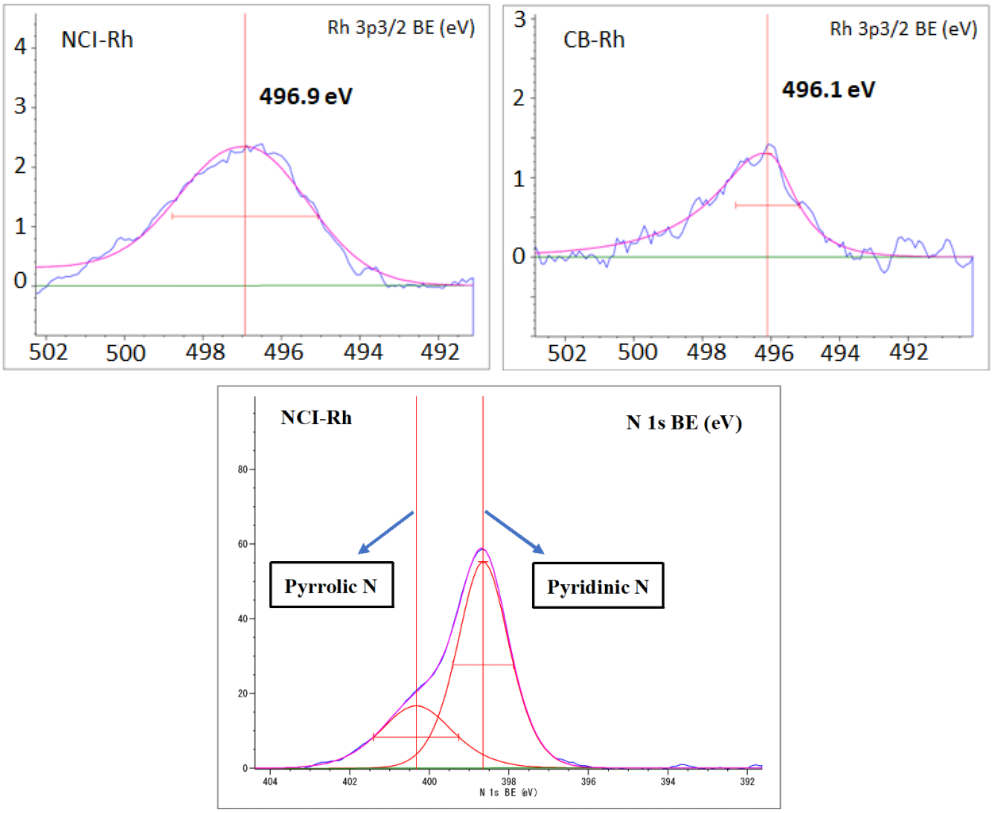

Figure 2. XPS analysis of NCI-Rh and CB-Rh

To get insight into the active species, hot filtration tests were conducted (Table 5). The result showed that no further reaction occurred in the filtrate obtained from the middle of the reaction, which means leached Rh species did not catalyze the reaction even if trace amounts of Rh were leached out.

Table 5. Hot filtration tests

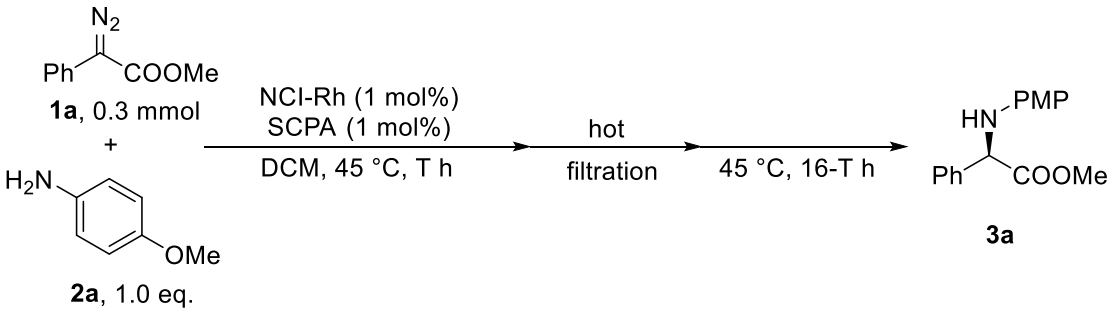

entry	T (h)	yield[a] (ee)[b] (%) at T h	yield[a] (ee)[b] (%) at 16 h
1*	16	-	91 (83)
2	3	42 (82)	40 (82)
3	6	68 (83)	70 (83)

*: No hot filtration. a: Determined by ^{1}H NMR analysis. b: Determined by HPLC analysis.

Stoichiometric reactions were performed under flow conditions to confirm whether the reaction proceeded on the heterogeneous phase (Scheme 21). A solution of diazo substrate **1a** was first flowed into a column packed with NCI-Rh. After washing thoroughly with DCM, a solution of amine substrate **2a** and SCPA was flowed. The desired product was obtained in 28% yield with respect to the amount of Rh. On the other hand, in the case of packing nitrogen-doped carbon instead of NCI-Rh, no absorption of **1a** in the column was observed in the same study. The results indicated that the Rh of NCI-Rh played an important role in keeping **1a** in the column while nitrogen-doped carbon did not.

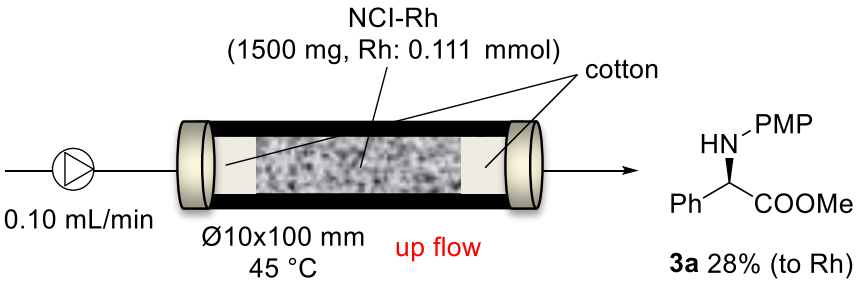

1) DCM (20 mL)
2) **1a** (3.3 mL, 0.1 M DCM solution)
3) DCM (40 mL)
4) **2a** (1.2 mL, 0.1 M DCM solution) and SCPA (1 mol%)
5) DCM (20 mL)

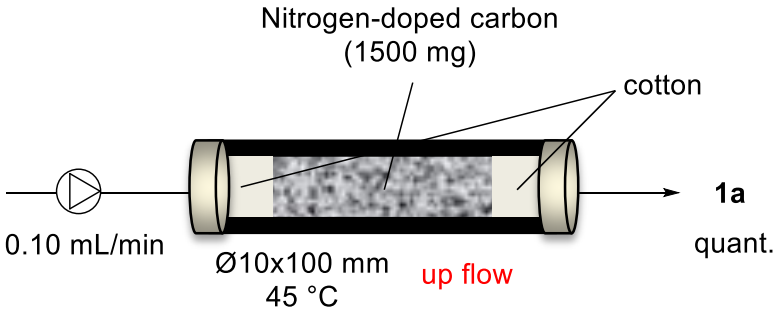

1) DCM (20 mL)
2) **1a** (3.3 mL, 0.1 M DCM solution)
3) DCM (40 mL)

Scheme 21. Stoichiometric reactions under flow conditions

Infrared absorption spectrometry (IR) and solid-state NMR measurements were performed on NCI-Rh treated with **1a** to directly observe the reaction intermediates. However, no clear peaks were obtained probably because the amount of intermediate was small or the intermediate was unstable in the air.

Finally, STEM analysis and EDS mapping of NCI-Rh treated with 2-(4-bromophenyl)-2-diazoacetate was conducted to detect the position of the substrate on NCI-Rh (Figure 3). The results showed that Rh and Br appeared to be mainly located in the same place. Based on the above mechanistic studies, I guess that the reaction proceeded via the formation of Rh carbenoid in the solid state.

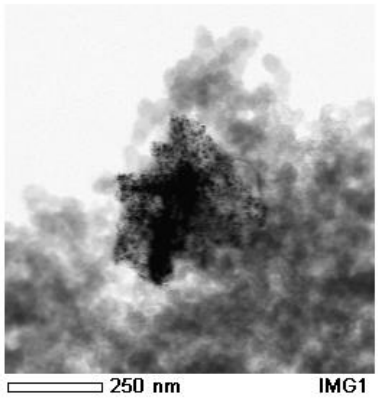
250 nm
IMG1

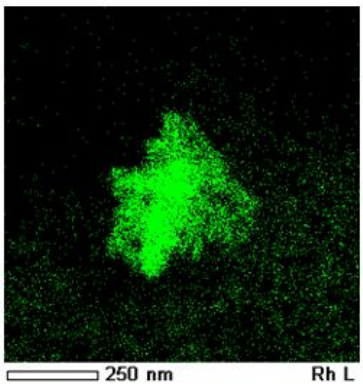
250 nm
Rh L

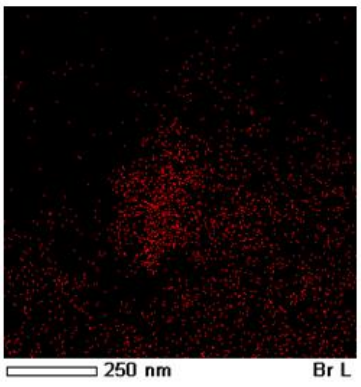
250 nm
Br L

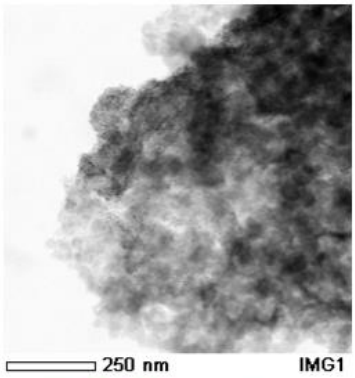
250 nm
IMG1

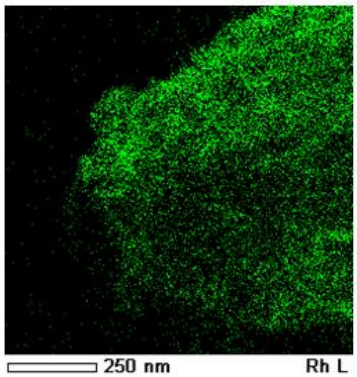
250 nm
Rh L

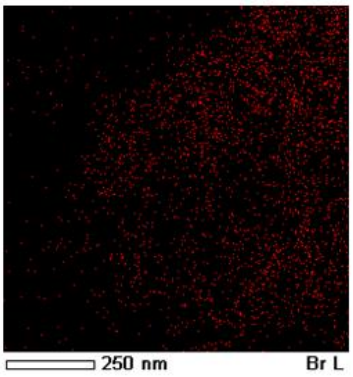
250 nm
Br L

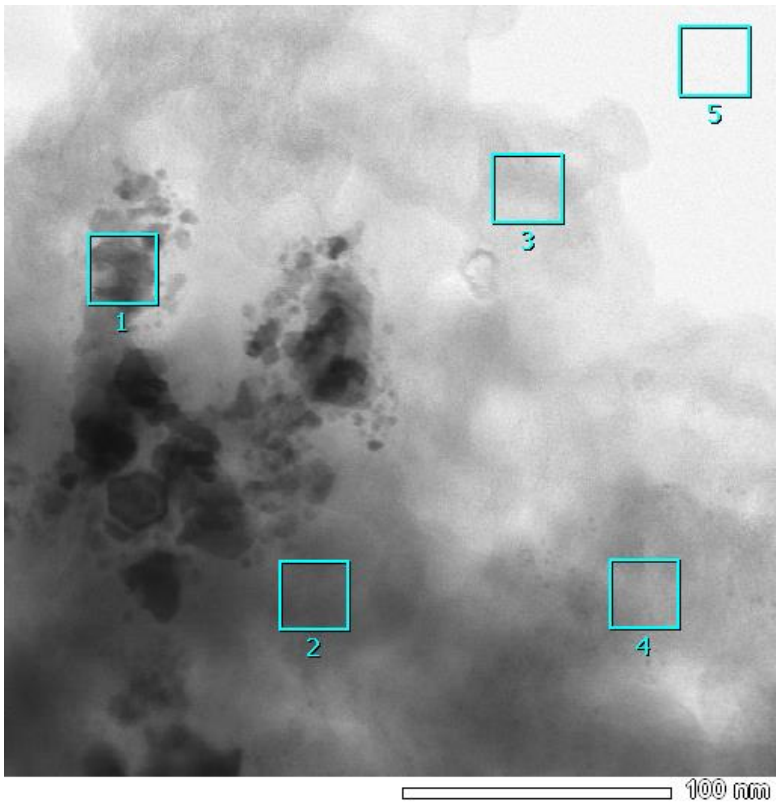
1
2
3
4
5
100 nm

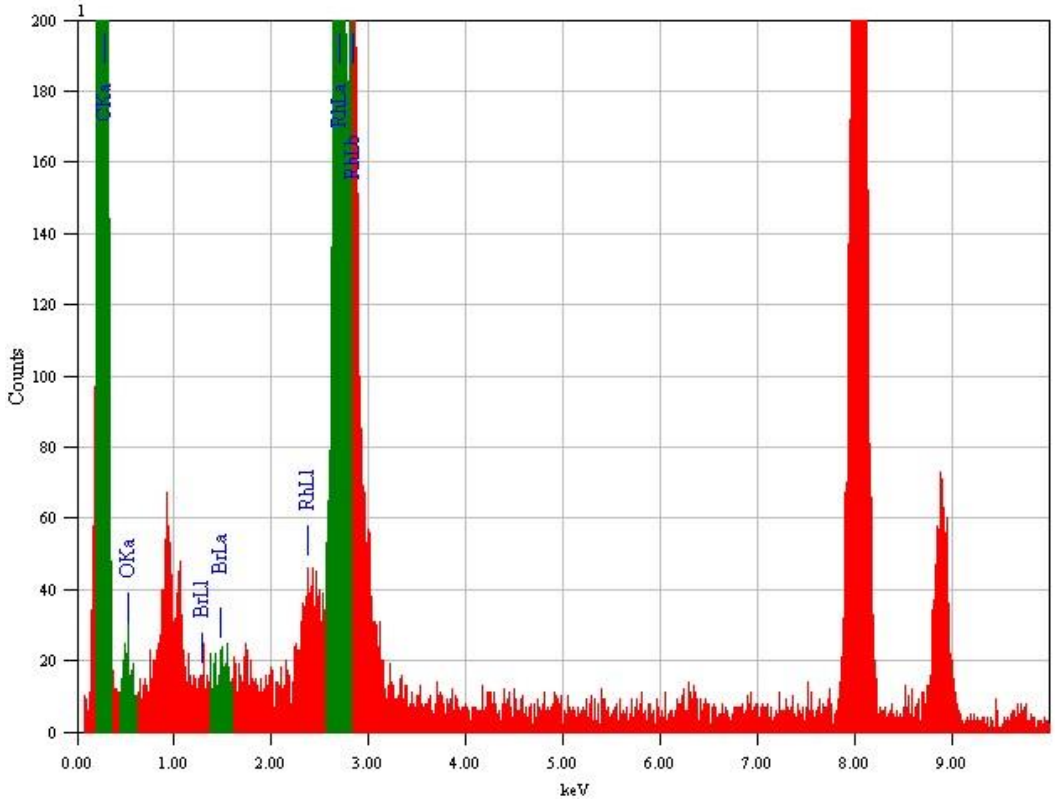
1
Counts
keV
OKa
RhLa
RhLl
OKa
BrLl
BrLa
RhLl

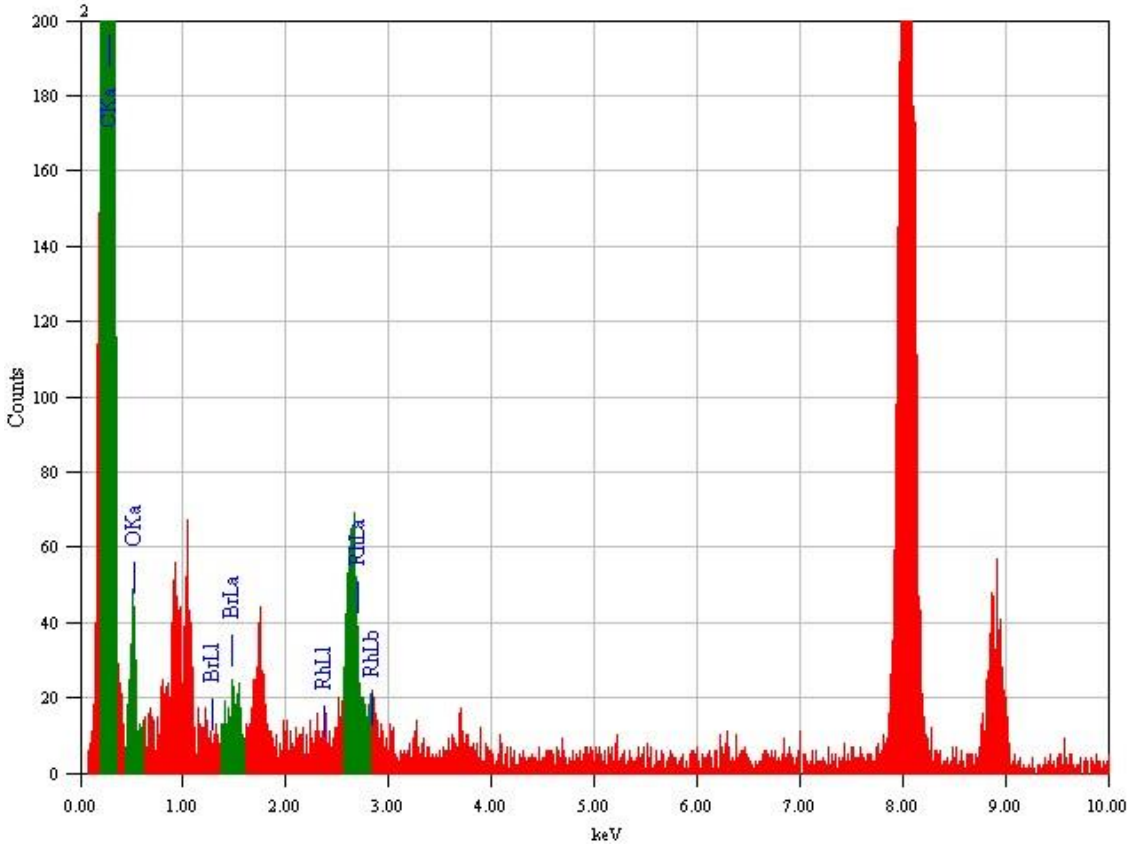
2
Counts
keV
OKa
OKa
BrLl
BrLa
RhLl
RhLa
RhLb

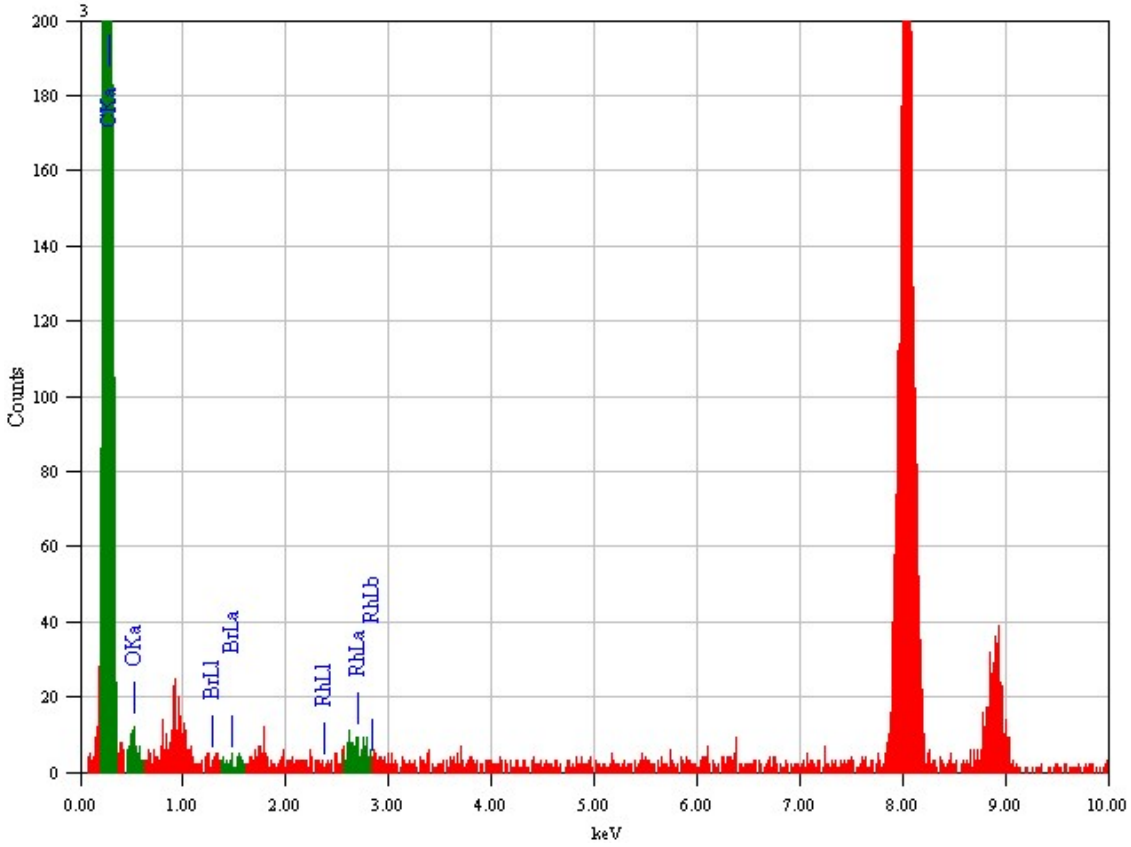
3
Counts
keV
OKa
OKa
BrLl
BrLa
RhLl
RhLa
RhLb

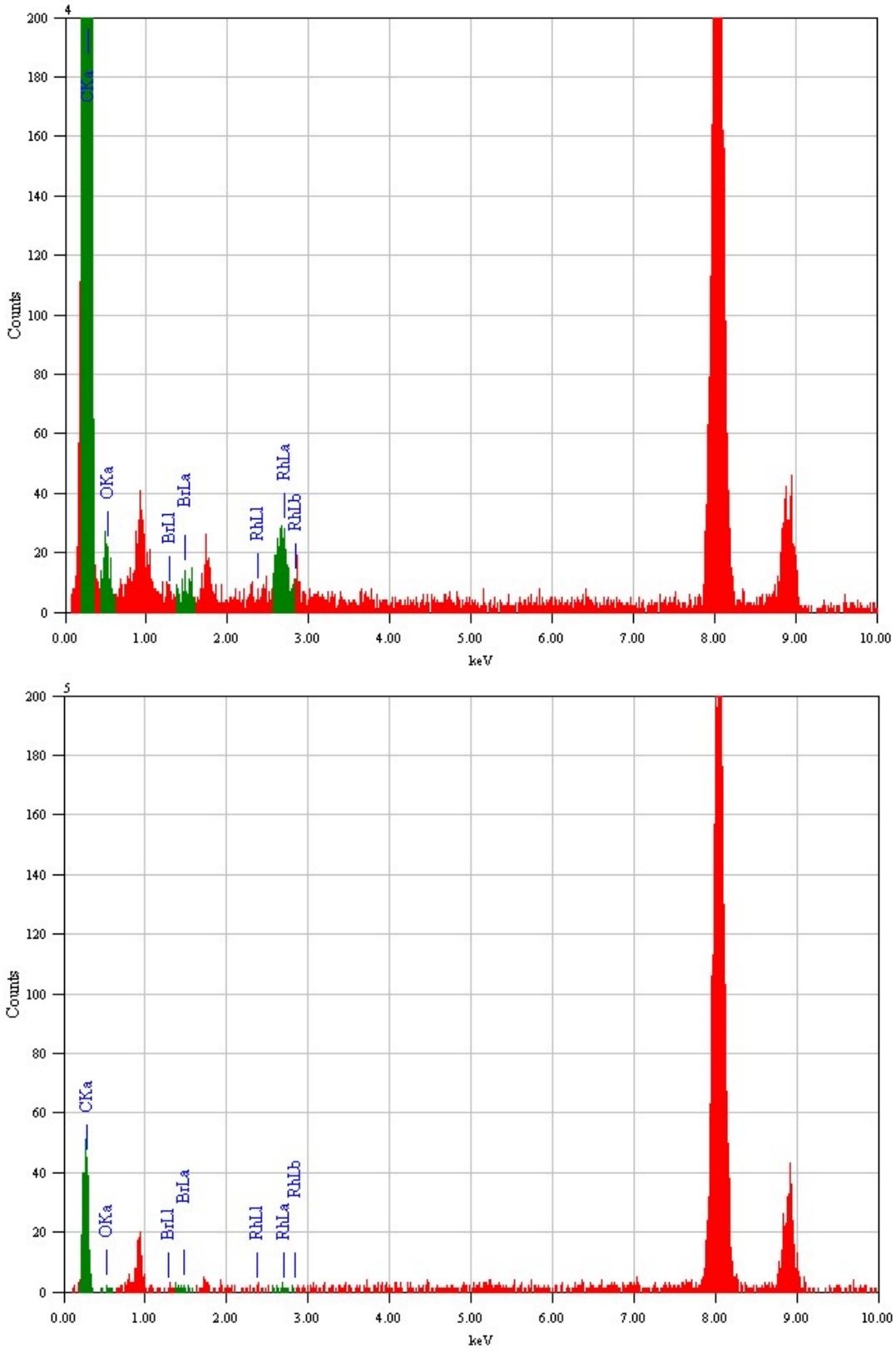

Figure 3. STEM analysis and EDS mapping of NCI-Rh treated with methyl 2-(4-bromophenyl)-2-diazoacetate

In this chapter, I have developed nitrogen-doped carbon incarcerated rhodium nanoparticle catalysts (NCI-Rh) for the asymmetric insertion of carbenoids derived from diazoesters into amines. By employing SPINOL-derived chiral phosphoric acids as cocatalysts, various types of α-amino acid derivatives were synthesized in high yields with high enantioselectivities. In this catalyst system, nitrogen-dopants played a crucial role in both activity and enantioselectivity. Furthermore, NCI-Rh was applied successfully to a flow system. Several control studies and analyses suggested the formation of intermediates derived from diazo compounds on the surface of NCI-Rh. This work has not only established an efficient synthetic system, but also opened the door to asymmetric reactions catalyzed by metal nanoparticles.

Chapter 3: Development of Nitrogen-Doped Carbon Incarcerated Zinc Nanoparticle Catalysts for Electrochemical Allylations of Carbonyl Compounds

3-1. Introduction

Organometallic reagents hold a special place in organic synthesis because they have widespread synthetic applications based on carbon−carbon bond formation.[67] The most popular reaction is the Grignard reaction, which is the addition reaction of an organomagnesium halide (Grignard reagent) to a carbonyl compound to afford a tertiary or secondary alcohol (Scheme 22).

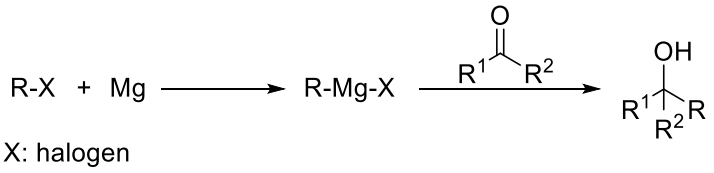

Scheme 22. Grignard reaction

Organometallic reagents are not only utilized for addition reactions to various electrophiles but also applied to cross-coupling reactions such as Kumada-Tamao-Corriu reaction[68] or Negishi reaction (Scheme 23).[69] However, stoichiometric amounts of metal reagents are usually required in such transformations, which can result in the generation of large amounts of metallic waste.

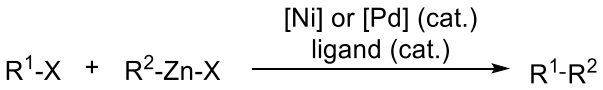

Scheme 23. Negishi cross coupling reaction

In another aspect, because organometallic reagents are highly reactive and unstable in air and water, special care is required in large-scale synthesis. To address this problem, approaches to continuously produce organometallic reagents under flow conditions have been reported (Scheme 24).[70-75] The process involves flowing aryl or alkyl halides into a column packed with activated metals to generate organometallic reagents in situ for subsequent reactions. However, this method consumes a stoichiometric amount of metal and still generates a large amount of waste, and the amounts of organometallic reagents accessible are finite. Therefore, catalytic carbon−carbon bond forming reactions that proceed without the generation of metallic waste are in high demand.

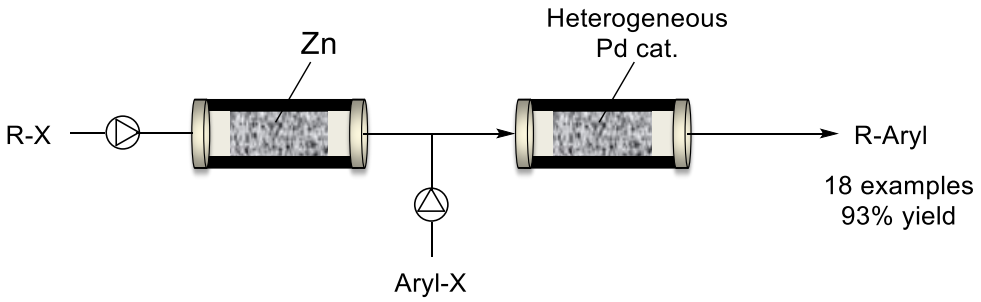

Scheme 24. Continuous-flow generation of organozinc reagents

I envisioned an electrochemical approach in which metal catalysts on the cathode form organometallic reagents and the subsequent electroreduction after the reaction regenerate metal(0) on the cathode (Scheme 25). Electrochemistry has recently gained much attention as a versatile strategy for achieving challenging transformations at the forefront of synthetic organic chemistry.[76-78] Electrochemical reactions realize the powerful and clean redox process, in which electrons work as redox reagents without chemical oxidants or reductants.

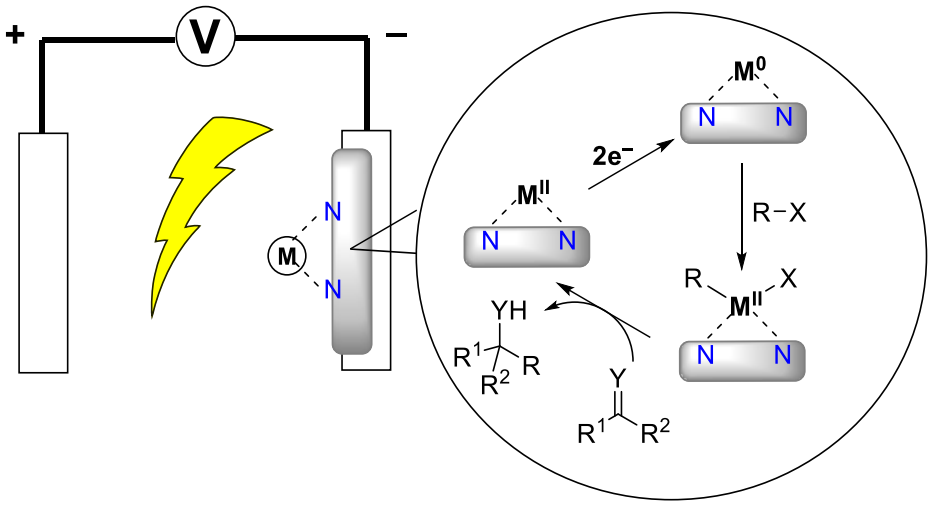

Scheme 25. Electrochemical approach with heterogeneous catalyst electrode

Allylation of carbonyl compounds is an efficient C−C bond-forming reaction and an essential synthetic transformation because homoallylic alcohols are ubiquitous building blocks for materials and bioactive compounds.[79,80] Allylation reactions using organometallics have been developed extensively[81,82] and zinc has been demonstrated to be a particularly good reagent to mediate the Barbier-type reaction (Scheme 26). However, such systems generally consume stoichiometric amounts of metals.

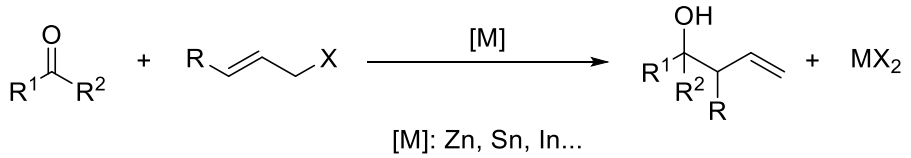

Scheme 26. Barbier-type allylation reactions

In 2009, electrochemical allylation of aldehydes in aqueous ammonia was reported by Huang's group (Scheme 27).[83] This reaction was mediated by zinc generated from zinc electrodes and achieved in an undivided cell. However, a stoichiometric amount of zinc were leached out from the electrodes to the solution.

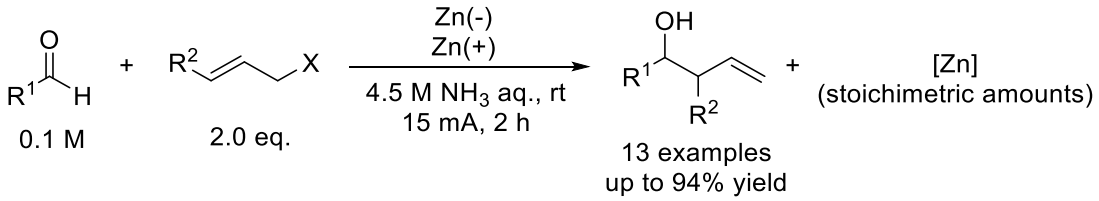

Scheme 27. Electrochemical allylation of aldehydes using zinc electrodes

In 2010, Huang's group achieved electrochemical allylation of carbonyl compounds in aqueous media using zinc cathode with a catalytic amount of zinc consumption (Scheme 28).[84] Nevertheless, a large amount of zinc still leached out, and zinc was used excessively. Moreover, the system required a divided cell, and the substrate scope was limited.

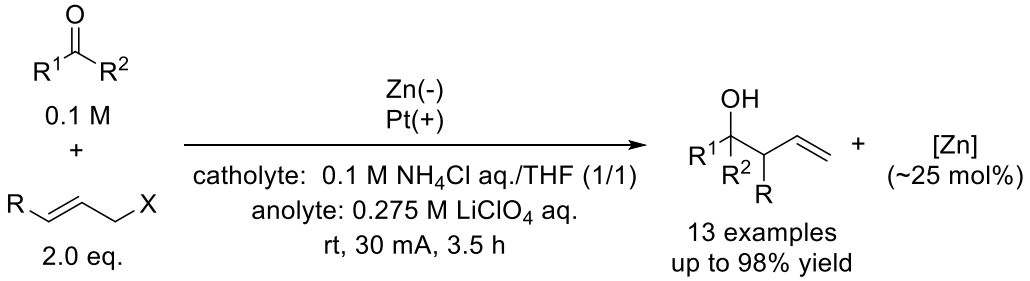

Scheme 28. Electrochemical allylation of carbonyls catalyzed by zinc

A conceivable main challenge in the development of catalyst electrodes for electrochemical C−C bond-forming reaction is to suppress metal leaching. To overcome this issue, I reasoned that nitrogen-doped carbon-supported metal species would be suitable materials for the electrodes inspired by the robustness of NCI catalysts (Scheme 25).[85] Metal leaching was not observed not only in the presence of radicals in NCI-Co catalyzed oxygenation of styrenes,[24] but also in the presence of chiral catalysts in NCI-

Rh catalyzed asymmetric insertion reactions (Chapter 2). Nitrogen-doped carbon-supported metal-based electrodes have been extensively studied to catalyze hydrogen evolution or oxygen reduction in the field of electrochemistry.[9,86,87] However, electrochemical organic transformations, especially carbon−carbon forming-reactions, catalyzed by nitrogen-doped carbon-supported metal catalysts remain undeveloped.[88]

Based on these backgrounds, I attempted to develop efficient electrochemical allylation reactions of carbonyl compounds using nitrogen-doped carbon-supported zinc catalyst electrodes to achieve C−C bond forming-reactions without metallic wastes.

3-2. Optimizations and characterizations of catalysts

NCI-Zn was prepared based on the preparation of NCI-Rh (Scheme 29). A zinc salt was treated with $NaBH_4$ in the presence of a 1:1 (w/w) ratio of PVP and ketjen black (CB). A poor solvent was added to the mixture to generate polymer-encapsulated zinc species. The precipitation was pyrolyzed at 400 ℃ or 800 ℃ to afford NCI-Zn. To prepare the electrode, NCI-Zn was mixed with a Nafion solution at 0 ℃ under sonication for 1 h, and the composite was pasted on a carbon cloth. After dried at 50 ℃ for 1 h, The carbon cloth was fixed to a graphite electrode with carbon tape and used as an electrode (Scheme 30).

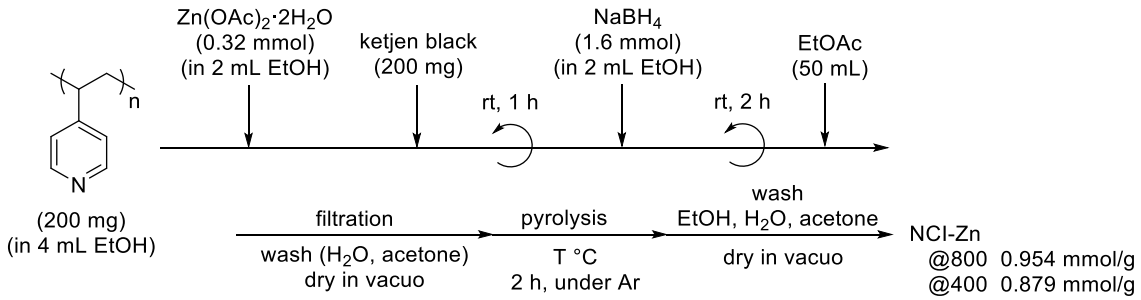

Scheme 29. Preparation of NCI-Zn

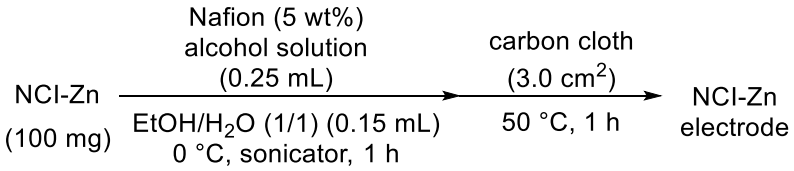

Scheme 30. Preparation of NCI-Zn electrode

The activity of the prepared NCI-Zn electrodes was evaluated in electrochemical allylation of benzaldehydes **5a** with allyl bromide **6a** using a Pt anode in an undivided cell (Table 6). The reaction conditions were based on the previous report.[83] When a graphite cathode was used, the desired homoallylic alcohol **7a** was not detected (entry 1). On the other hand, NCI-Zn cathode gave a small amount of **7a**, and it was found that pyrolysis at 800 ℃ was more effective to suppress zinc leaching than pyrolysis at 400 ℃ (entries 2,3). Although the yield was very low and the turnover number (TON) was less than 2 (entry 2), catalytic amounts of zinc mediated the reaction considering that the maximum amounts of zinc on the NCI-Zn cathode was 0.095 mmol, which was promising to realize my strategy.

Table 6. Evaluation of NCI-Zn electrode

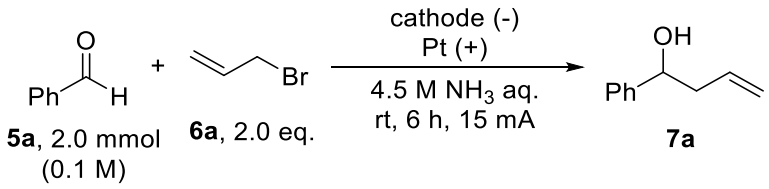

entry	cathode	Zn on cathode (mmol)	yield (%)[a]	Zn leaching (mol%)[b]
1	graphite	-	N.D.	-
2	NCI-Zn@800	0.095	9	1.7
3	NCI-Zn@400	0.088	5	2.4

a: Isolated yield. b: Determined by ICP analysis. Based on the amount of **5a**.

I thought that the low yield was attributed to small loading of zinc on the electrode. To increase the loading of zinc, the effects of the ratio of PVP and ketjen black were examined (Table 7). Treatment with HCl was also investigated to remove largely aggregated zinc species that might cause the leaching of zinc. As expected, a larger amount of PVP lead to a higher loading of zinc, which gave a higher yield in the model reaction (entries 1,3,5). Furthermore, HCl treatment was found to be efficient to suppress the leaching of zinc (entries 2,4,6).

Table 7. Effects of the ratio of PVP and ketjen black

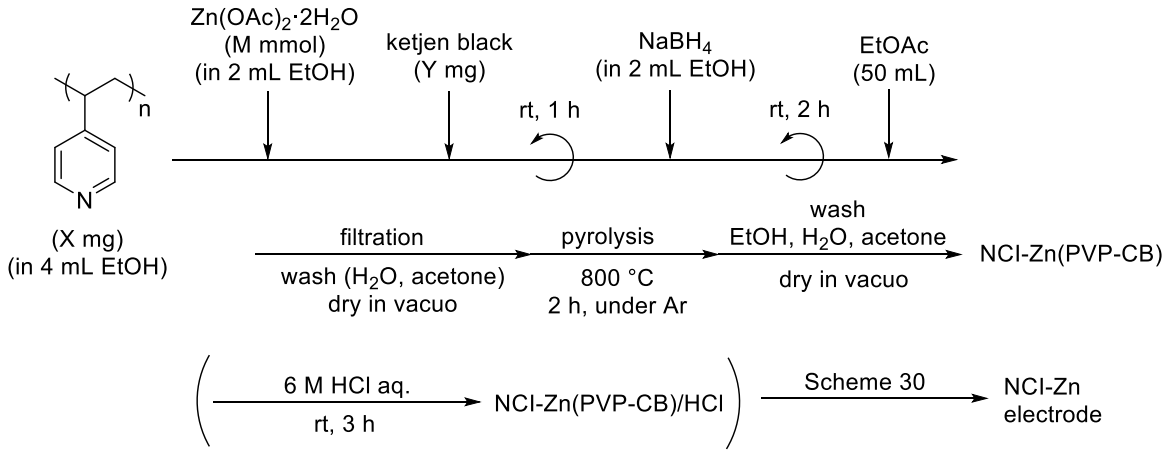

NCI-Zn	X (mg)	Y (mg)	Zn loading (mmol/g)[a]
NCI-Zn(1-1)	200	200	0.954
NCI-Zn(1-1)/HCl	200	200	0.799
NCI-Zn(3-1)	300	100	2.66
NCI-Zn(3-1)/HCl	300	100	1.93
NCI-Zn(5-1)	667	133	3.61
NCI-Zn(5-1)/HCl	667	133	2.99

a: Determined by ICP analysis.

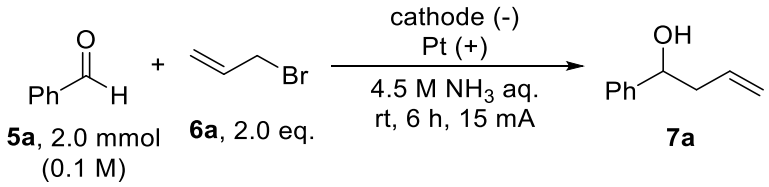

entry	cathode	Zn on cathode (mmol)	yield (%)[a]	Zn leaching (mol%)[b]
1	NCI-Zn(1-1)	0.095	9	1.7
2	NCI-Zn(1-1)/HCl	0.080	6	0.8
3	NCI-Zn(3-1)	0.266	16	3.5
4	NCI-Zn(3-1)/HCl	0.193	11	1.9
5	NCI-Zn(5-1)	0.361	19	5.3
6	NCI-Zn(5-1)/HCl	0.299	16	2.2

a: Isolated yield. b: Determined by ICP analysis. Based on the amount of **5a**.

Optimizations of reaction conditions were conducted to improve the yield (Table 8). A lower concentration of **5a** and a longer reaction time increased the yield to 27% (entries 2,3). On the other hand, higher current or high temperature did not improve the yield,

because of the formation of side products in a messy crude mixture (entries 4,5). The lower concentration of the aqueous ammonia solution decreased the leaching of zinc although the yield was kept (entry 6).

Table 8. Optimizations of reaction conditions

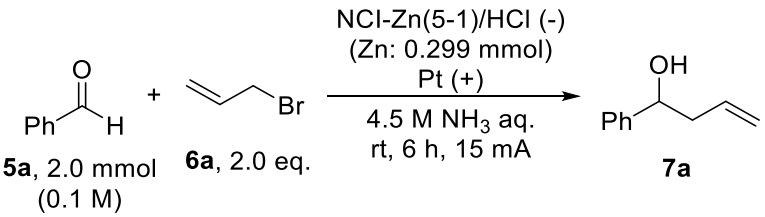

entry	derivation	yield (%)[a]	Zn leaching (mol%)[b]
1	-	16	2.2
2	0.05 M	21	3.4
3	0.05 M, 12 h	27	6.5
4	0.05 M, 30 mA	10	3.5
5	0.05 M, 60 ℃	24	5.8
6	0.05 M, 1.5 M NH_3 aq.	20	2.0

a: Isolated yield. b: Determined by ICP analysis. Based on the amount of **5a**.

I envisioned that a large amount of catalysts could be fixed on an electrode by using XC-72, which has a higher density than ketjen black, as carbon black. Four types of NCI-Zn were prepared from PVP and XC-72 with different ratios and with or without an acid treatment (Table 9). The electrodes could be prepared using 200 mg of NCI-Zn, twice as much as before, and the model reaction was performed using each NCI-Zn cathode. The catalyst, which was prepared from a 5:1 (w/w) ratio of PVP and XC-72, and treated with HCl, showed the best performance (entry 5, 35% yield, 4.1 mol% Zn leaching).

Table 9. Examination of XC-72 as carbon black

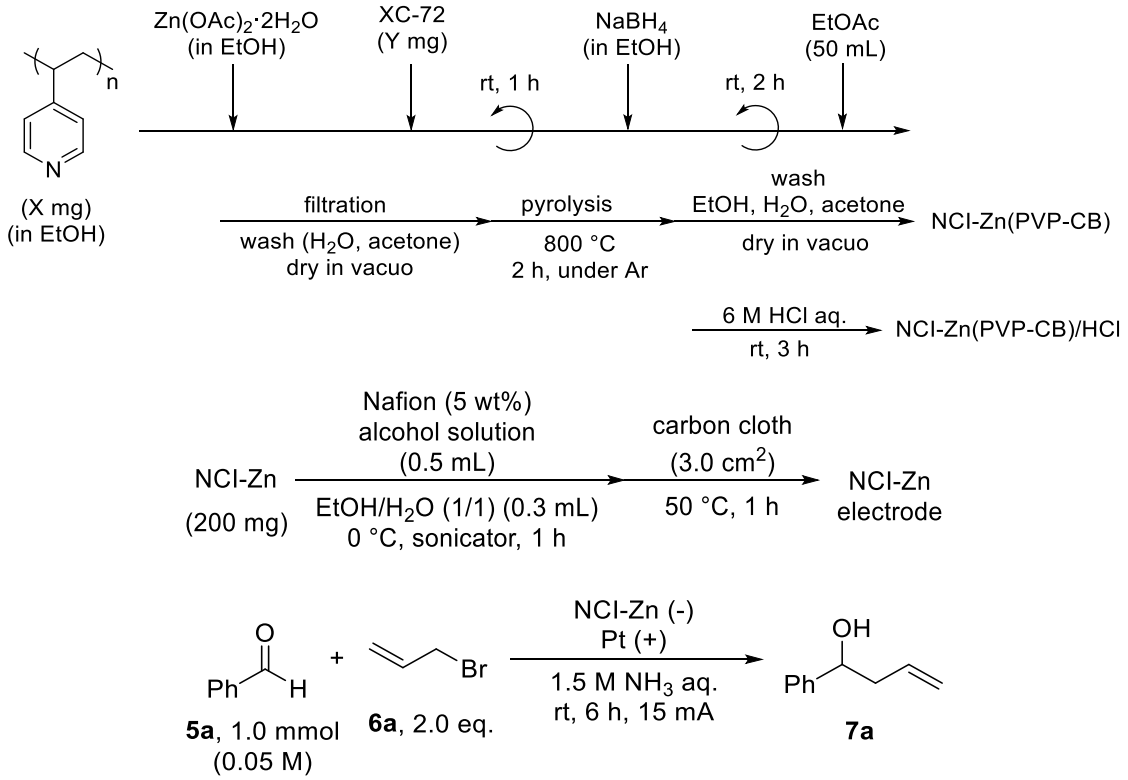

entry	NCI-Zn	Zn loading (mmol/g)	yield (%)[a]	Zn leaching (mol%)[b]
1	NCI-Zn(5-1)/HCl*	3.01	20	2.0
2	NCI-Zn(1-1)	0.874	15	2.3
3	NCI-Zn(1-1)/HCl	0.805	15	1.8
4	NCI-Zn(5-1)	3.39	40	8.0
5	NCI-Zn(5-1)/HCl	2.90	35	4.1

a: Isolated yield. b: Determined by ICP analysis. Based on the amount of **5a**.

*: Ketjen black was used as CB.

The electrolyte solution was optimized using the best catalyst were performed (Table 10). Initially, among electrolytes, a 0.3 M $LiClO_4$ aqueous solution gave the desired product **7a** with a less amount of zinc leaching (entry 4). Additionally, the use of THF as a cosolvent was found to be effective for improving the yield because it enhanced the solubility of the substrates (entry 6). The use of a buffer solution had almost no positive effects, which indicated that the formation of acid did not affect the reaction (entries 12,13). Finally, when the reaction was carried out in a 0.5 mmol scale for a longer reaction time (15 h) using the same cathode as before, in which the amount of zinc relative to the substrate **5a** was increased, **7a** was obtained in 77% yield with 7.2 mol% zinc leaching (entries 14,15).

Table 10. Optimizations of the solvent system

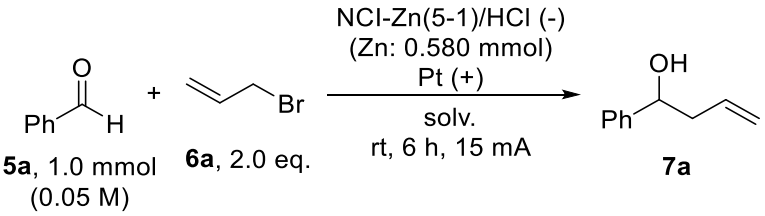

5a, 1.0 mmol (0.05 M) **6a**, 2.0 eq. **7a**

entry	solv.	yield (%)[a]	Zn leaching (mol%)[b]
1	1.5 M NH_3 aq.	35	4.1
2	0.1 M H_2SO_4 aq.	49	19.3
3	0.1 M $LiClO_4$ aq.	30	2.4
4	0.3 M $LiClO_4$ aq.	41	2.8
5	1.0 M $LiClO_4$ aq.	39	3.6
6	0.3 M $LiClO_4$ aq./THF (1:1)	49	3.0
7	0.3 M $LiClO_4$ aq./DMF (1:1)	32	3.3
8	0.3 M $LiClO_4$ aq./CH_3CN (1:1)	25	2.7
9	0.3 M Et_4NI aq./THF (1:1)	36	2.7
10	0.3 M $^nBu_4NBF_4$ aq./THF (1:1)	32	1.6
11	0.3 M $^nBu_4NPF_6$ aq./THF (1:1)	29	1.5
12	1 M ammonium buffer (pH 8.0)/THF (1:1)	29	4.1
13	1 M phosphate buffer (pH 5.9)/THF (1:1)	54	4.4
14[c]	0.3 M $LiClO_4$ aq./THF (1:1)	55	5.0
15[c,d]	0.3 M $LiClO_4$ aq./THF (1:1)	77	7.2

a: Isolated yield. b: Determined by ICP analysis. Based on the amount of **5a**. c: 0.5 mmol (0.05 M) scale. d: 15 h.

I then examined the effects of dopants added for NCI-Zn preparation to suppress zinc leaching (Table 11). A precursor for additional dopants (triphenylphosphine, phenyl sulfide, and phenanthroline) was incorporated before pyrolysis. Regardless of the kind of additives, almost the same loading of zinc was observed before acid treatment (entries 1,3,5). In addition, the loading of zinc after the acid treatment was also similar (entries 2,4,6). The loading of phosphorus in P-NCI-Zn was determined to be 0.84 mmol/g by ICP analysis (entry 1), which did not change after the acid treatment (entry 2).

Table 11. Preparation of NCI-Zn using source of additional dopants

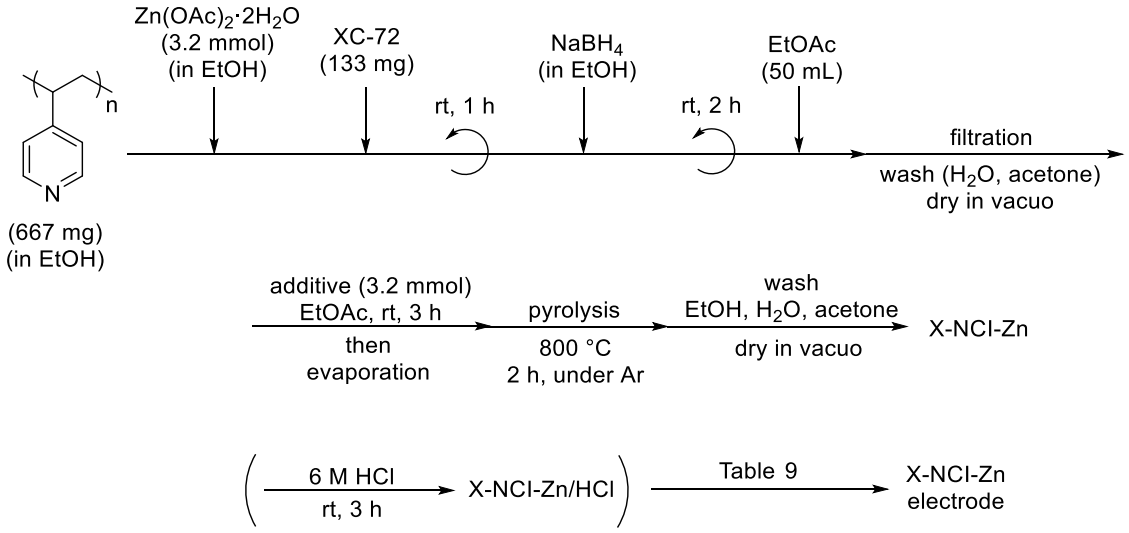

entry	additive	cat.	loading (mmol/g)[a]
1	PPh_3	P-NCI-Zn	Zn: 3.20, P: 0.84
2		P-NCI-Zn/HCl	Zn: 2.88, P:0.80
3	SPh_2	S-NCI-Zn	Zn: 3.33
4		S-NCI-Zn/HCl	Zn: 3.03
5	phenanthroline	N-NCI-Zn	Zn: 3.19
6		N-NCI-Zn/HCl	Zn: 2.97

a: Determined by ICP analysis.

NCI-Zn with additional dopants (X-NCI-Zn) was evaluated in the electrochemical allylation reaction (Table 12). Additional nitrogen dopants had positive effects on the suppression of zinc leaching (entries 6,7), while phosphorus and sulfur dopants decrease the reactivity (entries 2-5). This result indicated that additional nitrogen dopants enhanced interactions between zinc and nitrogen-doped carbon supports.

Table 12. Effects of additional dopants

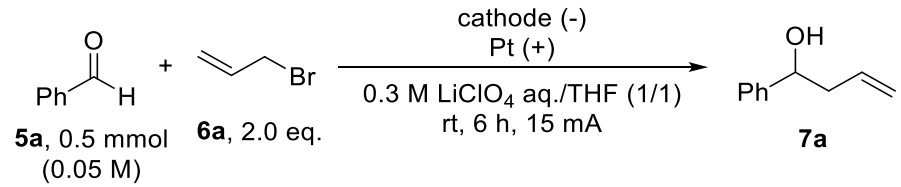

entry	cathode	Zn on cathode (mmol)	yield (%)[a]	Zn leaching (mol%)[b]
1	NCI-Zn(5-1)/HCl	0.580	55	5.0
2	P-NCI-Zn	0.640	39	3.9
3	P-NCI-Zn/HCl	0.576	29	2.9
4	S-NCI-Zn	0.666	29	1.5
5	S-NCI-Zn/HCl	0.606	21	0.6
6	N-NCI-Zn	0.638	49	4.4
7	N-NCI-Zn/HCl	0.594	47	2.4

a: Isolated yield. b: Determined by ICP analysis. Based on the amount of **5a**.

The effects of additional nitrogen dopants in N-NCI-Zn were focused. The timing of the addition of phenanthroline and its equivalent to zinc were investigated (Table 13). The addition of phenanthroline during the formation of zinc nanoparticles was not effective (entries 4,5), and the addition to polymer-encapsulated zinc species before pyrolysis was found to be the best procedure (entries 2,3). In addition, 3 eq. of phenanthroline to zinc increased the catalytic activity (entry 3, N-NCI-Zn/HCl **A2**).

Table 13. Detail examination of N-NCI-Zn

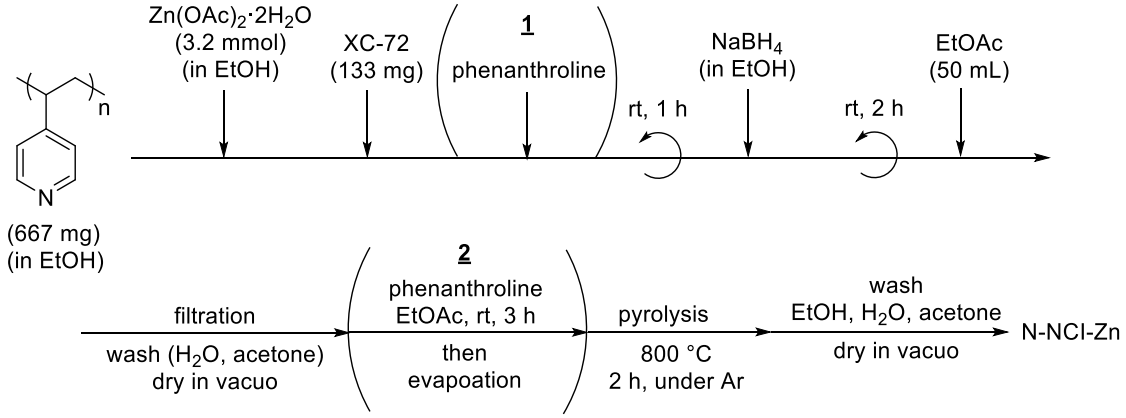

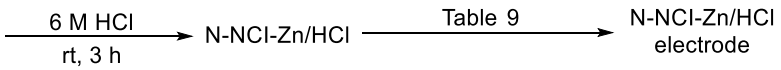

entry	timing of addition	eq. of phenanthroline (to Zn)	catalyst
1	-	-	NCI-Zn(5-1)/HCl
2	2	1	N-NCI-Zn/HCl **A1**
3	2	3	N-NCI-Zn/HCl **A2**
4	1	1	N-NCI-Zn/HCl **A3**
5	1	3	N-NCI-Zn/HCl **A4**

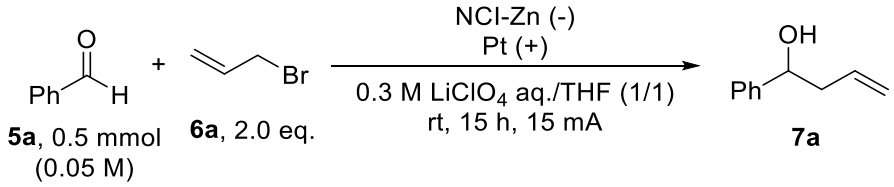

entry	cathode	Zn on cathode (mmol)	yield (%)[a]	Zn leaching (mol%)[b]
1	NCI-Zn(5-1)/HCl	0.580	77	7.2
2	N-NCI-Zn/HCl **A1**	0.594	68	5.4
3	N-NCI-Zn/HCl **A2**	0.572	80	6.6
4	N-NCI-Zn/HCl **A3**	0.560	72	5.0
5	N-NCI-Zn/HCl **A4**	0.548	66	5.3

a: Isolated yield. b: Determined by ICP analysis. Based on the amount of **5a**.

In parallel, I conducted the optimizations of reaction conditions with NCI-Zn(5-1)/HCl (Table 14). The prolonged reaction time improved the yield (entry 2), while higher current gave a lower yield (entry 3). The smaller reaction scale, in which the amount of zinc

relative to the substrate **5a** was increased, was most efficient to obtain a high yield, and the reaction in 0.3 mmol scale gave **7a** in 84% yield with 8.5 mol% zinc leaching (entries 4,5).

Table 14. Optimizations of reaction conditions

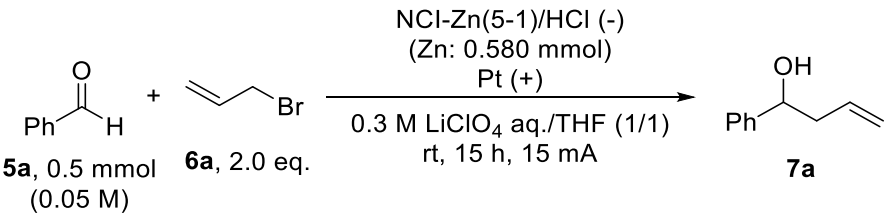

entry	derivation	yield (%)[a]	Zn leaching (mol%)[b]
1	-	77	7.2
2	24 h	80	7.2
3	30 mA	71	7.8
4	0.3 mmol scale	85	8.5
5	0.3 mmol scale, 24 h	84	9.2

a: Isolated yield. b: Determined by ICP analysis. Based on the amount of **5a**.

Finally, I checked the effects of the source of additional nitrogen dopants (Table 15). After examination of phenanthroline, bipyridine, or pyrazine, it was found that pyrazine was the best additional dopant, with the resulting catalyst (N-NCI-Zn/HCl **C1**) giving excellent yield with 7.3 mol% zinc leaching (entry 5). I determined that this N-NCI-Zn/HCl **C1** was the optimal catalyst, which was used for further investigations.

Table 15. Effects of nitrogen sources

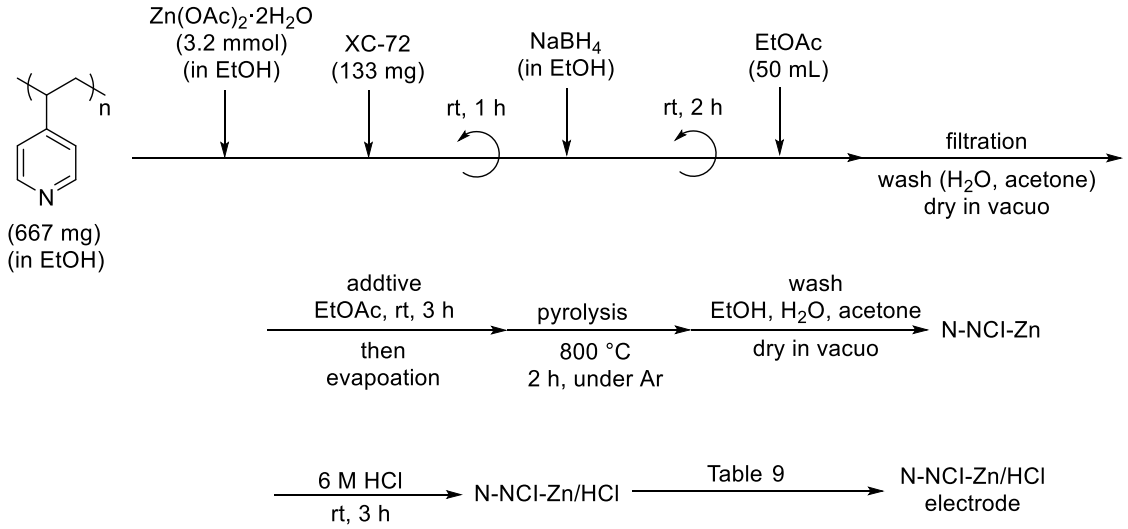

entry	additive	eq. of additive (to Zn)	catalyst
1	-	-	NCI-Zn(5-1)/HCl
2	phenanthroline	3	N-NCI-Zn/HCl **A2**
3	phenanthroline	10	N-NCI-Zn/HCl **A5**
4	bipyridine	3	N-NCI-Zn/HCl **B**
5	pyrazine	3	N-NCI-Zn/HCl **C1**
6	pyrazine	10	N-NCI-Zn/HCl **C2**

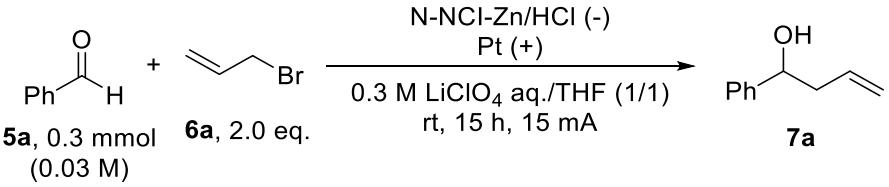

entry	cathode	Zn on cathode (mmol)	yield (%)[a]	Zn leaching (mol%)[b]
1	NCI-Zn(5-1)/HCl	0.580	85	8.5
2	N-NCI-Zn/HCl **A2**	0.572	89	8.3
3	N-NCI-Zn/HCl **A5**	0.576	84	8.4
4	N-NCI-Zn/HCl **B**	0.552	80	7.0
5	N-NCI-Zn/HCl **C1**	0.526	92	7.3
6	N-NCI-Zn/HCl **C2**	0.516	87	7.0

a: Isolated yield. b: Determined by ICP analysis. Based on the amount of **5a**.

STEM analysis and EDS mapping of N-NCI-Zn **C1** were performed before and after

treatment with HCl (Figure 4). The results suggested that acid washing removed the large, aggregated zinc species and that N-NCI-Zn/HCl **C1** had uniform distribution of zinc on the surface of the nitrogen-doped carbon support.

N-NCI-Zn **C1**

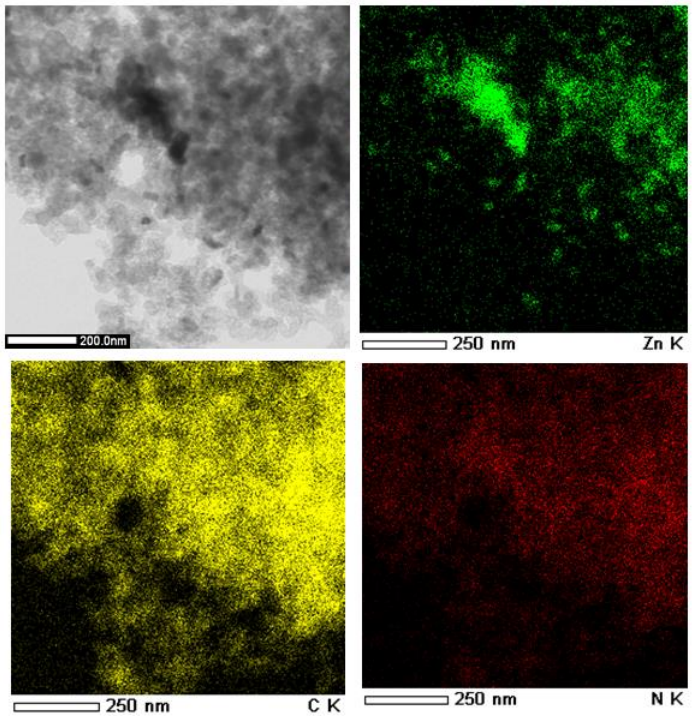

N-NCI-Zn/HCl **C1**

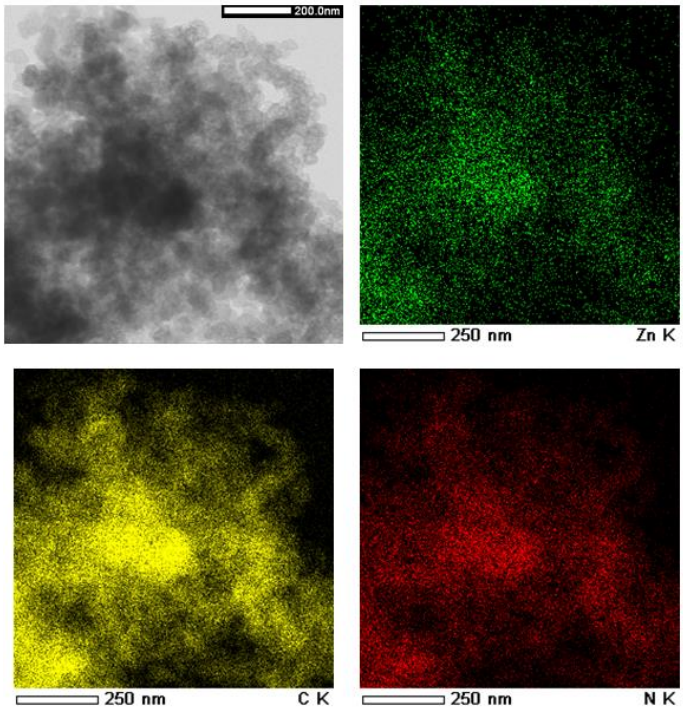

Figure 4. STEM analysis and EDS mapping

Three kinds of zinc catalysts, NCI-Zn(5-1), NCI-Zn(5-1)/HCl, and N-NCI-Zn/HCl **C1**, were characterized by XPS analysis (Figure 5). The spectra of Zn $2p_{3/2}$ revealed that both treatment with HCl and the addition of pyrazine contributed to lower binding energy of zinc, which means the higher ratio of Zn(0) species.

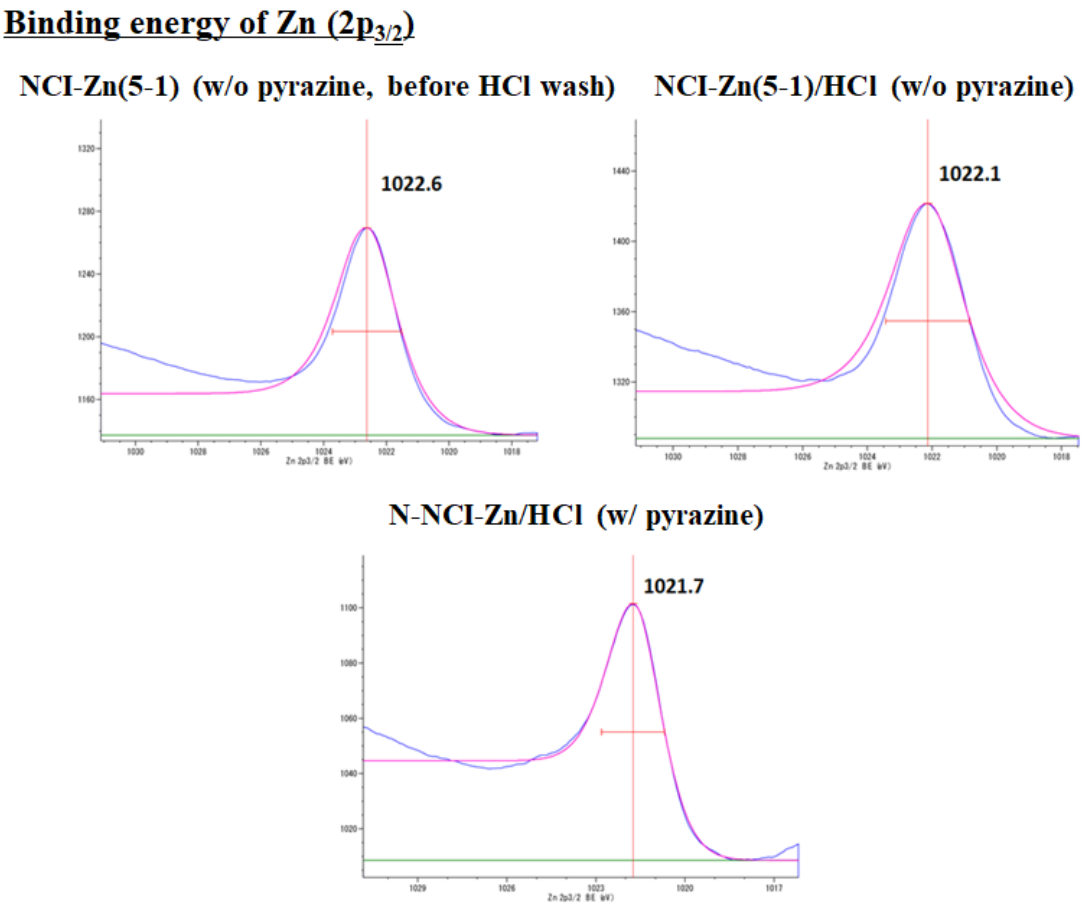

Figure 5. XPS analysis

3-3. Synthetic utilities and mechanistic studies

With the optimized reaction system in hand, I investigated the substrate scope for the electrochemical allylation of aldehydes (Scheme 31). Regardless of the electronic properties and positions of the substituents, the desired allyl alcohols **7a**-**e**, **7g**, **7h**, and **7j**-**l** were obtained from a series of aromatic aldehydes in high yields with less than 10 mol% Zn leaching. 4-Hydroxybenzaldehyde gave a complex crude reaction mixture in which the desired product **7f** was not detected. Almost no reaction occurred with 4-nitrobenzaldehyde (**7i**), probably because of the low solubility of this substrate. Reactions with aliphatic aldehydes and α,β-unsaturated aldehydes also gave the desired products **7m**-**q** in moderate to high yields with less than 10 mol% Zn leaching. A variety of heteroaromatic aldehydes, which were not investigated extensively in previous reports, were tolerated under the conditions. Pyridine, thiophene, furan, and quinoline derivatives were smoothly converted to the desired allyl alcohols **7r**-**v**, although only indole-3-carboxaldehyde did not give the desired product (**7w**). γ-substituted products **7x** and **7y** could be obtained in excellent yields with regioselectivities by replacing allyl bromide with crotyl bromide or cinnamyl bromide. Furthermore, both aromatic and aliphatic ketones were applicable to give the corresponding allyl alcohols **7z**, **7aa**, and **7ab** in high yields.

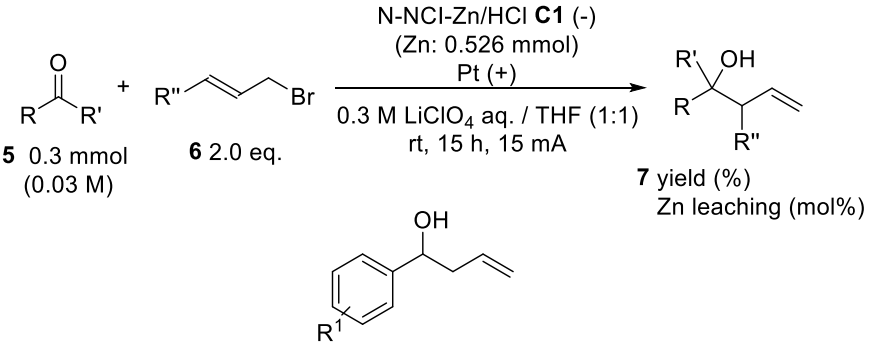

7a (R^1 = H): 92%, 7.3 mol%
7b (R^1 = 4-Cl): 82%, 7.3 mol%
7c (R^1 = 3,4-Cl): 75%, 6.7 mol%
7d (R^1 = 4-Me): 95%, 6.7 mol%
7e (R^1 = 4-OMe): 97%, 7.0 mol%
7f (R^1 = 4-OH): N.D.
7g (R^1 = 3-OMe): 93%, 7.7 mol%
7h (R^1 = 2-CF_3): 90%, 7.0 mol%
7i (R^1 = 4-NO_2): trace
7j (R^1 = 4-Ph): 88%, 5.0 mol%

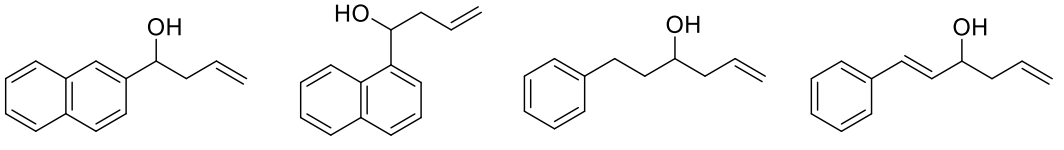

7k: 98%, 10.0 mol% **7l**: 91%, 8.3 mol% **7m**: 84%, 7.7 mol% **7n**: 67%, 4.0 mol%

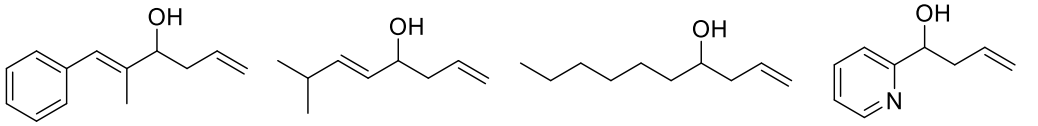

7o: 75%, 6.3 mol% **7p**: 88%, 7.0 mol% **7q**: 81%, 7.3 mol% **7r**: 70%, 7.3 mol%

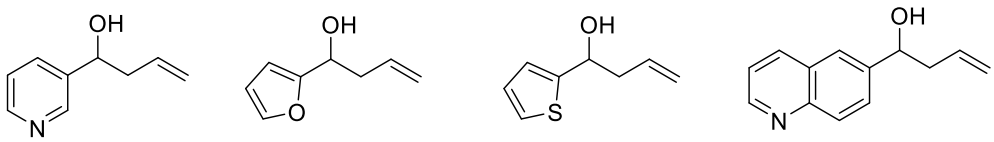

7s: 75%, 8.3 mol% **7t**: 92%, 8.7 mol% **7u**: 72%, 8.3 mol% **7v**: 90%, 9.7 mol%

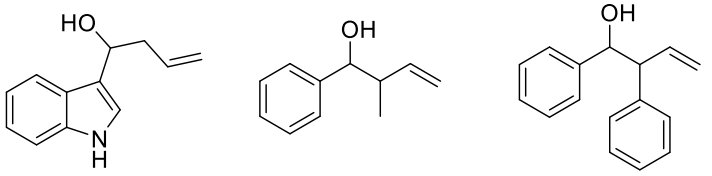

7w: N.D.
7x: 95%, 9.7 mol% (*syn*:*anti* = 58:42)
7y: 90%, 8.3 mol% (*syn*:*anti* = 17:83)

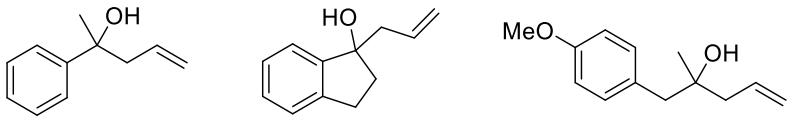

7z: 89%, 6.3 mol% **7aa**: 73%, 5.7 mol% **7ab**: 70%, 4.0 mol%

Scheme 31. Substrate scope

Recovery and reuse of N-NCI-Zn/HCl **C1** electrode were examined (Table 16). When the recovered electrode was washed with THF and water respectively in this order, the catalysts were physically removed from the cathode during the 3rd run of the reaction. In addition, drying of the recovered electrode after washing was not good. Therefore, the recovered electrode, which was washed with a mixture of water and THF after the reaction, was used in the next run without drying. The catalyst electrode maintained high activity until the 3rd run. Considering that the maximum amount of zinc on the cathode was about 0.5 mmol, N-NCI-Zn/HCl **C1** mediated the reaction in a catalytic way and the total TON through the reuse experiments was 1.6.

Table 16. Recovery and reuse experiments

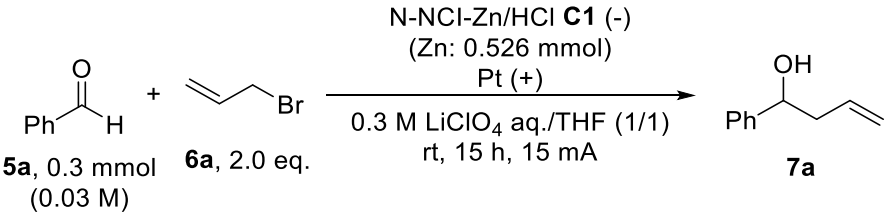

Recovery method	run	yield (%)[a]	Zn leaching (mol%)[b]
Washed with THF→H_2O then not dry	1	91	7.3
	2	92	8.3
	3	49	3.3
Washed with THF→H_2O then dry at 50 °C for 1 h	1	90	7.3
	2	57	4.7
Washed with THF/H_2O then not dry	1	91	7.3
	2	91	7.3
	3	84	7.7
	4	41	2.7

a: Isolated yield. b: Determined by ICP analysis. Based on the amount of **5a**.

The reactions using Zn cathode were also carried out for comparisons (Scheme 32). Substrates (**5a**, **5v**, **5ab**) gave lower yields and higher zinc leaching compared than in the reaction using N-NCI-Zn/HCl **C1** as a cathode. These results indicate that N-NCI-Zn/HCl **C1** exhibits unique activities thar differ from those of bulk zinc electrodes.

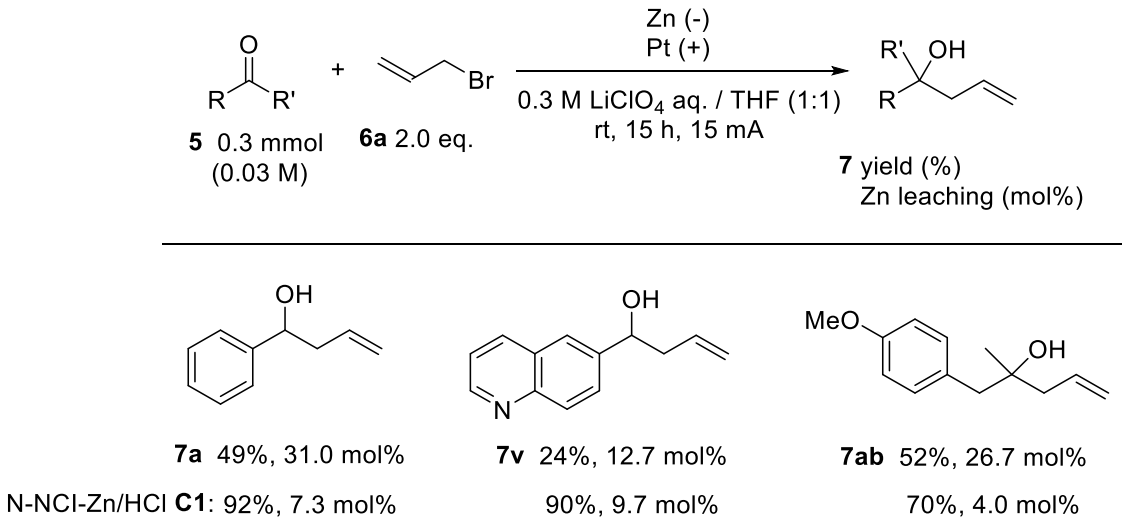

Scheme 32. Comparison with bulk Zn electrode

To get more insight, I conducted several control experiments (Table 17). In the reactions using graphite or carbon cloth on graphite, no desired products were detected (entries 2, 3). The cathode containing no nitrogen-dopants gave a low yield (entry 4), which suggested that nitrogen dopants had a crucial role in catalytic activities. I also confirmed that nitrogen-doped carbon itself did not catalyze the reaction (entry 5). When the catalyst was fixed on the cathode with a larger amount of Nafion^{TM} than the optimal conditions, the yield decreased probably because a large amount of Nafion^{TM} blocks active sites physically (entry 6). Finally, the reaction hardly proceeded without any current applied (entry 7), which implied that electricity contributed to the turnover of N-NCI-Zn/HCl **C1**.

Table 17. Control experiments

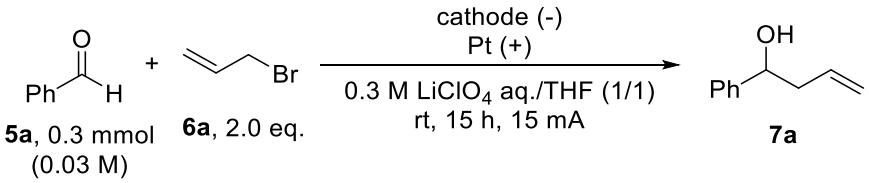

entry	cathode	yield (%)[a]	Zn leaching (mol%)[b]
1	N-NCI-Zn/HCl **C1**	92	7.3
2	graphite	N.D.	-
3	C cloth on graphite	N.D.	-
4	CB-Zn/HCl[c]	24	3.7
5	NDC[d]	N.D.	-
6[e]	N-NCI-Zn/HCl **C1**	56	4.7
7[f]	N-NCI-Zn/HCl **C1**	7	1.0

a: Isolated yield. b: Determined by ICP analysis. Based on the amount of **5a**. c: Prepared without PVP. d: prepared without zinc. e: the catalyst was fixed on the electrode using 20 wt % Nafion solution instead of 5 wt % Nafion solution. f: Without electricity.

I then conducted hot filtration tests to confirm whether the leached species could catalyze the reaction (Table 18). After the reaction was performed for several hours using N-NCI-Zn/HCl **C1** cathode, the cathode was changed to a graphite electrode. No further reaction took place after replacing the cathode during the reaction. Based on these results, zinc species leached out in the solution were not active species.

Table 18. Hot filtration tests

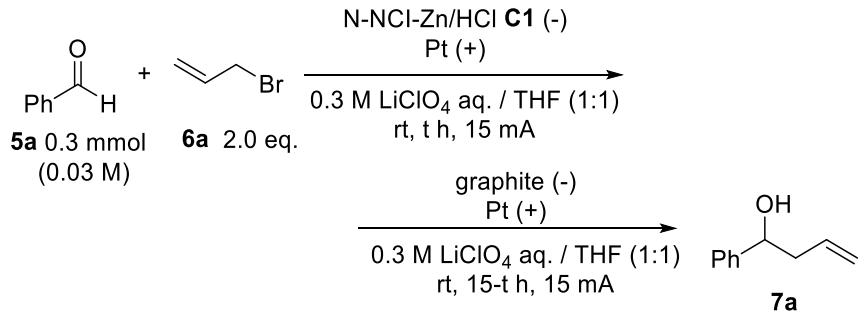

entry	t (h)	yield (%)[a] at T h	yield (%)[a] at 15 h
1[b]	15	-	92
2	3	41	40
3	6	67	70

a: Isolated yield. b: Replacement of the cathode was not conducted.

Cyclic voltammetry (CV) experiments were performed to monitor the progress of the reaction (Figure 6). When N-NCI-Zn/HCl **C1** cathode was used, CV curves showed reductive peaks of Zn(II) at 5 min or 3 h after the reaction starts, and no such peaks were observed at 15 h. These peaks did not appear when graphite was used as a cathode. This indicated that Zn(II) species were reduced to Zn(0) on the cathode until the reaction was complete.

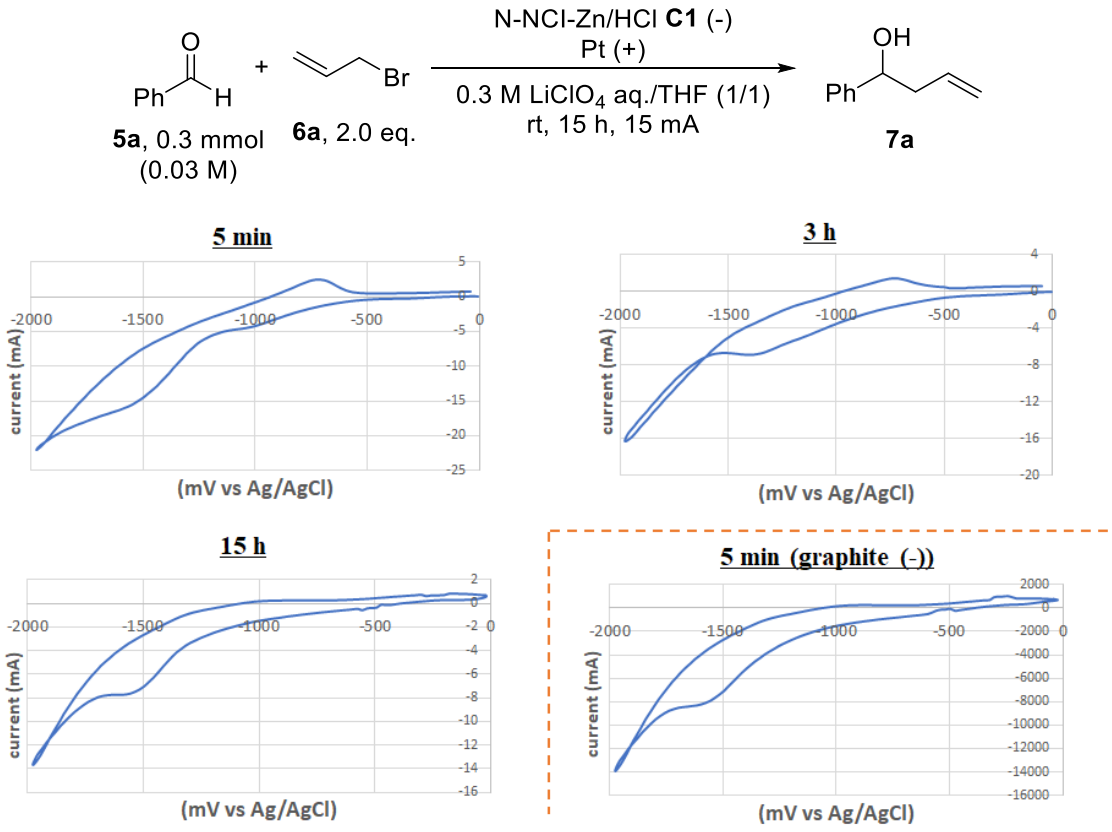

Figure 6. Cyclic voltammetry experiments

Finally, I attempted to apply this system to asymmetric reactions with chiral ligands (Table 19). When chiral diamine ligand **L1**, Bolm's ligand **L2**, and (1*R*,2*S*)-(-)-2-amino-1,2-diphenylethanol **L3** were utilized, in all cases, no enantioselectivities were observed although the allylation reaction proceeded (entries 1-3). Furthermore, no enantioselectivity was obtained by changing the reaction conditions, such as the electrolyte, the amounts of chiral ligands, and the ratio of solvents (entries 4-9). I thought that it was difficult that chiral ligands coordinate to zinc in the reaction system because the oxidative addition to allyl bromide was fast enough.

Table 19. Examination of asymmetric reaction using chiral ligands

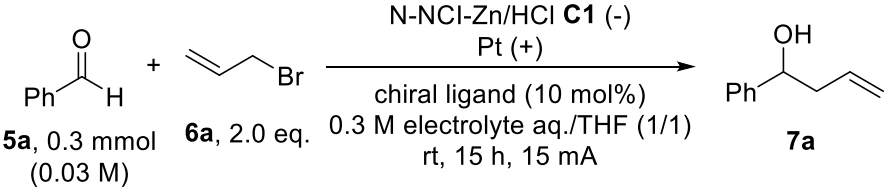

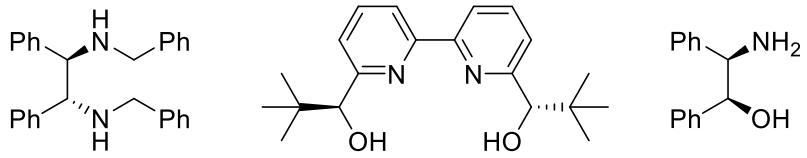

L1 L2 L3

entry	L	electrolyte	yield (%)[a]	ee (%)[b]	Zn leaching (mol%)[c]
1	**L1**	$LiClO_4$	82	0	7.4
2	**L2**	$LiClO_4$	56	0	5.0
3	**L3**	$LiClO_4$	85	0	8.1
4	**L1**	$TBAPF_6$	49	0	2.5
5	**L3**	$TBAPF_6$	44	0	3.1
6[d]	**L1**	$LiClO_4$	77	0	7.7
7[d]	**L3**	$LiClO_4$	72	0	7.2
8[d,e]	**L1**	$LiClO_4$	62	0	5.8
9[d,e]	**L3**	$LiClO_4$	60	0	5.4

a: Isolated yield. b: Determined by HPLC analysis. c: Determined by ICP analysis. Based on the amount of **5a**. d: Chiral ligand (100 mol%) was used. e: 0.3 M $LiClO_4$ aq./THF = 1/9.

I tried to modify N-NCl-Zn/HCl **C1** with chiral ligands in advance of the electrochemical reaction (Table 20). Unfortunately, N-NCl-Zn/HCl **C1** treated with **L1** or **L3** did not give any enantioselectivities (entries 1,2). Even when a stoichiometric amount of **L1** or **L3** was added in the electrochemical reaction, no enantioselectivities were observed (entries 3,4). Based on these results, it was likely that the desired chiral complexes could not be formed during the reaction.

Table 20. Examination of chiral ligand modified catalysts

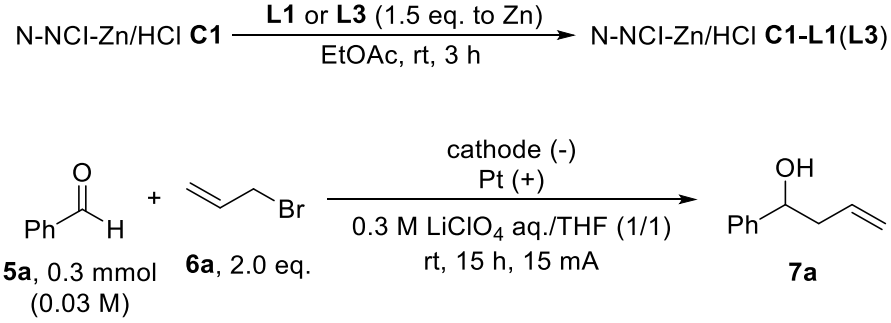

entry	cathode	yield (%)[a]	ee (%)[b]	Zn leaching (mol%)[c]
1	N-NCI-Zn/HCl **C1-L1**	87	0	7.0
2	N-NCI-Zn/HCl **C1-L3**	71	0	5.7
3[d]	N-NCI-Zn/HCl **C1-L1**	75	0	6.8
4[e]	N-NCI-Zn/HCl **C1-L3**	64	0	5.8

a: Isolated yield. b: Determined by HPLC analysis. c: Determined by ICP analysis. Based on the amount of **5a**. d: **L1** (100 mol%) was added. e: **L3** (100 mol%) was added.

In this chapter, I have developed an electrochemical system using nitrogen-doped carbon incarcerated zinc nanoparticle catalysts (N-NCI-Zn/HCl **C1**) for the allylation of carbonyls. This reaction system efficiently produced a range of homoallylic alcohols with low levels of zinc consumption. It was found that additional nitrogen dopants contributed to the suppression of zinc leaching. Hot filtration tests indicated that the reaction was mediated by zinc species on the surface of the cathode.

Chapter 4

本章については、5 年以内に雑誌等で刊行予定のため、非公開。

Chapter 5

本章については、5 年以内に雑誌等で刊行予定のため、非公開。

Chapter 6: Conclusion

Heterogeneous catalysts have great advantages over homogeneous catalysts due to their reusability, easy separation from products and reducing wastes significantly. Especially, continuous-flow reactions using heterogeneous catalysts can provide efficient synthetic methods of organic compounds with environmental compatibility, efficiency and safety.

Nitrogen-doped carbon (NDC) is an attractive support to stabilize metal nanoparticles or single-atoms by strong metal-nitrogen interactions. Despite the extensive investigations in electrocatalysts, the applications of nitrogen-doped carbon-supported heterogeneous catalysts to organic reactions are still less explored. Our laboratory has recently developed nitrogen-doped carbon incarcerated metal nanoparticle catalysts (NCI-M) prepared from poly(4-vinylpyridine) through a polymer-incarceration method, in which metal nanoparticles are encapsulated and stabilized by NDC layers. Although NCI-M catalysts have enabled several organic transformations, the development of more challenging organic reactions such as enantioselective reactions and C−C bond-forming reactions using nitrogen-doped carbon-supported heterogeneous catalysts are desired.

In Chapter 2, I developed nitrogen-doped carbon incarcerated rhodium nanoparticle catalyst (NCI-Rh) for the asymmetric insertion of carbenoids derived from diazoesters into amines (Scheme 33). By employing SPINOL-derived chiral phosphoric acid as cocatalysts, various types of α-amino acid derivatives were synthesized in high yields with high enantioselectivities (Scheme 34). In this catalyst system, nitrogen dopants played a crucial role in both activity and enantioselectivity. Furthermore, NCI-Rh was applied successfully to continuous-flow synthesis. Several control studies and analyses suggested the formation of intermediates derived from diazo compounds on the surface of NCI-Rh. This work presents a novel example of asymmetric reactions catalyzed by metal nanoparticles.

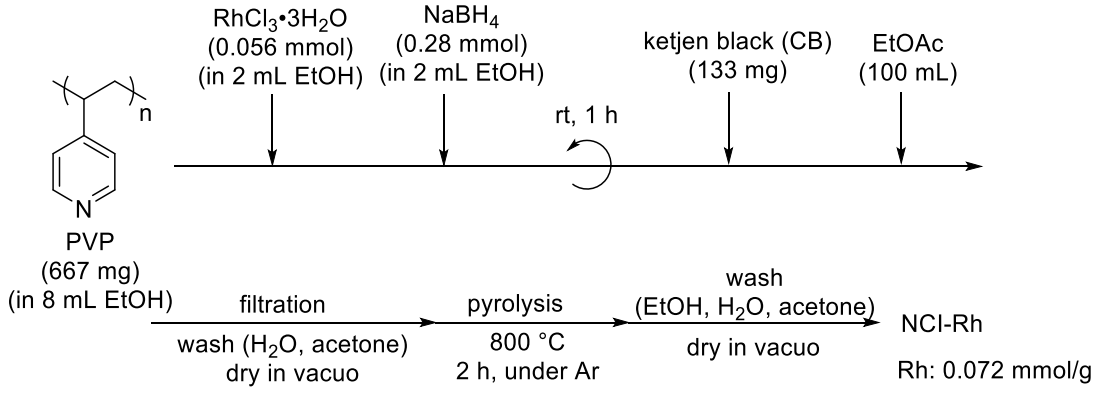

Scheme 33. Preparation of NCI-Rh

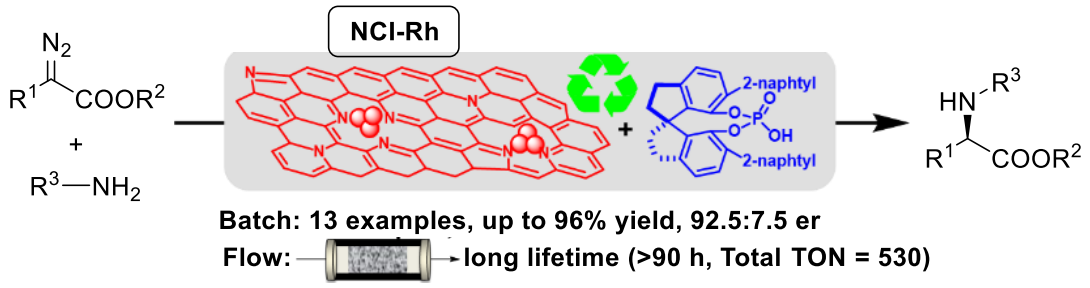

Scheme 34. NCI-Rh catalyzed asymmetric insertions of carbenoids into amines

Organometallic reagents hold a special place in organic synthesis because they have widespread synthetic applications based on carbon-carbon bond formation. Conventionally, stoichiometric amounts of organometallic reagents are required in such transformations and large amounts of metallic wastes are generated, which hindered applications to continuous-flow synthesis. To develop the catalytic carbon-carbon bond-forming reactions without metallic waste, I envisioned an electrochemical approach in which catalytic amounts of metals supported on the nitrogen-doped carbon-based cathode form organometallic reagents and the subsequent electroreduction after the reaction regenerates metal(0) on the cathode (Scheme 35).

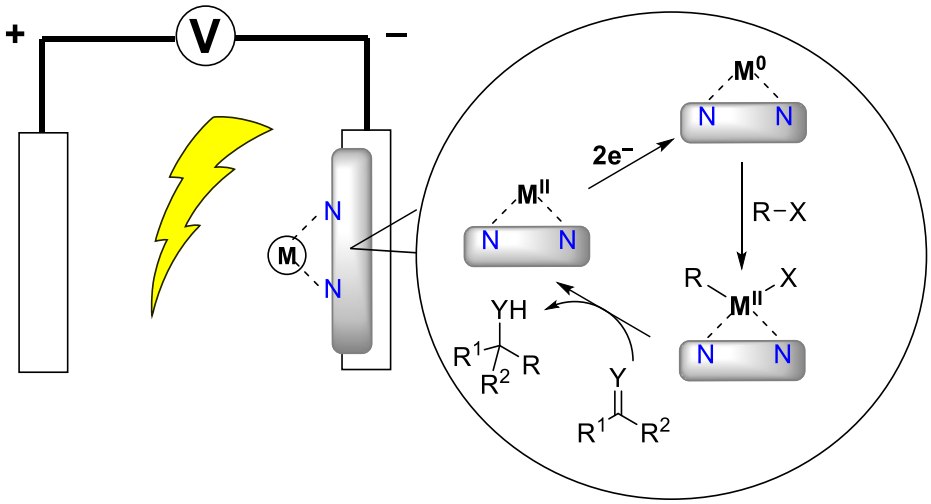

Scheme 35. Electrochemical approach with heterogeneous catalyst electrode

In Chapter 3, I developed an electrochemical system using nitrogen-doped carbon-incarcerated zinc nanoparticles (N-NCI-Zn/HCl **C1**) as a cathode for the allylation of carbonyls (Scheme 36). This reaction system efficiently produced a range of homoallylic alcohols with low levels of zinc consumption (Scheme 37). It was found that additional nitrogen dopants contributed to the suppression of zinc leaching. Hot filtration tests indicated that the reaction was mediated by zinc species on the surface of the cathode. Considering these phenomena and the good performance of the system with

heteroaromatic substrates, nitrogen-doped carbon-stabilized zinc nanoparticle species showed unique activities that differ from those of bulk zinc electrodes.

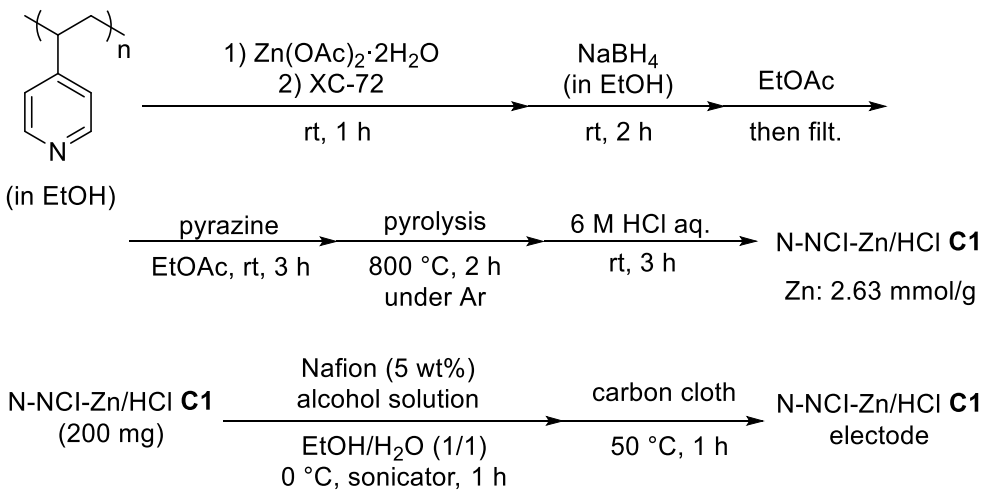

Scheme 36. Preparation of N-NCI-Zn/HCl C1 and its electrode

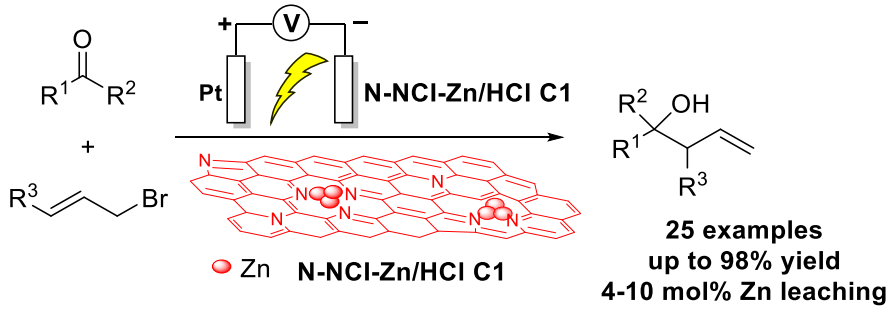

Scheme 37. Electrochemical allylation of carbonyl compounds using N-NCI-Zn/HCl C1 cathode

Through my doctoral course studies, I have demonstrated the applicability of nitrogen-doped carbon-supported heterogenous catalysts toward challenging organic transformations. The asymmetric insertion reaction catalyzed by NCI-Rh is the first example of asymmetric reactions using nitrogen-doped carbon supported heterogeneous catalysts, and N-NCI-Zn/HCl and Zn-N-C/HCl electrodes catalyzed electrochemical allylation reactions have opened the door to a novel strategy for catalytic carbon−carbon bond-forming reactions without metallic waste. This work certainly has broadened the world of nitrogen-doped carbon-supported heterogeneous catalysts and will trigger their further application to fine chemical synthesis. I believe that the achievement of electrochemical organic transformations using heterogenous catalysts as electrodes opens a new possibility for heterogenous catalysis and continuous-flow reactions.

Chapter 7: Experimental section

General information

- JEOL JNM-ECX600, ECA500 or ECZ500 spectrometers were used for NMR measurement. Chloroform ($\delta = 7.24$) was used as an internal standard for ^{1}H NMR and $CDCl_3$ ($\delta = 77.0$) for ^{13}C NMR. Structures of known compounds were confirmed by comparison with data shown in literature.
- FTIR analysis was conducted with a Shimadzu IRSpirit-T.
- Preparative thin-layer chromatography was carried out using Wakogel B-5F.
- ICP analysis was performed on Shimadu ICPS-7510 equipment. The sample was prepared by heating with THERMO BLOCK ND-M11.
- HPLC analysis was performed on Shimadu LC-20AB, SPD-20A, and DGU-$20A_3$.
- Daicel Chiralpak column were used for HPLC analysis.
- The absolute configuration of reported compounds was determined by comparison to literature and that of other products was assumed by analogy.
- DART mass spectra were recorded on JEOL JMS-T100TD mass spectrometer.
- STEM/EDS images were obtained using a JEOL JEM-2100F instrument operated at 200 kV. All STEM specimens were prepared by placing a drop of the solution on carbon-coated copper grids and allowed to dry in air (without staining).
- XPS analysis was performed on JPS-9010MC with a Mg Kα X-ray source and the C 1s line at 284.2 eV was used as reference to correct the binding energy.
- Pyrolysis was conducted with an ARF-40K ceramic tube furnace and the temperature was controlled with a YKC-11 instrument.
- Cyclic voltammetry experiments were conducted with ElectraSyn 2.0 from IKA with Ag/AgCl as a reference electrode.
- Nitrogen absorption/desorption isotherm was recorded on a BELSORP-mini Microtrac Bell.
- XRD analysis was performed on MiniFlex 600 from Rigaku.
- $RhCl_3 \bullet 3H_2O$ was purchased from Wako Pure Chemical Company.
- 4-Vinylpyridine (stabilized with HQ) was purchased from Tokyo Chemical Industry Co., Ltd. And was treated through alumina, activated before use.
- $NaBH_4$ was purchased from Wako Pure Chemical Company and recrystallized from diglyme by heating according to the literature and store in a glove box.
- Ketjen black EC300J was purchased from Lion Corporation.
- $Zn(OAc)_2 \bullet 2H_2O$ was purchased from Wako Pure Chemical Company.
- Nafion^{TM} perfluorinated resin solution (5 wt.%) in mixture of lower aliphatic alcohols and water (contains 45% water) was purchased from Sigma-Aldrich Co. LLC and used without further purification.

- $Zn(NO_3)•6H_2O$ was purchased from Sigma-Aldrich Co. LLC and used without further purification.
- 2-Methylimidazole was purchased from Sigma-Aldrich Co. LLC and used without further purification.
- Benzylamine was purchased from Tokyo Chemical Industry Co., Ltd. and used without further purification.
- $NiCl_2•6H_2O$ was purchased from Wako Pure Chemical Company.
- Ag(OAc) was purchased from Wako Pure Chemical Company.
- Deionized water from a MILLIPORE MilliQ machine (Gradient A 10) was used as solvent without further treatment.
- Methanol was distilled over Mg and dried over MS3A.
- Ethanol was distilled over Na and dried over MS3A.
- Other solvents were purchased in dried grade from Wako Pure Chemical Company and used without further purification.
- Asymmetric N-H insertion reactions were conducted with Carousel^{TM}.
- Diazoesters **1** were prepared by following the literature.[139]
- $BocNH_2$ and $FmocNH_2$ were prepared by following the literature[140,141] and other amines for asymmetric N-H insertion reactions were purchased from Tokyo Chemical Industry Co., Ltd and used without further purification.
- TRIP and SCPA were prepared by following the literature.[142-144]
- For asymmetric N-H insertion reactions under flow system,
  Pump : Minato Concept, Inc. MCRP204
  Column : 10Φ x 10 cm from Tokyo Rikakikai Co. Ltd.
  Aluminium heating block and its controller: Custom-made by Tokyo Rika Kikai Co. Ltd (EYELA)
- Electrochemical allylation reactions at 1 mmol scale were conducted in a 50 mL-three-necked flask with power supply (AD-8724D from P4LT18-0.1 from Matsusada Precision).
- Electrochemical allylation reactions at less than 0.5 mmol scale were conducted with ElectraSyn 2.0 from IKA.
- Pt and graphite electrode were purchased from IKA.
- Carbon cloth (EC-CC1-060T) was purchased from TOYO Corporation.
- Carbon Double-Sided Tape was purchased from NISSHIN EM Co., Ltd.
- Allyl bromide **6a** was purchased from Sigma-Aldrich Co. LLC and used without further purification.
- Carbonyl compounds **5** for electrochemical allylation reactions were purchased from Tokyo Chemical Industry Co., Ltd and used without further purification.
- Electrolytes were purchased from Tokyo Chemical Industry Co., Ltd and used without further purification.

Development of Nitrogen-Doped Carbon Incarcerated Rhodium Nanoparticle Catalysts for Asymmetric Insertion Reactions

Preparation of poly(4-vinylpyridine)[23]

To a solution of 4-vinylpyridine (83.9 g, 0.80 mol) in chloroform (150 mL), V-70 (2.41 g, 7.8 mmol) was added at room temperature, and the mixture was stirred until fully dissolved. The solution was degassed with sonication under Ar atmosphere and stirred for 48 h at room temperature. The mixture was added slowly to ethyl acetate/diethyl ether (1 L, 1/4) to generate precipitation, and the suspension was decanted. The precipitation was washed with diethyl ether (200 mL) three times. The polymer was dried in vacuo after grinding to afford poly(4-vinylpyridine) (72.3 g, 86.2% yield).

Preparation of NCI-Rh

To a stirring solution of poly(4-vinylpyridine) (667 mg) in ethanol (8 mL), a solution of $RhCl_3 \bullet 3H_2O$ (14.7 mg, 0.056 mmol) in ethanol (2 mL) was added dropwise at room temperature under air. To this solution, $NaBH_4$ (10.6 mg, 0.28 mmol) in ethanol (2 mL) was added dropwise, and the mixture was stirred for 1 h at room temperature under air. To this mixture was added ketjen black (133 mg), followed by addition of ethyl acetate (100 mL) at room temperature dropwise, and stirred for 30 min. The catalyst was filtered and the collected catalysts was stirred in water (50 mL) for 10 min at room temperature. The catalyst was filtered, and the collected catalyst was stirred in acetone (50 mL) for 10 min at room temperature, followed by filtration and drying in vacuo. The catalyst was pyrolyzed at 800 °C for 2 h under Ar atmosphere. After cooling to room temperature, the catalyst was washed in ethanol (50 mL) with stirring. The catalyst was filtered, washed with ethanol, water and acetone, and dried in vacuo to afford NCI-Rh (601.3 mg). NCI-Rh (~10 mg) was heated in sulfuric acid (1.0 mL) at 200 °C, and some drops of nitric acid was added. After evaporating all nitric acid, the mixture was cooled to room temperature and diluted to 50 mL aqueous solution. The loading of Rh was determined to be 0.072 mmol/g by ICP analysis.

General procedure for asymmetric N-H insertion reactions

To a suspension of amine **2** (0.3 mmol), NCI-Rh (Rh: 1 mol%) and SCPA (1 mol%) in DCM (2.0 mL), a solution of diazoester **1** (0.3 mmol) in DCM (1.0 mL) was added at room temperature. The mixture was stirred for 16 h at 45 °C and filtered after cooling to room temperature. The filtrate was concentrated and the residue was purified by preparative thin-layer chromatography to afford **3**. The enantiomeric excess of **3** was determined by HPLC analysis.

Recovery and reuse of NCI-Rh

After the reaction, the resulting suspension was transferred to centrifugation tube. By

centrifugation (3500 rpm, 10 min), NCI-Rh was washed with DCM three times. The residue was used in the next run directly without drying completely. Almost no change in the Rh loading of the recovered catalyst after eight runs was confirmed by ICP analysis (before use: 0.072 mmol/g, after 8th run: 0.074 mmol/g).

Flow system and reactivation of NCI-Rh

A column (Φ10x100 mm) was packed with NCI-Rh (1.50 g) and cotton was put at each end. A DCM solution of methyl phenyldiazoacetate **1a** (0.05 M), *p*-anisidine **2a** (0.05 M) and SCPA (1 mol%) was flowed into the column, which was heated at 45 °C, using peristaltic pump at a rate of 0.10-0.11 mL/min without pre-wetting the catalyst. The column was set vertically and the flow reactions were performed with upward flow. One fraction was collected for several hours or overnight, and the solvent was evaporated. The residue was purified by preparative thin-layer chromatography and the ee was determined by HPLC analysis.

NCI-Rh recovered after the above flow reaction was treated at 800 °C for 2 h under Ar. Using the reactivated NCI-Rh (1.38 g), the second run of flow reaction was performed. One fraction was collected for several hours or overnight, and the solvent was evaporated. The residue was purified by preparative thin-layer chromatography and the ee was determined by HPLC analysis.

Recovery of SCPA under flow system

Under the flow system, the column (Φ10x50 mm) packed with a basic resin (AMBERLITE IRA900) was connected after the column packed with NCI-Rh. After the first run, DCM (100 mL) was flowed to wash the inside of columns. The basic resin which was taken out from the column was stirred in toluene (30 mL) in the presence of 1 M HCl aqueous solution (30 mL) at ambient temperature for 1 h. The resin was removed by filtration and the aqueous phase was extracted with toluene twice. The combined organic extracts were dried over sodium sulfate and concentrated. The residue was purified by column chromatography to afford pure SCPA (48% recovery) The recovered SCPA was successfully reused for the asymmetric insertion reaction to afford **3a** (91% yield, 82% ee).

Deprotection of PMP group of 3a and enhancement of the ee[146]

To a solution of **3a** (542.5 mg, 2.0 mmol) in MeCN (15 mL), a H_2O (4.5 mL) solution of cerium ammonium nitrate (CAN, 2.19 g, 4.0 mmol) was added at 0 °C. After stirring at 0 °C for 2 h, the resulting solution was treated with 2 M HCl to pH = 1. The aqueous phase was washed with ethyl acetate and brought to basic by $NaHCO_3$ aqueous solution. The resulting suspension was extracted with DCM. The combined organic extracts were dried over Na_2SO_4 and concentrated to afford free amine product **4a** (271.3 mg, 82% yield). **4a** was treated with HCl to form HCl salts and recrystallized from EtOH. The ee

was determined by HPLC analysis after derivatization with Ac_2O in DCM.

Hot filtration test

To a suspension of amine **2a** (0.3 mmol), NCI-Rh (Rh: 1 mol%) and SCPA (1 mol%) in DCM (2.0 mL), a solution of diazoester **1a** (0.3 mmol) in DCM (1.0 mL) was added at room temperature. After stirring at 45 °C for 3 h or 6 h, NCI-Rh was removed by filtration with keeping temperature, then filtrate was further stirred at 45 °C for 13 h or 10 h, respectively. At each point, yield was determined by ^1H NMR analysis, and ee was determined by HPLC analysis.

Stoichiometric reactions under flow conditions

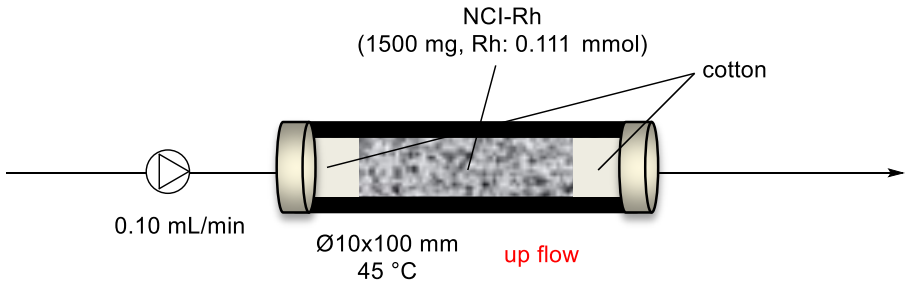

A column (Φ10x100 mm) was packed with NCI-Rh (1.50 g) and cotton was put at each end. After flowing 20 mL of DCM, a DCM solution of methyl phenyldiazoacetate **1a** (0.33 mmol, 0.1 M)) was flowed into the column, which was heated at 45 °C, using peristaltic pump at a rate of 0.10 mL/min. After washing by flowing 40 mL of DCM, a DCM solution of *p*-anisidine **2a** (0.12mmol, 0.1 M) and SCPA (1 mol%) was flowed followed by flowing additional 20 mL of DCM. Final 25 mL resulting solution was concentrated and purified by preparative thin-layer chromatography to afford **3a** and the ee was determined by HPLC analysis (28% yield to Rh, 83% ee).

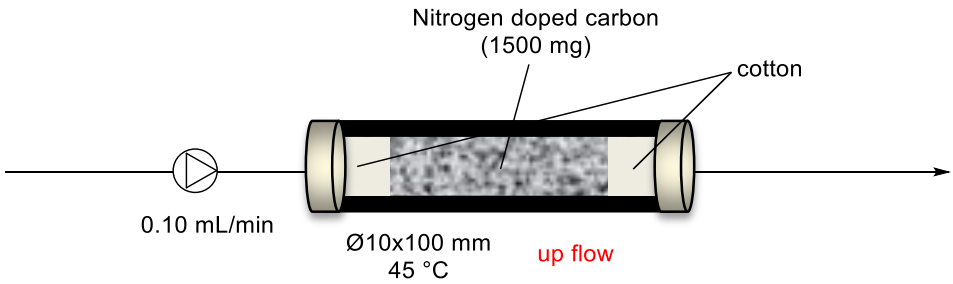

A column (Φ10x100 mm) was packed with nitrogen-doped carbon (1.50 g) and cotton was put at each end. After flowing 20 mL of DCM, a DCM solution of methyl

phenyldiazoacetate **1a** (0.33 mmol, 0.1 M)) was flowed into the column, which was heated at 45 °C, using peristaltic pump at a rate of 0.10 mL/min. The resulting solution after flowing additional 20 mL of DCM was concentrated to afford **1a** (57.9 mg, 0.33 mmol). The fact that **1a** was fully recovered indicated no adsorption and reaction of **1a** occurred on the nitrogen-doped carbon.

Characterization date of products

(4-Methoxyphenylamino)phenylacetic acid methyl ester (3a)[146]

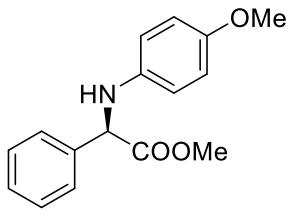

Yellow liquid. ^{1}H NMR ($CDCl_3$, 500 MHz) δ = 3.69 (s, 3H), 3.70 (s, 3H), 4.65 (br, 1H), 5.00 (s, 1H), 6.50-6.53 (m, 2H), 6.70-6.71 (m, 2H), 7.28-7.30 (m, 1H), 7.32-7.35 (m, 2H), 7.46-7.50 (m, 2H) ppm. ^{13}C NMR ($CDCl_3$, 125 MHz) δ = 52.7, 55.7, 61.7, 114.7, 114.8, 127.2, 128.2, 128.8, 137.8, 140.2, 152.5, 172.5 ppm. HPLC (OJ-H, eluate: hexane / *i*-PrOH = 7 / 3, detector: 254 nm, flow rate: 1.0 mL / min), (*R*) t_1 = 8.3 min, (*S*) t_2 = 11.3 min. $[\alpha]^{20}_D$ = -82.4 (c = 1.09, $CHCl_3$).

(2-Methoxyphenylamino)phenylacetic acid methyl ester (3b)

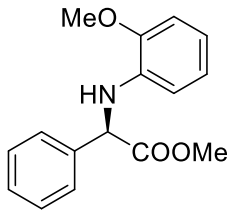

Yellow liquid. ^{1}H NMR ($CDCl_3$, 600 MHz) δ = 3.72 (s, 3H), 3.87 (s, 3H), 5.07 (s, 1H), 5.46 (br, 1H), 6.33-6.34 (m, 1H), 6.64-6.67 (m, 1H), 6.70-6.76 (m, 1H), 6.77-6.78 (m, 1H),7.28-7.30 (m, 1H), 7.33-7.35 (m, 2H), 7.49 (d, 2H, *J* = 3.8 Hz) ppm. ^{13}C NMR ($CDCl_3$, 150 MHz) δ = 52.7, 55.4, 60.7, 109.5, 110.6, 117.4, 121.0, 127.2, 128.2, 128.8, 135.9, 137.7, 147.0, 172.3 ppm. HPLC (OJ-H, eluate: hexane / *i*-PrOH = 7 / 1, detector: 254 nm, flow rate: 0.8 mL / min), (*R*) t_1 = 36.3 min, (*S*) t_2 = 40.8 min. IR (neat) 3417, 1739, 1514, 1266, 1171, 1037, 820, 637 cm^{-1}. HRMS (DART) calculated for $C_{16}H_{18}NO_3^+$ [*M*+H^+] 272.12867, found 272.12822. $[\alpha]^{20}_D$ = -88.5 (c = 1.22, $CHCl_3$).

Methyl 2-(*tert*-butoxycarbonylamino)-2-phenylacetate (3c)[147]

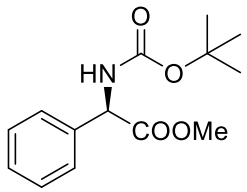

transparent liquid. ^{1}H NMR ($CDCl_3$, 500 MHz) δ = 1.41 (s, 9H), 3.70 (s, 3H), 5.31 (s, 1H), 5.52 (br, 1H), 7.31-7.34 (m, 5H) ppm. ^{13}C NMR ($CDCl_3$, 125 MHz) δ = 28.3, 52.7, 57.6, 80.2, 127.1, 128.4, 128.9, 136.9, 154.8, 171.6 ppm. HPLC (OD-H, eluate: hexane / *i*-PrOH = 9 / 1, detector: 254 nm, flow rate: 0.5 mL / min), (*S*) t_1 = 19.3 min, (*R*) t_2 = 21.2 min.

Methyl 2-((((9H-fluoren-9-yl)methoxy)carbonyl)amino)-2-phenylacetate (3d)[148]

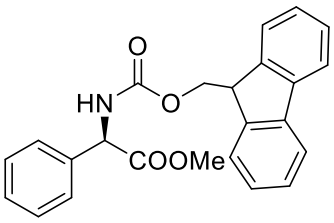

transparent liquid. ^{1}H NMR ($CDCl_3$, 600 MHz) δ =3.71 (s, 3H), 3.72 (d, 2H, *J* = 3.4 Hz), 3.99 (t, 1H, *J* = 6.9 Hz), 5.28 (s, 1H), 7.28-7.38 (m, 4H), 7.45-7.51 (m, 5H), 7.66 (d, 2H, *J* = 4.5 Hz), 7.84 (d, 2H, *J* = 4.6 Hz) ppm. ^{13}C NMR ($CDCl_3$, 150 MHz) δ = 41.1, 46.8, 49.3, 52.0, 120.0, 124.9, 127.0, 127.1, 128.0, 128.5, 129.2, 133.9, 141.1, 143.3, 144.0, 172.0 ppm. HPLC (OJ-H, eluate: hexane / *i*-PrOH = 8 / 2, detector: 254 nm, flow rate: 1.0 mL / min), (*R*) t_1 = 14.4 min, (*S*) t_2 = 20.9 min.

Methyl 2-(((benzyloxy)carbonyl)amino)-2-phenylacetate (3e)[147]

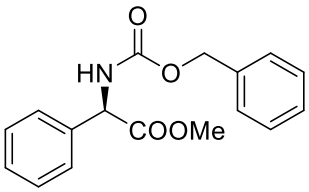

transparent liquid. ^{1}H NMR ($CDCl_3$, 600 MHz) δ =3.70 (s, 3H), 5.05-5.12 (m, 2H), 5.37 (s, 1H), 5.84 (br, 1H), 7.31-7.35 (m, 10H) ppm. ^{13}C NMR ($CDCl_3$, 150 MHz) δ = 52.8, 57.9, 67.1, 127.1, 128.1, 128.2, 128.5, 128.6, 128.9, 136.1, 136.5, 155.3, 171.3 ppm. HPLC (OJ-H, eluate: hexane / *i*-PrOH = 9 / 1, detector: 254 nm, flow rate: 1.0 mL / min), (*R*) t_1 = 17.9 min, (*S*) t_2 = 20.6 min.

(4-Methoxyphenylamino)phenylacetic acid ethyl ester (3f)[146]

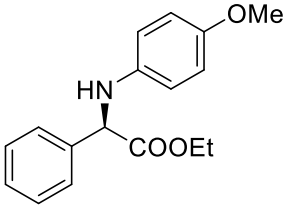

Yellow liquid. ^{1}H NMR ($CDCl_3$, 500 MHz) δ = 1.19 (t, 3H, *J* = 7.1 Hz), 3.69 (s, 3H), 4.08-4.24 (m, 2H), 4.99 (s, 1H), 6.53 (d, 2H, *J* = 4.3 Hz), 6.70 (d, 2H, *J* = 4.3 Hz), 7.27-7.29 (m, 1H), 7.32-7.35 (m. 2H), 7.46-7.48 (m, 2H) ppm. ^{13}C NMR ($CDCl_3$, 125 MHz) δ = 14.1, 55.7, 61.7, 61.7, 114.8, 127.2, 128.2, 128.8, 137.8, 140.1, 152.5, 168.6, 172.1 ppm. HPLC (OJ-H, eluate: hexane / *i*-PrOH = 8 / 2, detector: 254 nm, flow rate: 1.0 mL / min), (*R*) t_1 = 12.4 min, (*S*) t_2 = 17.4 min.

(4-Methoxyphenylamino)phenylacetic acid isopropyl ester (3g)[146]

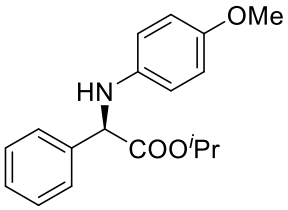

Yellow liquid. ^{1}H NMR ($CDCl_3$, 600 MHz) δ = 1.05 (d, 3H, *J* = 3.1 Hz), 1.23 (d, 3H, *J* = 3.1 Hz), 3.69 (s, 3H), 4.97 (s, 1H), 4.98-5.01 (m, 1H), 6.69-6.70 (m, 4H), 7.27-7.32 (m, 3H), 7.44-7.45 (m, 2H) ppm. ^{13}C NMR ($CDCl_3$, 150 MHz) δ = 21.7, 21.7, 41.7, 55.7, 68.1, 114.8, 116.4, 126.9, 128.5, 129.1, 134.3, 139.7, 152.8, 171.1 ppm. HPLC (OJ-H, eluate: hexane / *i*-PrOH = 8 / 2, detector: 254 nm, flow rate: 1.0 mL / min), (*R*) t_1 = 10.4 min, (*S*) t_2 = 12.2 min.

Methyl 2-((4-methoxyphenyl)amino)-2-(*p*-tolyl)acetate (3h)[146]

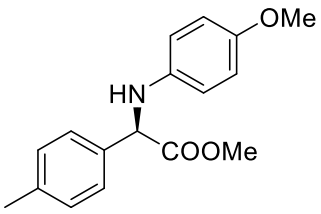

Yellow liquid. ^{1}H NMR ($CDCl_3$, 600 MHz) δ = 2.32 (s, 3H), 3.69 (s, 3H), 3.70 (s, 3H), 4.62 (br, 1H), 4.97 (s, 1H), 6.51 (d, 2H, *J* = 4.4 Hz), 6.70 (d, 2H, *J* = 4.5 Hz), 7.14 (d, 2H, *J* = 4.1 Hz), 7.35 (d, 2H, *J* = 4.1 Hz) ppm. ^{13}C NMR ($CDCl_3$, 150 MHz) δ =21.1, 52.7, 55.7, 61.3, 114.7, 114.8, 127.1, 129.5, 134.7, 138.0, 140.2, 152.4, 172.7 ppm. HPLC (OJ-H, eluate: hexane / *i*-PrOH = 9 / 1, detector: 254 nm, flow rate: 1.0 mL / min), (*R*) t_1 = 15.6 min, (*S*) t_2 = 21.9 min.

Methyl 2-(4-methoxyphenyl)-2-((4-methoxyphenyl)amino)acetate (3i)[146]

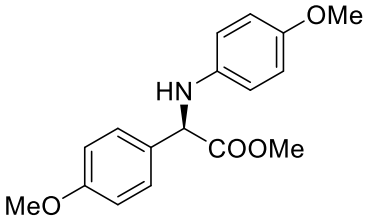

Yellow liquid. ^{1}H NMR ($CDCl_3$, 600 MHz) δ = 3.69(s, 3H), 3.70 (s, 3H), 3.77 (s, 3H), 4.65 (br, 1H), 4.95 (s, 1H), 6.51 (d, 2H, *J* = 4.5 Hz), 6.70 (d, 2H, *J* = 4.5 Hz), 6.86 (d, 2H, *J* = 4.4 Hz), 7.37 (d, 2H, *J* = 4.5 Hz) ppm. ^{13}C NMR ($CDCl_3$, 150 MHz) δ = 52.6, 55.2, 55.7, 61.0, 114.2, 114.7, 114.8, 128.4, 129.7, 140.2, 152.5, 159.5, 172.8 ppm. HPLC (OJ-H, eluate: hexane / *i*-PrOH = 9 / 1, detector: 254 nm, flow rate: 1.0 mL / min), (*R*) t_1 = 12.5 min, (*S*) t_2 = 17.4 min.

Methyl 2-(4-chlorophenyl)-2-((4-methoxyphenyl)amino)acetate (3j)[146]

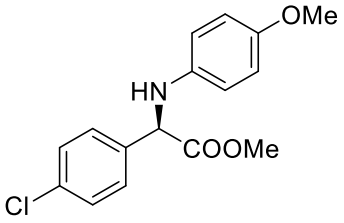

Yellow liquid. ^{1}H NMR ($CDCl_3$, 600 MHz) δ = 3.68 (s, 3H), 3.71 (s, 3H), 4.68 (br, 1H), 4.96 (s, 1H), 6.47-6.49 (m, 2H), 6.69-6.71 (m, 2H), 7.30 (d, 2H, *J* = 4.1 Hz), 7.41 (d, 2H, *J* = 4.1 Hz) ppm. ^{13}C NMR ($CDCl_3$, 150 MHz) δ = 52.9, 55.7, 61.0, 114.8, 114.9, 128.6, 129.0, 134.1, 136.4, 139.8, 152.6, 172.0 ppm. HPLC (AS-H, eluate: hexane / *i*-PrOH = 7 / 3, detector: 254 nm, flow rate: 0.8 mL / min), (*S*) t_1 = 8.5 min, (*R*) t_2 = 10.4 min.

Methyl 2-((4-methoxyphenyl)amino)-2-(*o*-tolyl)acetate (3k)

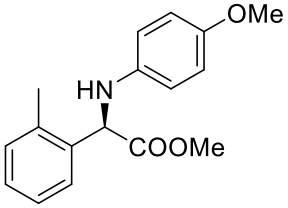

Transparent liquid. ^{1}H NMR ($CDCl_3$, 600 MHz) δ = 2.51 (s, 3H), 3.69 (s, 3H), 3.70 (s, 3H), 4.52 (br, 1H), 5.21 (s, 1H), 6.50 (d, 2H, *J* = 4.5 Hz), 6.71 (d, 2H, *J* = 4.5 Hz), 7.15-7.20 (m, 3H), 7.36-7.37 (m, 1H) ppm. ^{13}C NMR ($CDCl_3$, 150 MHz) δ = 19.5, 52.6, 55.7, 58.3, 114.6, 114.9, 126.4, 126.6, 128.1, 130.9, 136.0, 136.6, 140.5, 152.5, 173.0 ppm. HPLC (OJ-H, eluate: hexane / *i*-PrOH = 8 / 2, detector: 254 nm, flow rate: 1.0 mL / min), (*R*) t_1 = 16.6 min, (*S*) t_2 = 22.6 min. IR (neat) 3417, 1737, 1514, 1240, 1211, 1037, 903, 723, 648 cm^{-1}. HRMS (DART) calculated for $C_{17}H_{20}NO_3^+$ [*M*+H$^+$] 286.14432, found 286.14361. $[\alpha]^{20}_D$ = +79.7 (c = 0.95, $CHCl_3$).

Methyl 2-(2-methoxyphenyl)-2-((4-methoxyphenyl)amino)acetate (3l)[146]

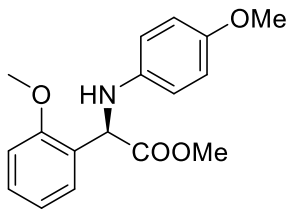

Transparent liquid. ^{1}H NMR ($CDCl_3$, 600 MHz) δ = 3.68 (s, 3H), 3.69 (s, 3H), 3.89 (s, 3H), 4.52 (br, 1H), 5.43 (s, 1H), 6.59 (d, 2H, *J* = 4.5 Hz), 6.71 (d, 2H, *J* = 4.5 Hz), 6.90-6.93 (m, 2H), 7.24-7.27 (m, 1H), 7.32-7.33 (m, 1H) ppm. ^{13}C NMR ($CDCl_3$, 150 MHz) δ = 52.5, 55.6, 55.8, 55.8, 111.1, 114.7, 115.0, 121.0, 126.5, 128.1, 129.4, 140.6, 152.5 157.1, 173.0 ppm. HPLC (OJ-H, eluate: hexane / *i*-PrOH = 8 / 2, detector: 254 nm, flow rate: 0.5 mL / min), (*R*) t_1 = 25.2 min, (*S*) t_2 = 35.6 min.

Methyl 2-((4-methoxyphenyl)amino)-2-(napthalen-2-yl)acetate (3m)[146]

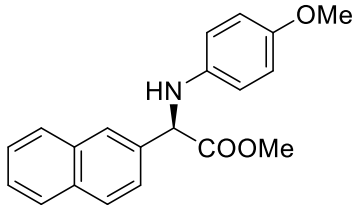

Yellow liquid. ^{1}H NMR ($CDCl_3$, 600 MHz) δ = 3.67 (s, 3H), 3.71 (s, 3H), 5.16 (s, 1H), 6.56 (d, 2H, *J* = 4.1 Hz), 6.69 (d, 2H, *J* = 4.4 Hz), 7.46-7.47 (m, 2H), 7.58-7.59 (m, 1H) 7.80-7.83 (m, 3H), 7.94 (s, 1H) ppm. ^{13}C NMR ($CDCl_3$, 150 MHz) δ = 52.8, 55.7, 61.8, 114.8, 114.8, 124.9, 126.2, 126.2, 126.5, 127.7, 128.0, 128.7, 133.2, 133.3, 135.3, 140.1, 152.5, 172.5 ppm. HPLC (AS-H, eluate: hexane / *i*-PrOH = 9 / 1, detector: 254 nm, flow rate: 1.0 mL / min), (*S*) t_1 = 26.8 min, (*R*) t_2 = 28.8 min.

Development of Nitrogen-Doped Carbon Incarcerated Zinc Nanoparticle Catalysts for Electrochemical Allylation of Carbonyl Compounds

Preparation of poly(4-vinylpyridine)[23]

To a solution of 4-vinylpyridine (83.9 g, 0.80 mol) in chloroform (150 mL), V-70 (2.41 g, 7.8 mmol) was added at room temperature, and the mixture was stirred until fully dissolved. The solution was degassed with sonication under Ar atmosphere and stirred for 48 h at room temperature. The mixture was added slowly to ethyl acetate/diethyl ether (1 L, 1/4) to generate precipitation, and the suspension was decanted. The precipitation was washed with diethyl ether (200 mL) three times. The polymer was dried in vacuo after grinding to afford poly(4-vinylpyridine) (72.3 g, 86.2% yield).

Representative procedure for preparation of NCI-Zn/HCl (NCI-Zn(5-1)/HCl)

To a stirring solution of poly(4-vinylpyridine) (667 mg) in ethanol (4 mL), a solution of $Zn(OAc)_2•2H_2O$ (700 mg, 3.2 mmol) in ethanol (12 mL) was added dropwise at room temperature under air. XC-72 (133 mg) was added to this solution, and the mixture was stirred for 1 h at room temperature. To this suspension was added a solution of $NaBH_4$ (600 mg, 16 mmol) in ethanol (6 mL), and the mixture was continued to stir for 2 h at room temperature. Ethyl acetate (100 mL) was added dropwise at room temperature, and stirred for 30 min. The catalyst was filtered and the collected catalyst was stirred in water (50 mL) for 10 min at room temperature. The catalyst was filtered, and the collected catalyst was stirred in acetone (50 mL) for 10 min at room temperature, followed by filtration and drying in vacuo. The catalyst was pyrolyzed at 800 °C for 2 h under Ar atmosphere. After cooling to room temperature, the catalyst was washed in ethanol (50 mL) with stirring. The catalyst was filtered, washed with ethanol, water and acetone, and dried in vacuo to afford NCI-Zn(5-1) (625 mg). NCI-Zn(5-1) (600 mg) was stirred in 6 M hydrochloric acid aqueous solution (30 mL) for 3 h at room temperature, and the filtered catalyst was washed with plenty amount of water and acetone to afford NCI-Zn(5-1)/HCl. NCI-Zn(5-1)/HCl (~5 mg) was heated in sulfuric acid (1.0 mL) at 200 °C, and some drops of nitric acid was added. After evaporating all nitric acid, the mixture was cooled to room temperature and diluted to 50 mL aqueous solution. The loading of Zn was determined to be 2.99 mmol/g by ICP analysis.

Representative procedure for preparation of X-NCI-Zn/HCl (N-NCI-Zn/HCl C1)

To a stirring solution of poly(4-vinylpyridine) (1.50 g) in ethanol (9 mL), a solution of $Zn(OAc)_2•2H_2O$ (1.58 g, 7.2 mmol) in ethanol (25 mL) was added dropwise at room temperature under air. XC-72 (300 mg) was added to this solution, and the mixture was stirred for 1 h at room temperature. To this suspension was added a solution of $NaBH_4$ (1.36 g, 36 mmol) in ethanol (10 mL), and the mixture was continued to stir for 2 h at room temperature. Ethyl acetate (200 mL) was added dropwise at room temperature, and

stirred for 30 min. The solid was filtered and stirred in water (50 mL) for 10 min at room temperature. After filtration, the collected solid was stirred in acetone (50 mL) for 10 min at room temperature. The filtered and dried solid was stirred in ethyl acetate (50 mL) in the presence of pyrazine (1.73 g, 21.6 mmol) for 3 h at room temperature, followed by evaporation and drying in vacuo. The catalyst was pyrolyzed at 800 °C for 2 h under Ar atmosphere. After cooling to room temperature, the catalyst was washed in ethanol (50 mL) with stirring. The catalyst was filtered, washed with ethanol, water and acetone, and dried in vacuo to afford N-NCI-Zn **C1** (1.28 g).

N-NCI-Zn **C1** (1.2 g) was stirred in 6 M hydrochloric acid aqueous solution (60 mL) for 3 h at room temperature, and the filtered catalyst was washed with plenty amount of water and acetone to afford N-NCI-Zn/HCl **C1**. N-NCI-Zn/HCl **C1** (~5 mg) was heated in sulfuric acid (1.0 mL) at 200 °C, and some drops of nitric acid was added. After evaporating all nitric acid, the mixture was cooled to room temperature and diluted to 50 mL aqueous solution. The loading of Zn was determined to be 2.63 mmol/g by ICP analysis.

Preparation of CB-Zn/HCl (without poly-4-vinylpyridine)

To a stirring solution of XC-72 (800 mg) in ethanol (4 mL), a solution of $Zn(OAc)_2•2H_2O$ (700 mg, 3.2 mmol) in ethanol (12 mL) was added dropwise at room temperature under air, and the mixture was stirred for 1 h at room temperature. To this suspension was added a solution of $NaBH_4$ (600 mg, 16 mmol) in ethanol (6 mL), and the mixture was continued to stir for 2 h at room temperature. Ethyl acetate (100 mL) was added dropwise at room temperature, and stirred for 30 min. The catalyst was filtered and the collected catalyst was stirred in water (50 mL) for 10 min at room temperature. The catalyst was filtered, and the collected catalyst was stirred in acetone (50 mL) for 10 min at room temperature, followed by filtration and drying in vacuo. The catalyst was pyrolyzed at 800 °C for 2 h under Ar atmosphere. After cooling to room temperature, the catalyst was washed in ethanol (50 mL) with stirring. The catalyst was filtered, washed with ethanol, water and acetone, and dried in vacuo to afford CB-Zn (660 mg). CB-Zn (600 mg) was stirred in 6 M hydrochloric acid aqueous solution (30 mL) for 3 h at room temperature, and the filtered catalyst was washed with plenty amount of water and acetone to afford CB-Zn/HCl. CB-Zn/HCl (~5 mg) was heated in sulfuric acid (1.0 mL) at 200 °C, and some drops of nitric acid was added. After evaporating all nitric acid, the mixture was cooled to room temperature and diluted to 50 mL aqueous solution. The loading of Zn was determined to be 2.40 mmol/g by ICP analysis.

Preparation of nitrogen-doped carbon (NDC)

To a solution of poly(4-vinylpyridine) (5.0 g) in ethanol (100 mL), XC-72 (5.0 g) was added. After stirring for 1 h at room temperature, ethyl acetate (800 mL) was added dropwise and the collected solids by filtration were washed with ethyl acetate and acetone. After drying in vacuo, a part of solids (2.2 g) were pyrolyzed at 800 °C for 2 h under Ar

atmosphere. After cooling to room temperature, the solids were washed in ethanol with stirring. The solids were filtered, washed with ethanol, water and acetone, and dried in vacuo to afford nitrogen-doped carbon (NDC) (1.5 g).

Representative procedure for preparation of N-NCI-Zn/HCl C1 electrode

The mixture of N-NCI-Zn/HCl **C1** (200 mg) and Nafion^{TM} resin (5 wt%) solution (0.5 mL) in water/ethanol (1/1, 0.3 mL) was sonicated at 0 °C for 1 h. The resulting mixture was pasted on carbon cloth (12 x 25 mm) which was dried at 50 °C in an oven for 1 h. The carbon cloth was fixed on a graphite plate (9 x 52 mm) with carbon tape to prepare N-NCI-Zn/HCl **C1** electrode.

General procedure for electrochemical allylation of carbonyls using N-NCI-Zn/HCl C1 cathode

To 0.3 M $LiClO_4$ aqueous solution (5 mL) and THF (5 mL) in a reaction vial, benzaldehyde **5a** (31.8 mg, 0.3 mmol) and allyl bromide **6a** (72.6 mg, 0.6 mmol) were added. The cap with Pt anode (9 x 52 mm) and N-NCI-Zn/HCl **C1** cathode (9 x 52 mm) was attached, and the reaction solution was stirred and electrolyzed at a constant current (15 mA) for 15 h at room temperature under air. After the electrolysis, ethyl acetate (10 mL) was added to the resulting solution, and the organic layer was separated. After washing aqueous layer with ethyl acetate twice, the combined organic extracts were concentrated. The residue was purified by preparative thin-layer chromatography to afford desired alcohol **7a** in 92% yield. Zn leaching was determined by ICP analysis of aqueous phases after extraction.

Hot filtration tests

The reactions were performed in the same way as the above procedure. After 3 h or 6 h, the cap was replaced with one with Pt anode and graphite cathode, and the stirring at constant current (15 mA) was continued for 12 h or 9 h, respectively. After the electrolysis, ethyl acetate (10 mL) was added to the resulting solution, and the organic layer was separated. After washing aqueous layer with ethyl acetate twice, the combined organic extracts were concentrated. The residue was purified by preparative thin-layer chromatography. Zn leaching was determined by ICP analysis of aqueous phases after extraction.

Recovery and reuse of N-NCI-Zn/HCl C1 cathode

The reactions were performed in the same way as the above procedure. After the reaction, N-NCI-Zn/HCl **C1** cathode was removed from the cap and washed with 30 mL of H_2O/THF (1/1). The recovered N-NCI-Zn/HCl **C1** cathode was attached the cap without complete drying, and the next run of the reaction was performed.

General procedure for electrochemical allylation of benzaldehyde 5a with chiral

ligands using N-NCI-Zn/HCl C1 cathode

To 0.3 M $LiClO_4$ aqueous solution (5 mL) and THF (5 mL) in a reaction vial, benzaldehyde **5a** (31.8 mg, 0.3 mmol), allyl bromide **6a** (72.6 mg, 0.6 mmol), and chiral ligand **L1** (11.8 mg, 0.03 mmol) were added. The cap with Pt anode (9 x 52 mm) and N-NCI-Zn/HCl **C1** cathode (9 x 52 mm) was attached, and the reaction solution was stirred and electrolyzed at a constant current (15 mA) for 15 h at room temperature under air. After the electrolysis, ethyl acetate (10 mL) was added to the resulting solution, and the organic layer was separated. After washing aqueous layer with ethyl acetate twice, the combined organic extracts were concentrated. The residue was purified by preparative thin-layer chromatography to afford desired alcohol **7a** in 82% yield. The enantiomeric excess of **7a** was determined by HPLC analysis (OD-H, eluate: hexane / *i*-PrOH = 49 / 1, detector: 254 nm, flow rate: 1.0 mL / min, (*R*) t_1 = 16.4 min, (*S*) t_2 = 19.7 min.). Zn leaching was determined by ICP analysis of aqueous phases after extraction.

Preparation of chiral ligand modified N-NCI-Zn/HCl C1 (N-NCI-Zn/HCl C1-L)

To a suspension of N-NCI-Zn/HCl **C1** (500 mg, Zn: 1.32 mmol) in ethyl acetate (10 mL), a solution of **L1** or **L3** (2.0 mmol) in ethyl acetate (10 mL) was added dropwise. After stirring for 3 h at room temperature, the solids were collected by filtration and washed with ethyl acetate. The collected catalyst was dried in vacuo to afford N-NCI-Zn/HCl **C1-L**.

Characterization date of products

1-phenylbut-3-en-1-ol (7a)[84]

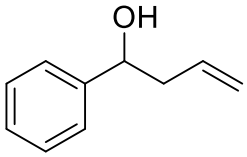

Transparent liquid. ^{1}H NMR ($CDCl_3$, 600 MHz) δ = 1.79 (br, 1H), 2.46-2.54 (m, 2H), 4.73 (dd, 1H, *J* = 7.6, 4.8 Hz), 5.12-5.17 (m, 2H), 5.76-5.82 (m, 1H), 7.25-7.28 (m, 1H), 7.32-7.34 (m, 4H) ppm. ^{13}C NMR ($CDCl_3$, 150 MHz) δ = 43.8, 73.3, 118.4, 125.8, 127.5, 128.4, 134.4, 143.8 ppm.

1-(4-chlorophenyl)but-3-en-1-ol (7b)[84]

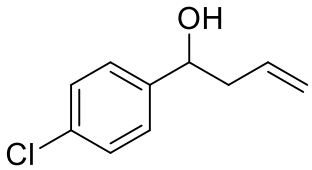

Transparent liquid. ^{1}H NMR ($CDCl_3$, 600 MHz) δ = 2.01 (br, 1H), 2.41-2.50 (m, 2H), 4.71 (dd, 1H, *J* = 8.3, 4.9 Hz), 5.13-5.16 (m, 2H), 5.73-5.80 (m, 1H), 7.27-7.31 (m, 4H) ppm. ^{13}C NMR ($CDCl_3$, 150 MHz) δ = 43.8, 72.5, 118.9, 127.2, 128.5, 133.1, 133.9, 142.2 ppm.

1-(3,4-dichlorophenyl)but-3-en-1-ol (7c)[149]

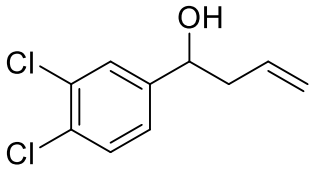

Transparent liquid. ^{1}H NMR ($CDCl_3$, 600 MHz) δ = 2.05 (br, 1H), 2.39-2.44 (m, 1H), 2.47-2.52 (m, 1H), 4.69 (dd, 1H, *J* = 7.6, 2.0 Hz), 5.14-5.18 (m, 2H), 5.72-5.79 (m, 1H), 7.16-7.18 (m, 1H), 7.40 (d, 1H, *J* = 8.2 Hz), 7.45 (d, 1H, *J* = 2.0 Hz) ppm. ^{13}C NMR ($CDCl_3$, 150 MHz) δ = 43.8, 71.9, 119.4, 125.2, 127.9, 130.3, 131.3, 132.5, 133.5, 144.0 ppm.

1-(*p*-tolyl)but-3-en-1-ol (7d)[150]

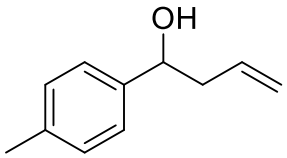

Transparent liquid. ^{1}H NMR ($CDCl_3$, 600 MHz) δ = 1.92 (br, 1H), 2.33 (s, 3H), 2.45-2.53 (m, 2H), 4.69 (dd, 1H, *J* = 7.6, 5.5 Hz), 5.11-5.16 (m, 2H), 5.76-5.83 (m, 1H), 7.14 (d, 2H, *J* = 8.3 Hz), 7.23 (d, 2H, *J* = 8.2 Hz) ppm. ^{13}C NMR ($CDCl_3$, 150 MHz) δ = 21.1, 43.7, 73.2, 118.2, 125.7, 129.0, 134.6, 137.2, 140.9 ppm.

1-(4-methoxyphenyl)but-3-en-1-ol (7e)[84]

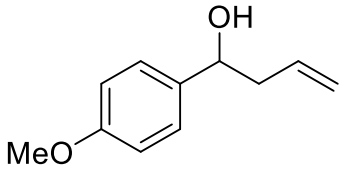

Transparent liquid. ^{1}H NMR ($CDCl_3$, 600 MHz) δ = 1.92 (br, 1H), 2.47-2.50 (m, 2H), 3.79 (s, 3H), 4.68 (dd, 1H, *J* = 6.8, 6.2 Hz), 5.10-5.15 (m, 2H), 5.75-5.82 (m, 1H), 6.87 (d, 2H, *J* = 8.9 Hz), 7.27 (d, 2H, *J* = 8.9 Hz) ppm. ^{13}C NMR ($CDCl_3$, 150 MHz) δ = 43.7, 55.2, 72.9, 113.8, 118.2, 127.0, 134.6, 136.0, 159.0 ppm.

1-(3-methoxyphenyl)but-3-en-1-ol (7g)[151]

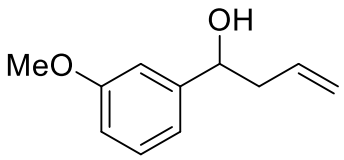

Transparent liquid. ^{1}H NMR ($CDCl_3$, 600 MHz) δ = 1.98 (br, 1H), 2.44-2.54 (m, 2H), 3.80 (s, 3H), 4.71 (dd, 1H, *J* = 7.6, 4.8 Hz), 5.12-5.17 (m, 2H), 5.76-5.83 (m, 1H), 6.79-6.81 (m, 1H), 6.91-6.92 (m, 2H), 7.23-7.26 (m, 1H) ppm. ^{13}C NMR ($CDCl_3$, 150 MHz) δ = 43.8, 55.2, 73.2, 111.3, 113.0, 118.1, 118.4, 129.4, 134.4, 145.6, 159.7 ppm.

1-(2-(trifluoromethyl)phenyl)but-3-en-1-ol (7h)[152]

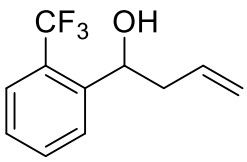

Transparent liquid. ^{1}H NMR ($CDCl_3$, 600 MHz) δ = 2.11 (br, 1H), 2.35-2.40 (m, 1H), 2.51-2.53 (m, 1H), 5.13-5.20 (m, 3H), 5.84-5.91 (m, 1H), 7.35-7.37 (m, 1H), 7.56-7.61 (m, 2H), 7.78 (d, 1H, *J* = 7.6 Hz) ppm. ^{13}C NMR ($CDCl_3$, 150 MHz) δ = 43.9, 68.6, 118.4, 124.3 (q, *J* = 273.8 Hz), 125.3 (q, *J* = 6.0 Hz), 126.7 (q, *J* = 30.2 Hz), 127.4, 127.5, 132.1, 134.3, 143.0 ppm.

1-([1,1'-biphenyl]-4-yl)but-3-en-1-ol (7j)[150]

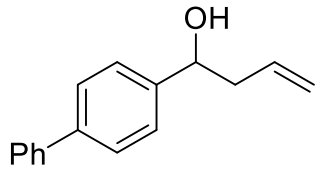

Transparent liquid. ^{1}H NMR ($CDCl_3$, 600 MHz) δ = 2.03 (br, 1H), 2.50-2.59 (m, 2H), 4.78 (dd, 1H, *J* = 8.3, 4.9 Hz), 5.15-5.20 (m, 2H), 5.80-5.87 (m, 1H), 7.32-7.34 (m, 1H), 7.41-7.43 (m, 4H), 7.56-7.58 (m, 4H) ppm. ^{13}C NMR ($CDCl_3$, 150 MHz) δ = 43.8, 73.0, 118.5, 126.2, 127.0, 127.1, 127.2, 128.7, 134.4, 140.4, 140.8, 142.9 ppm.

1-(naphthalen-2-yl)but-3-en-1-ol (7k)[153]

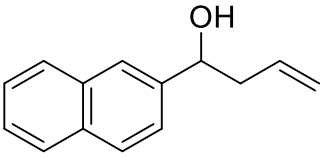

Transparent liquid. ^{1}H NMR ($CDCl_3$, 600 MHz) δ = 2.54-2.64 (m, 2H), 4.90 (dd, 1H, *J* = 7.6, 4.8 Hz), 5.13-5.19 (m, 2H), 5.79-5.86 (m, 1H), 7.45-7.48 (m, 3H), 7.80-7.83 (m, 4H) ppm. ^{13}C NMR ($CDCl_3$, 150 MHz) δ = 43.7, 73.4, 118.5, 124.0, 124.5, 125.8, 126.1, 127.6, 127.9, 128.2, 132.9, 133.2, 134.3, 141.2 ppm.

1-(naphthalen-1-yl)but-3-en-1-ol (7l)[153]

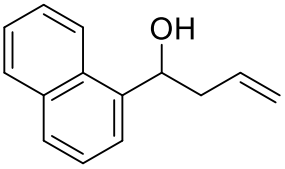

Transparent liquid. ^{1}H NMR ($CDCl_3$, 600 MHz) δ = 2.13 (br, 1H), 2.57-2.62 (m, 1H), 2.74-2.78 (m, 1H), 4.53 (dd, 1H, *J* = 8.9, 4.1 Hz), 5.17-5.23 (m, 2H), 5.89-5.96 (m, 1H), 7.46-7.53 (m, 3H), 7.66 (d, 1H, *J* = 6.9 Hz), 7.77 (d, 1H, *J* = 8.3 Hz), 7.87 (d, 1H, *J* = 8.3 Hz), 8.07 (d, 1H, *J* = 8.3 Hz) ppm. ^{13}C NMR ($CDCl_3$, 150 MHz) δ = 42.9, 70.0, 118.4, 122.8, 123.0, 125.4, 125.5, 126.0, 128.0, 128.9, 130.2, 133.8, 134.8, 139.4 ppm.

1-phenylhex-5-en-3-ol (7m)[84]

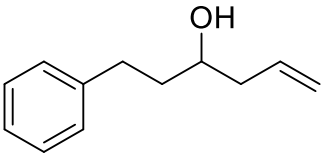

Transparent liquid. ^{1}H NMR ($CDCl_3$, 500 MHz) δ = 1.73 (br, 1H), 1.76-1.81 (m, 2H), 2.17-2.22 (m, 1H), 2.30- 2.34 (m, 1H), 2.66-2.72 (m, 1H), 2.78-2.84 (m, 1H), 3.66-3.69 (m, 1H), 5.13-5.16 (m, 2H), 5.78-5.85 (m, 1H), 7.17-7.22 (m, 3H), 7.27-7.30 (m, 2H) ppm. ^{13}C NMR ($CDCl_3$, 150 MHz) δ = 32.0, 38.4, 42.0, 69.9, 118.2, 125.8, 128.3, 128.4, 134.6, 142.0 ppm.

(*E*)-1-phenylhexa-1,5-dien-3-ol (7n)[84]

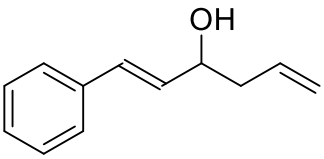

Transparent liquid. ^{1}H NMR ($CDCl_3$, 500 MHz) δ = 1.74 (br, 1H), 2.35-2.46 (m, 2H), 4.35 (dd, 1H, *J* = 12.0, 8.6 Hz), 5.14-5.20 (m, 2H), 5.80-5.89 (m, 1H), 6.23 (dd, 1H, *J* = 16.0, 6.9 Hz), 6.60 (d, 1H, *J* = 16.1 Hz), 7.21-7.23 (m, 1H), 7.28-

7.31 (m, 2H), 7.36-7.37(m, 2H) ppm. ^{13}C NMR ($CDCl_3$, 150 MHz) δ = 42.0, 71.7, 118.5, 126.4, 127.6, 128.5, 130.3, 131.5, 134.0, 136.6 ppm.

(*E*)-2-methyl-1-phenylhexa-1,5-dien-3-ol (7o)[154]

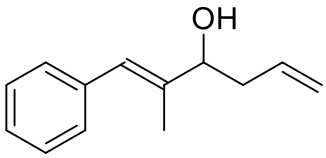

Transparent liquid. ^{1}H NMR ($CDCl_3$, 600 MHz) δ = 1.75 (br, 1H), 1.87 (d, 3H, *J* = 1.3 Hz), 2.35-2.47 (m, 2H), 4.21 (dd, 1H, *J* = 6.2, 2.8 Hz), 5.12-5.19 (m, 2H), 5.79-5.86 (m, 1H), 6.52 (s, 1H), 7.19-7.21 (m, 1H), 7.26 (d, 2H, *J* = 7.6 Hz), 7.30-7.33 (m, 2H) ppm. ^{13}C NMR ($CDCl_3$, 150 MHz) δ = 13.7, 40.1, 76.5, 118.1, 125.7, 126.4, 128.1, 129.0, 134.5, 137.5, 139.5 ppm.

(*E*)-7-methylocta-1,5-dien-4-ol (7p)

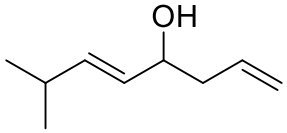

Transparent liquid. ^{1}H NMR ($CDCl_3$, 500 MHz) δ = 0.96 (d, 3H, *J* = 1.8 Hz), 0.97 (d, 3H, *J* = 1.7 Hz), 1.76 (br, 1H), 2.22-2.32 (m, 3H), 4.08-4.11 (m, 1H), 5.08-5.12 (m, 2H), 5.38-5.43 (m, 1H), 5.60-5.65 (m, 1H), 5.74-5.82 (m, 1H) ppm. ^{13}C NMR ($CDCl_3$, 125 MHz) δ = 22.2, 22.3, 30.6, 42.1, 71.9, 118.0, 129.0, 134.4, 139.2 ppm. IR (neat) 3345, 2960, 2870, 1642, 1464, 1027, 971, 913, 636 cm^{-1}. HRMS (DART) calculated for $C_9H_{17}O^+$ [*M*+H^+] 141.12794, found 141.12805.

dec-1-en-4-ol (7q)[84]

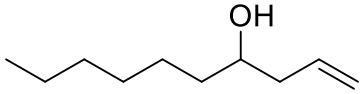

Transparent liquid. ^{1}H NMR ($CDCl_3$, 500 MHz) δ = 0.86 (t, 3H, *J* = 6.9 Hz), 1.24-1.31 (m, 8H), 1.42-1.45 (m, 2H), 1.55 (br, 1H), 2.09-2.15 (m, 1H), 2.26-2.31 (m, 1H), 3.60-3.65 (m, 1H), 5.10-5.13 (m, 2H), 5.77-5.85 (m, 1H) ppm. ^{13}C NMR ($CDCl_3$, 125 MHz) δ = 14.0, 22.6, 25.6, 29.3, 31.8, 36.8, 41.9, 70.7, 118.0, 134.9 ppm.

1-(pyridine-2-yl)but-3-en-1-ol (7r)[84]

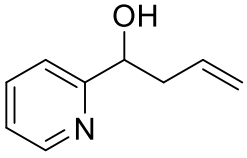

Transparent liquid. ^{1}H NMR ($CDCl_3$, 600 MHz) δ = 2.47-2.52 (m, 1H), 2.62-2.66 (m, 1H), 4.85 (dd, 1H, *J* = 7.6, 4.8 Hz), 5.08-5.12 (m, 2H), 5.79-5.86 (m, 1H), 7.23-7.25 (m, 1H), 7.32 (d, 1H, *J* = 7.6 Hz), 7.71-7.74 (m, 1H), 8.56 (d, 1H, *J* = 4.8 Hz) ppm. ^{13}C NMR ($CDCl_3$, 150 MHz) δ = 42.8, 72.1, 118.1, 120.6, 122.4, 134.0, 136.8, 148.2, 161.3 ppm.

1-(pyridin-3-yl)but-3-en-1-ol (7s)[153]

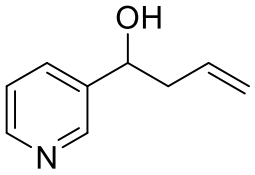

Transparent liquid. ^{1}H NMR ($CDCl_3$, 600 MHz) δ = 1.64 (br, 1H), 2.43-2.56 (m, 2H), 4.80 (dd, 1H, *J* = 8.2, 4.8 Hz), 5.14-5.18 (m, 2H), 5.74-5.81 (m, 1H), 7.37 (dd, 1H, *J* = 7.6, 4.8 Hz), 7.82 (d, 1H, *J* = 8.2 Hz), 8.58 (d, 1H, *J* = 4.8 Hz), 8.64 (s, 1H) ppm. ^{13}C NMR ($CDCl_3$, 150 MHz) δ = 43.2, 70.2, 119.5, 125.3, 132.8, 138.2, 142.0, 146.4, 147.3 ppm.

1-(furan-2-yl)but-3-en-1-ol (7t)[84]

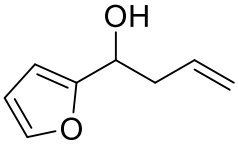

Pale yellow liquid. ^{1}H NMR ($CDCl_3$, 600 MHz) δ = 2.16 (br, 1H), 2.56-2.64 (m, 2H), 4.72 (t, 1H, *J* = 6.5 Hz), 5.11-5.17 (m, 2H), 5.75-5.81 (m, 1H), 6.23 (d, 1H, *J* = 3.5 Hz), 6.30-6.31 (m, 1H), 7.35 (d, 1H, *J* = 2.0 Hz) ppm. ^{13}C NMR ($CDCl_3$, 150 MHz) δ = 40.0, 66.9, 106.0, 110.1, 118.5, 133.7, 141.9, 156.0 ppm.

1-(thiophen-2-yl)but-3-en-1-ol (7u)[155]

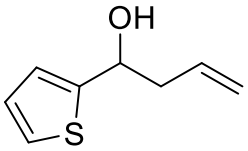

Transparent liquid. ^{1}H NMR ($CDCl_3$, 500 MHz) δ = 2.12 (d, 1H, *J* = 4.0 Hz), 2.59-2.63 (m, 2H), 4.99 (t, 1H, *J* = 8.0 Hz), 5.14-5.20 (m, 2H), 5.78-5.86 (m, 1H), 6.94-6.97 (m, 2H), 7.23 (d, 1H, *J* = 1.2 Hz) ppm. ^{13}C NMR ($CDCl_3$, 125 MHz) δ = 43.8, 69.3, 118.8, 123.7, 124.5, 126.6, 133.8, 147.8 ppm.

1-(quinolin-6-yl)but-3-en-1-ol (7v)[156]

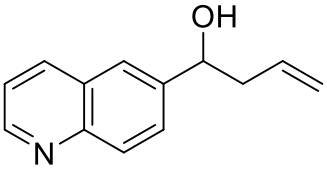

Orange liquid. ^{1}H NMR ($CDCl_3$, 500 MHz) δ = 2.48-2.54 (m, 1H), 2.57-2.62 (m, 1H), 4.91 (dd, 1H, *J* = 8.0, 4.6 Hz), 5.14-5.18 (m, 2H), 5.75-5.83 (m, 1H), 7.45 (dd, 1H, *J* = 8.0, 4.6 Hz), 7.67 (dd, 1H, *J* = 8.6, 1.7 Hz), 7.82 (s, 1H), 8.22-8.23 (m, 2H), 9.05 (br, 1H) ppm. ^{13}C NMR ($CDCl_3$, 125 MHz) δ = 43.5, 72.5, 118.3, 121.2, 124.4, 127.8, 128.2, 128.7, 133.9, 137.9, 143.2, 146.1, 150.2 ppm.

2-methyl-1-phenylbut-3-en-1-ol (7x)[84]

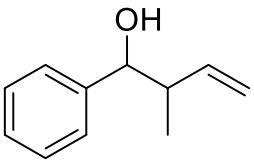

Transparent liquid. ^{1}H NMR ($CDCl_3$, 500 MHz) (*syn* isomer) δ = 0.99 (d, 3H, *J* = 7.5 Hz), 1.90 (br, 1H), 2.55-2.59 (m, 1H), 4.61 (d, 1H, *J* = 2.9 Hz), 5.02-5.06 (m, 2H), 5.71-5.83 (m, 1H), 7.25-7.34 (m, 5H) ppm. (*anti* isomer) δ = 0.86 (d, 3H, *J* = 6.9 Hz), 2.11 (br, 1 H), 2.45-2.49 (m, 1H), 4.35 (d, 1H, *J* = 8.0 Hz), 5.16-5.21 (m, 2H), 5.71-5.83 (m, 1H), 7.25-7.34 (m, 5H) ppm. ^{13}C NMR ($CDCl_3$, 125 MHz) (*syn* isomer) δ = 14.0, 46.3,

77.2, 115.5, 126.5, 127.3, 128.1, 140.3, 142.4 ppm. (*anti* isomer) δ = 16.5, 44.6, 77.9, 116.9, 126.8, 127.7, 128.2, 140.6, 142.5 ppm.

1,2-diphenylbut-3-en-1-ol (7y)[157]

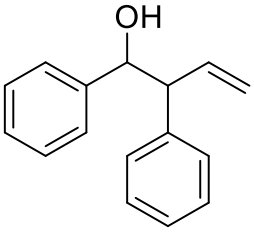

Transparent liquid. ^{1}H NMR ($CDCl_3$, 600 MHz) (*anti* isomer) δ = 2.27 (d, 1H, *J* = 2.0 Hz), 3.53 (t, 1H, *J* = 8.3 Hz), 4.83 (d, 1H, *J* = 2.0 Hz), 5.20-5.26 (m, 2H), 6.21-6.27 (m, 1H), 7.04 (d, 2H, *J* = 7.6 Hz), 7.12-7.20 (m, 8H) ppm. (*syn* isomer) δ = 1.90 (d, 1H, *J* = 3.4 Hz), 3.62 (t, 1H, *J* = 8.3 Hz), 4.84-4.90 (m, 2H), 4.97 (d, 1H, *J* = 10.3 Hz), 5.85-5.91 (m, 1H), 7.26-7.35 (m, 10H) ^{13}C NMR ($CDCl_3$, 125 MHz) (*anti* isomer) δ = 59.1, 77.2, 118.3, 126.5, 126.6, 127.4, 127.9, 128.3, 128.7, 137.8, 140.6, 141.8 ppm. (*syn* isomer) δ = 58.4, 77.5, 117.2, 127.0, 127.0, 127.3, 127.7, 128.1, 128.6, 137.6, 140.2, 141.8 ppm.

2-phenylpent-4-en-2-ol (7z)[84]

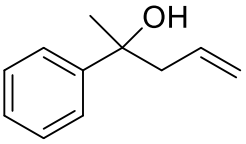

Transparent liquid. ^{1}H NMR ($CDCl_3$, 600 MHz) δ = 1.53 (s, 3H), 2.01 (s, 1H), 2.49 (dd, 1H, *J* = 13.7, 8.2 Hz), 2.67 (dd, 1H, *J* = 13.7, 6.9 Hz), 5.09-5.14 (m, 2H), 5.57-5.64 (m, 1H), 7.21-7.24 (m, 1H), 7.31-7.34 (m, 2H), 7.42 (d, 2H, *J* = 7.6 Hz) ppm. ^{13}C NMR ($CDCl_3$, 150 MHz) δ = 29.9, 48.4, 73.6, 119.4, 124.7, 126.6, 128.1, 133.6, 147.6 ppm.

1-allyl-2,3-dihydro-1*H*-inden-1-ol (7aa)[158]

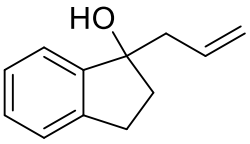

Transparent liquid. ^{1}H NMR ($CDCl_3$, 600 MHz) δ = 1.94 (br, 1H), 2.05-2.09 (m, 1H), 2.30-2.34 (m, 1H), 2.50 (dd, 1H, *J* = 13.7, 6.8 Hz), 2.62 (dd, 1H, *J* = 13.7, 7.6 Hz), 2.78-2.83 (m, 1H), 2.96-3.01 (m, 1H), 5.13-5.18 (m, 2H), 5.81-5.88 (m, 1H), 7.22-7.23 (m, 3H), 7.31-7.32 (m, 1H) ppm. ^{13}C NMR ($CDCl_3$, 150 MHz) δ = 29.4, 39.6, 44.9, 82.7, 118.8, 122.8, 124.9, 126.6, 128.2, 133.7, 143.0, 147.0 ppm.

1-(4-methoxyphenyl)-2-methylpent-4-en-2-ol (7ab)[159]

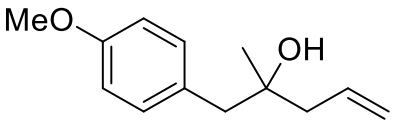

Transparent liquid. ^{1}H NMR ($CDCl_3$, 500 MHz) δ = 1.12 (s, 3H), 2.21 (d, 1H, *J* = 3.4 Hz), 2.22 (d, 1H, *J* = 3.4 Hz), 2.65-2.73 (m, 2H), 3.78 (s, 3H), 5.09-5.16 (m, 2H), 5.86-5.95 (m, 1H), 6.83 (d, 2H, *J* = 8.6 Hz), 7.12 (d, 2H, *J* = 8.6 Hz) ppm. ^{13}C NMR ($CDCl_3$, 125 MHz) δ = 26.5, 46.1, 46.9, 55.2, 72.1, 113.6, 118.6, 129.4, 131.5, 134.1, 158.3 ppm.

Chapter 8: References

1. Rothenberg, G. Catalysis: Concepts and Green Applications. *Wiley-VCH* (2008).
2. Kobayashi, S. Flow "Fine" Synthesis: High Yielding and Selective Organic Synthesis by Flow Methods. *Chem. Asian J. 11*, 425–436 (2016).
3. Tsubogo, T. *et al*. Multistep continuous-flow synthesis of (*R*)- and (*S*)-rolipram using heterogeneous catalysts. *Nature 520*, 329–332 (2015).
4. Ross, J. R. H. Heterogeneous Catalysis: Fundamentals and Applications. *Elsevier* (2011).
5. Marsh, H. Activated Carbon. *Elsevier* (2006).
6. Serp, P. Carbon Materials for Catalysis. *Wiley-VCH* (2008).
7. Liu, P. *et al*. Cobalt and nitrogen doped porous carbon nanofibers as an efficient electrocatalyst for high performance oxygen reduction reaction. *J. Mater. Sci. Mater. Electron. 31*, 7596–7605 (2020).
8. Zhou, N. *et al.* Probing Active Sites on Metal-Free, Nitrogen-Doped Carbons for Oxygen Electroreduction: A Review. *Catalysts 8*, 509-524 (2018).
9. Wei, Q. *et al*. Nitrogen-Doped Carbon Nanotube and Graphene Materials for Oxygen Reduction Reactions. *Catalysts 5*, 1574-1602 (2015).
10. He, L. *et al.* Synthesis, Characterization, and Application of Metal Nanoparticles Supported on Nitrogen-Doped Carbon: Catalysis beyond Electrochemistry. *Angew. Chem. Int. Ed. 55*, 12582–12594 (2016).
11. Su, H. *et al.* Activating cobalt nanoparticles via the Mott-Schottky effect in nitrogen-rich carbon shells for base-free aerobic oxidation of alcohols to esters. *J. Am. Chem. Soc. 139*, 811–818 (2017).
12. Zhou, Y. X. *et al*. Conversion of a metal–organic framework to N-doped porous carbon incorporating Co and CoO nanoparticles: direct oxidation of alcohols to esters. *Chem. Commun. 51*, 8292–8295 (2015).
13. Zhong, W. *et al.* Base-free oxidation of alcohols to esters at room temperature and atmospheric conditions using nanoscale Co-based catalysts. *ACS Catal. 5*, 1850–1856 (2015).
14. Jagadeesh, R. V. *et al.* Selective oxidation of alcohols to esters using heterogeneous Co_3O_4-N@C catalysts under mild conditions. *J. Am. Chem. Soc. 135*, 10776–10782 (2013).
15. Jiang, Y. *et al*. Solvent-free aerobic selective oxidation of hydrocarbons catalyzed by porous graphitic carbon encapsulated cobalt composites. *New J. Chem. 42*, 16829–16835 (2018).
16. Lin, X. *et al*. Nitrogen-doped carbon nanotubes encapsulate cobalt nanoparticles as efficient catalysts for aerobic and solvent-free selective oxidation of hydrocarbons. *Green Chem. 19*, 2164–2173 (2017).
17. Li, W. *et al*. Superior activity and selectivity of heterogenized cobalt catalysts for hydrogenation of nitroarenes. *Catal. Sci. Technol. 9*, 157–162 (2019).

18. Murugesan, K. *et al*. Cobalt-based nanoparticles prepared from MOF–carbon templates as efficient hydrogenation catalysts. *Chem. Sci. 9*, 8553–8560 (2018).
19. Duan, Y. *et al*. Enhanced catalytic performance of cobalt nanoparticles coated with a N,P-codoped carbon shell derived from biomass for transfer hydrogenation of functionalized nitroarenes. *Green Chem. 20*, 2821–2828 (2018).
20. Chen, F. *et al.* Hydrogenation of Pyridines Using a Nitrogen-Modified Titania-Supported Cobalt Catalyst. *Angew. Chem. Int. Ed. 57*, 14488–14492 (2018).
21. Chen, F. *et al*. Selective cobalt nanoparticles for catalytic transfer hydrogenation of N-heteroarenes. *Chem. Sci. 8*, 6239–6246 (2017).
22. Chen, F. *et al.* Selective Semihydrogenation of Alkynes with N-Graphitic-Modified Cobalt Nanoparticles Supported on Silica. *ACS Catal. 7*, 1526–1532 (2017).
23. Yasukawa, T. *et al.* Development of N-Doped Carbon-Supported Cobalt/Copper Bimetallic Nanoparticle Catalysts for Aerobic Oxidative Esterifications Based on Polymer Incarceration Methods. *Org. Lett. 20*, 5172–5176 (2018).
24. Yasukawa, T. *et al*. Oxygenation of Styrenes Catalyzed by N-Doped Carbon Incarcerated Cobalt Nanoparticles. *Bull. Chem. Soc. Jpn. 92*, 1980–1985 (2019).
25. Yang, X. *et al.* Development of Trifluoromethanesulfonic Acid-Immobilized Nitrogen-Doped Carbon-Incarcerated Niobia Nanoparticle Catalysts for Friedel-Crafts Acylation. *J. Org. Chem. 86*, 15800–15806 (2021).
26. Yang, X. *et al.* Well-Dispersed Trifluoromethanesulfonic Acid-Treated Metal Oxide Nanoparticles Immobilized on Nitrogen-Doped Carbon as Catalysts for Friedel–Crafts Acylation. *Chem. Asian J. 16*, 232–236 (2021).
27. Yasukawa, T. *et al.* Olefination of Aldehydes with Ethyl Diazoacetate Catalyzed by Nitrogen-doped Carbon-supported Metal. *Chem. Lett. 50*, 1733–1735 (2021).
28. Yu, T. *et al*. Recent Advances in Continuous-Flow Enantioselective Catalysis. *Chem. Eur. J. 26*, 5729–5747 (2020).
29. Zhao, D. *et al.* Recent advances in asymmetric catalysis in flow. *ACS Catal. 3*, 928–944 (2013).
30. Altava, B. *et al.* Chiral catalysts immobilized on achiral polymers: Effect of the polymer support on the performance of the catalyst. *Chem. Soc. Rev. 47*, 2722–2771 (2018).
31. McMorn, P. *et al.* Heterogeneous enantioselective catalysts: strategies for the immobilisation of homogeneous catalysts. *Chem. Soc. Rev. 33*, 108–122 (2004).
32. Schmid, G. Large clusters and colloids. Metals in the embryonic state. *Chem. Rev. 92*, 1709–1727 (1992).
33. Astruc, D. *et al.* Nanoparticles as recyclable catalysts: The frontier between homogeneous and heterogeneous catalysis. *Angew. Chem. Int. Ed. 44*, 7852–7872 (2005).
34. Meemken, F. *et al.* A. Recent Progress in Heterogeneous Asymmetric Hydrogenation of C=O and C=C Bonds on Supported Noble Metal Catalysts. *Chem. Rev. 117*, 11522–11569 (2017).
35. Yasukawa, T. *et al.* Chiral Ligand-Modified Metal Nanoparticles as Unique

Catalysts for Asymmetric C–C Bond-Forming Reactions: How Are Active Species Generated? *ACS Catal. 6*, 7979–7988 (2016).
36. Yasukawa, T. *et al.* Chiral metal nanoparticle-catalyzed asymmetric C-C bond formation reactions. *Chem. Soc. Rev. 43*, 1450–1461 (2014).
37. Zhu, J. *et al.* Enantioselective Dihydroxylation of Alkenes Catalyzed by 1,4-Bis(9-O-dihydroquinidinyl)phthalazine-Modified Binaphthyl–Osmium Nanoparticles. *ChemCatChem 10*, 1788–1792 (2018).
38. Chen, M. Y. *et al*. Catalytic Asymmetric Huisgen Alkyne–Azide Cycloaddition of Bisalkynes by Copper(I) Nanoparticles. *ChemCatChem 10*, 280–286 (2018).
39. Miyamura, H. *et al.* Rhodium-catalyzed asymmetric 1,4-addition reactions of aryl boronic acids with nitroalkenes: Reaction mechanism and development of homogeneous and heterogeneous catalysts. *Chem. Sci. 8*, 8362–8372 (2017).
40. Ma, H. C. *et al.* Pd NPs-Loaded Homochiral Covalent Organic Framework for Heterogeneous Asymmetric Catalysis. *Chem. Mater. 29*, 6518–6524 (2017).
41. Yasukawa, T. *et al.* Chiral Nanoparticles/Lewis Acids as Cooperative Catalysts for Asymmetric 1,4-Addition of Arylboronic Acids to *α,β*-Unsaturated Amides. *Angew. Chem. Int. Ed. 55*, 8058–8061 (2016).
42. Yasukawa, T. *et al.* Asymmetric Arylation of Imines Catalyzed by Heterogeneous Chiral Rhodium Nanoparticles. *Org. Lett. 18*, 2716–2718 (2016).
43. Yasukawa, T. *et al.* Chiral Metal Nanoparticle Systems as Heterogeneous Catalysts beyond Homogeneous Metal Complex Catalysts for Asymmetric Addition of Arylboronic Acids to *α,β*-Unsaturated Carbonyl Compounds. *J. Am. Chem. Soc. 137*, 6616–6623 (2015).
44. Yasukawa, T. *et al*. Polymer-incarcerated chiral Rh/Ag nanoparticles for asymmetric 1,4-addition reactions of arylboronic acids to enones: Remarkable effects of bimetallic structure on activity and metal leaching. *J. Am. Chem. Soc. 134*, 16963–16966 (2012).
45. Ranganath, K. V. S. *et al.* Asymmetric Nanocatalysis: N-Heterocyclic Carbenes as Chiral Modifiers of Fe3O4/Pd nanoparticles. *Angew. Chem. Int. Ed. 49*, 7786–7789 (2010).
46. Ortunõ, M. A. *et al*. Reaction mechanisms at the homogeneous-heterogeneous frontier: Insights from first-principles studies on ligand-decorated metal nanoparticles. *Catal. Sci. Technol. 9*, 5173–5185 (2019).
47. Ye, R. *et al.* Supported Au Nanoparticles with N-Heterocyclic Carbene Ligands as Active and Stable Heterogeneous Catalysts for Lactonization. *J. Am. Chem. Soc. 140*, 4144–4149 (2018).
48. Fedorov, A. *et al*. Silica-Supported Cu Nanoparticle Catalysts for Alkyne Semihydrogenation: Effect of Ligands on Rates and Selectivity. *J. Am. Chem. Soc. 138*, 16502–16507 (2016).
49. Ernst, J. B. *et al.* Tunable Heterogeneous Catalysis: N-Heterocyclic Carbenes as Ligands for Supported Heterogeneous Ru/K-Al_2O_3 Catalysts to Tune Reactivity and

Selectivity. *J. Am. Chem. Soc. 138*, 10718–10721 (2016).
50. Eremin, D. B. *et al.* Understanding active species in catalytic transformations: From molecular catalysis to nanoparticles, leaching, "Cocktails" of catalysts and dynamic systems. *Coord. Chem. Rev. 346*, 2–19 (2017).
51. Reimann, S. *et al.* Identification of the active species generated from supported Pd catalysts in heck reactions: An in situ quick scanning EXAFS investigation. *J. Am. Chem. Soc. 133*, 3921–3930 (2011).
52. Xue, Y. P. *et al.* Enzymatic asymmetric synthesis of chiral amino acids. *Chem. Soc. Rev. 47*, 1516–1561 (2018).
53. Nájera, C. *et al.* Catalytic Asymmetric Synthesis of α-Amino Acids. *Chem. Rev. 107*, 4584–4671 (2007).
54. Ford, A. *et al.* Modern Organic Synthesis with *α*-Diazocarbonyl Compounds. *Chem. Rev. 115*, 9981–10080 (2015).
55. Moody, C. J. Enantioselective Insertion of Metal Carbenes into N-H Bonds: A Potentially Versatile Route to Chiral Amine Derivatives. *Angew. Chem. Int. Ed. 46*, 9148–9150 (2007).
56. Hou, Z. *et al.* Highly Enantioselective Insertion of Carbenoids into N-H Bonds Catalyzed by Copper(I) Complexes of Binol Derivatives. *Angew. Chem. Int. Ed. 49*, 4763–4766 (2010).
57. Lee, E. C. *et al.* Copper-Catalyzed Asymmetric N−H Insertion Reactions: Couplings of Diazo Compounds with Carbamates to Generate α-Amino Acids. *J. Am. Chem. Soc. 129*, 12066–12067 (2007).
58. Liu, B. *et al.* Highly Enantioselective Insertion of Carbenoids into N−H Bonds Catalyzed by Copper Complexes of Chiral Spiro Bisoxazolines. *J. Am. Chem. Soc. 129*, 5834–5835 (2007).
59. Saito, H. *et al.* Asymmetric Intermolecular N-H Insertion Reaction of Phenyldiazoacetates with Anilines Catalyzed by Achiral Dirhodium(II) Carboxylates and Cinchona Alkaloids. *Heterocycles 81*, 1149 (2010).
60. Li, M.-L. *et al.* Highly enantioselective carbene insertion into N-H bonds of aliphatic amines. *Science 366*, 990–994 (2019).
61. Guo, J. X. *et al.* Enantioselective synthesis of *α*-alkenyl *α*-amino acids via N-H insertion reactions. *Chem. Sci. 7*, 1104–1108 (2016).
62. Xu, B. *et al.* Asymmetric N-H Insertion Reaction Cooperatively Catalyzed by Rhodium and Chiral Spiro Phosphoric Acids. *Angew. Chem. Int. Ed. 50*, 11483–11486 (2011).
63. Miyamura, H. *et al.* Polysilane-Immobilized Rh-Pt Bimetallic Nanoparticles as Powerful Arene Hydrogenation Catalysts: Synthesis, Reactions under Batch and Flow Conditions and Reaction Mechanism. *J. Am. Chem. Soc. 140*, 11325–11334 (2018).
64. Ambrusi, R. E. *et al.* DFT study of Rh and Ti dimers decorating N-doped pyridinic and pyrrolic graphene for molecular and dissociative hydrogen adsorption. *Appl. Surf. Sci. 464*, 243–254 (2019).

65. He, Z. *et al.* Elucidating Interaction between Palladium and N-Doped Carbon Nanotubes: Effect of Electronic Property on Activity for Nitrobenzene Hydrogenation. *ACS Catal. 9*, 2893–2901 (2019).
66. Deming, C. P. *et al.* Oxygen Electroreduction Catalyzed by Palladium Nanoparticles Supported on Nitrogen-Doped Graphene Quantum Dots: Impacts of Nitrogen Dopants. *ACS Sustain. Chem. Eng. 4*, 6580–6589 (2016).
67. E. Negishi. Organometallics in Organic Synthesis Vol. 1. *Wiley* (1980).
68. Tamao, K. *et al.* Selective Carbon-Carbon Bond Formation by Cross-Coupling of Grignard Reagents with Organic Halides. Catalysis by Nickel-Phosphine Complexes. *J. Am. Chem. Soc. 94*, 4374–4376 (1972).
69. Negishi, E. Palladium- or Nickel-Catalyzed Cross Coupling. A New Selective Method for Carbon-Carbon Bond Formation. *Acc. Chem. Res. 15*, 340–348 (1982).
70. Harenberg, J. H. *et al.* Continuous Flow Preparation of Benzylic Sodium Organometallics. *Angew. Chem. Int. Ed. 61*, e202203807 (2022).
71. Harenberg, J. H. *et al.* (2-Ethylhexyl)sodium: A Hexane-Soluble Reagent for Br/Na-Exchanges and Directed Metalations in Continuous Flow. *Angew. Chem. Int. Ed. 60*, 14296–14301 (2021).
72. Menges-Flanagan, G. *et al.* Scalable Continuous Synthesis of Grignard Reagents from in Situ-Activated Magnesium Metal. *Org. Process Res. Dev. 24*, 315–321 (2020).
73. Herath, A. *et al.* Generation and Cross-Coupling of Organozinc Reagents in Flow. *Org. Lett. 20*, 7429–7432 (2018).
74. Huck, L. *et al.* Grignard Reagents on a Tab: Direct Magnesium Insertion under Flow Conditions. *Org. Lett. 19*, 3747–3750 (2017).
75. Alonso, N. *et al.* Continuous Synthesis of Organozinc Halides Coupled to Negishi Reactions. *Adv. Synth. Catal. 356*, 3737–3741 (2014).
76. Malapit, C. A. *et al.* Advances on the Merger of Electrochemistry and Transition Metal Catalysis for Organic Synthesis. *Chem. Rev. 122*, 3180-3218 (2022).
77. Novaes, L. F. T. *et al.* Electrocatalysis as an enabling technology for organic synthesis. *Chem. Soc. Rev. 50*, 7941–8002 (2021).
78. Yan, M. *et al.* Synthetic Organic Electrochemical Methods Since 2000: On the Verge of a Renaissance. *Chem. Rev. 117*, 13230–13319 (2017).
79. Huo, H. X. *et al.* Catalytic asymmetric allylation of carbonyl compounds and imines with allylic boronates. *Org. Chem. Front. 1*, 303–320 (2014).
80. Yus, M. *et al.* Diastereoselective allylation of carbonyl compounds and imines: Application to the synthesis of natural products. *Chem. Rev. 113*, 5595–5698 (2013).
81. Haydl, A. M. *et al.* Alkynes as Electrophilic or Nucleophilic Allylmetal Precursors in Transition-Metal Catalysis. *Angew. Chem. Int. Ed. 56*, 11312–11325 (2017).
82. Yamamoto, Y. et al. Selective Reactions Using Allylic Metals. *Chem. Rev. 93*, 2207–2293 (1993).
83. Huang, J. M. *et al.* Zn-mediated electrochemical allylation of aldehydes in aqueous ammonia. *Chem. Commun. 45*, 3943-3945 (2009).

84. Huang, J. M. *et al.* Electrochemical allylation of carbonyl compounds in aqueous electrolyte catalyzed by zinc. *Chem. Commun. 46*, 2286–2288 (2010).
85. Heard, D. M. *et al.* Electrode Materials in Modern Organic Electrochemistry. *Angew. Chem. Int. Ed. 59*, 18866–18884 (2020).
86. Cheng, Y. *et al.* An Ingenious Strategy to Integrate Multiple Electrocatalytically Active Components within a Well-Aligned Nitrogen-Doped Carbon Nanotube Array Electrode for Electrocatalysis. *ACS Catal. 11*, 3958–3974 (2021).
87. Masa, J. *et al.* On the Role of Metals in Nitrogen-Doped Carbon Electrocatalysts for Oxygen Reduction. *Angew. Chem. Int. Ed. 54*, 10102–10120 (2015).
88. Cui, T. *et al.* Atomically Dispersed Pt–N_3C_1 Sites Enabling Efficient and Selective Electrocatalytic C–C Bond Cleavage in Lignin Models under Ambient Conditions. *J. Am. Chem. Soc. 143*, 9429-9439 (2021).
89. Kaiser, S. K. *et al.* Single-Atom Catalysts across the Periodic Table. *Chem. Rev. 120*, 11703–11809 (2020).
90. Samantaray, M. K. *et al.* Surface organometallic chemistry in heterogeneous catalysis. *Chem. Soc. Rev. 47*, 8403–8437 (2018).
91. Wang, A. *et al.* Heterogeneous single-atom catalysis. *Nat. Rev. Chem. 2*, 65–81 (2018).
92. Yang, X. F. *et al.* Single-atom catalysts: A new frontier in heterogeneous catalysis. *Acc. Chem. Res. 46*, 1740–1748 (2013).
93. Qiao, B. *et al.* Single-atom catalysis of CO oxidation using Pt_1/FeOx. *Nat. Chem. 3*, 634–641 (2011).
94. Shi, Z. *et al.* Metal-Nitrogen-Doped Carbon Materials as Highly Efficient Catalysts: Progress and Rational Design. *Adv. Sci. 7*, 2001069 (2020).
95. Guo, J. *et al.* Nitrogen-Doped Porous Carbon Supported Nonprecious Metal Single-Atom Electrocatalysts: from Synthesis to Application. *Small Methods 3*, 1900159 (2019).
96. Cui, X. *et al.* Bridging homogeneous and heterogeneous catalysis by heterogeneous single-metal-site catalysts. *Nat. Catal. 1*, 385–397 (2018).
97. Liu, W. *et al.* A Durable Nickel Single-Atom Catalyst for Hydrogenation Reactions and Cellulose Valorization under Harsh Conditions. *Angew. Chem. Int. Ed. 57*, 7071–7075 (2018).
98. Wu, H. *et al.* Highly doped and exposed Cu(I)–N active sites within graphene towards efficient oxygen reduction for zinc–air batteries. *Energy Environ. Sci. 9*, 3736–3745 (2016).
99. Fei, H. *et al.* Atomic cobalt on nitrogen-doped graphene for hydrogen generation. *Nat. Commun. 6*, 1–8 (2015).
100. Mi, X. *et al.* Almost 100 % Peroxymonosulfate Conversion to Singlet Oxygen on Single-Atom CoN_{2+2} Sites. *Angew. Chem. Int. Ed. 60*, 4588–4593 (2021).
101. Mohd Adli, N. *et al.* Engineering Atomically Dispersed FeN_4 Active Sites for CO_2 Electroreduction. *Angew. Chem. Int. Ed. 60*, 1022–1032 (2021).

102. Li, Z. *et al.* Iridium single-atom catalyst on nitrogen-doped carbon for formic acid oxidation synthesized using a general host–guest strategy. *Nat. Chem. 12*, 764–772 (2020).
103. Tian, H. *et al*. High-power lithium–selenium batteries enabled by atomic cobalt electrocatalyst in hollow carbon cathode. *Nat. Commun. 11*, 1–12 (2020).
104. Bajada, M. A. *et al.* Interfacing single-atom catalysis with continuous-flow organic electrosynthesis. *Chem. Soc. Rev. 51*, 3898–3925 (2022).
105. Kudo, F. *et al.* Mutational Biosynthesis of Hitachimycin Analogs Controlled by the *β*-Amino Acid-Selective Adenylation Enzyme HitB. *ACS Chem. Biol. 16*, 539–547 (2021).
106. Ramadhar, T. R. *et al.* Allylation of Imines and Their Derivatives with Organoboron Reagents: Stereocontrolled Synthesis of Homoallylic Amines. *Synthesis 2011*, 1321–1346 (2011).
107. Kropf, J. E. *et al.* Studies on a total synthesis of the microbial immunosuppresive agent FR901483. *J. Org. Chem. 71*, 2046–2055 (2006).
108. Ochoa Puentes, C. *et al.* Recent advancements in the homoallylamine chemistry. *J. Heterocyclic Chem. 39,* 595–614 (2002).
109. Lai, Y. L. et al. Palladium-Catalyzed Electrochemical Allylic Alkylation between Alkyl and Allylic Halides in Aqueous Solution. *Org. Lett. 19*, 2022–2025 (2017).
110. Yang, Y. S. *et al.* Indium (Zinc)-copper-mediated barbier-type alkylation reaction of nitrones in water: Synthesis of amines and hydroxylamines. *Org. Lett. 11*, 1209–1212 (2009).
111. Shen, Z. L. *et al.* Indium/copper-mediated conjugate addition of unactivated alkyl iodides to *α*,*β*-unsaturated carbonyl compounds in water. *Tetrahedron Lett. 50*, 1051–1054 (2009).
112. Fleming, F. F. *et al.* Alkenenitriles: Conjugate additions of alkyl iodides with a silica-supported zinc-copper matrix in water. *J. Org. Chem. 72*, 6961–6969 (2007).
113. Keh, C. C. K. *et al.* The Barbier - Grignard-type carbonyl alkylation using unactivated alkyl halides in water. *J. Am. Chem. Soc. 125*, 4062–4063 (2003).
114. Mondal, B. *et al.* Making and breaking of Zn–C bonds in the cases of allyl and propargyl organozincs. *Tetrahedron 90*, 132169 (2021).
115. Sun, X. W. *et al.* Remarkable salt effect on in-mediated allylation of N-tert-butanesulfinyl imines in aqueous media: Highly practical asymmetric synthesis of chiral homoallylic amines and isoindolinones. *Org. Lett. 10*, 1259–1262 (2008).
116. Bernardi, L. *et al.* Organometallic reactions in aqueous media: Indium-promoted additions to 2-pyridyl and glyoxylic acid oxime ethers. *J. Org. Chem. 68*, 3348–3351 (2003).
117. Wang, D. K. *et al.* Mg and Zn mediated allylation of imines with allyl bromide. *Tetrahedron Lett. 37*, 4187–4188 (1996).
118. Huang, J. M. *et al.* Electrochemical Allylation Reactions of Simple Imines in Aqueous Solution Mediated by Nanoscale Zinc Architectures. *Angew. Chem. Int. Ed. 50*,

924–927 (2011).
119. Zhang, Y. *et al.* Rational Fabrication of Low-Coordinate Single-Atom Ni Electrocatalysts by MOFs for Highly Selective CO_2 Reduction. *Angew. Chem. Int. Ed. 60*, 7607–7611 (2021).
120. Yang, F. *et al.* Highly Efficient CO_2 Electroreduction on ZnN_4-based Single-Atom Catalyst. *Angew. Chem. Int. Ed. 57*, 12303–12307 (2018).
121. Agrawal, T. *et al.* Recent Developments in C–C Bond Formation Using Catalytic Reductive Coupling Strategies. *Synthesis 52*, 2623–2638 (2020).
122. Gu, J. *et al.* Nickel-catalyzed reductive coupling of alkyl halides with other electrophiles: Concept and mechanistic considerations. *Org. Chem. Front. 2*, 1411–1421 (2015).
123. Everson, D. A. *et al.* Cross-electrophile coupling: Principles of reactivity and selectivity. *J. Org. Chem. 79*, 4793–4798 (2014).
124. Moragas, T. *et al.* Metal-Catalyzed Reductive Coupling Reactions of Organic Halides with Carbonyl-Type Compounds. *Chem. Eur. J. 20*, 8242–8258 (2014).
125. Ullmann, F. *et al.* Ueber Synthesen in der Biphenylreihe. Berichte der Dtsch. *Chem. Gesellschaft 34*, 2174–2185 (1901).
126. Novaes, L. F. T. *et al*. Electrocatalysis as an enabling technology for organic synthesis. *Chem. Soc. Rev. 50*, 7941-8002 (2021).
127. Yi, L. *et al.* Nickel-Catalyzed Reductive Cross-Couplings: New Opportunities for Carbon–Carbon Bond Formations through Photochemistry and Electrochemistry. *CCS Chem. 4*, 9–30 (2022).
128. Wang, X. *et al.* Nickel-Catalyzed Reductive Couplings. *Top. Curr. Chem. 374*, 1–29 (2016).
129. Mori, M. *et al.* Preparation and synthetic use of the zerovalent nickel complex by electrochemical reduction. *Tetrahedron Lett. 21*, 631–634 (1980).
130. Oliveira, J. L. *et al.* Electrochemical coupling of mono and dihalopyridines catalyzed by nickel complex in undivided cell. *Tetrahedron 68*, 2383–2390 (2012).
131. De França, K. W. R. *et al.* Electrochemical homocoupling of 2-bromomethylpyridines catalyzed by nickel complexes. *J. Org. Chem. 67*, 1838–1842 (2002).
132. Cassol, T. M. *et al.* Two convenient and high-yielding preparations of 6,6′-dimethyl-2,2′-bipyridine by homocoupling of 6-bromopicoline. *Tetrahedron Lett. 41*, 8203–8206 (2000).
133. Rahil, R. *et al.* Nickel-Catalyzed Electrochemical Reductive Homocouplings of Aryl and Heteroaryl Halides: A Useful Route to Symmetrical Biaryls. *Synthesis 50*, 146–154 (2018).
134. Biswas, S. *et al.* Mechanism and selectivity in nickel-catalyzed cross-electrophile coupling of aryl halides with alkyl halides. *J. Am. Chem. Soc. 135*, 16192–16197 (2013).
135. Le Gall, E. *et al.* Cobalt-catalyzed electrochemical cross-coupling of

functionalized phenyl halides with 4-chloroquinoline derivatives. *Tetrahedron Lett. 42*, 267–269 (2001).
136. Gosmini, C. *et al.* Electrochemical cross-coupling between functionalized aryl halides and 2-chloropyrimidine or 2-chloropyrazine catalyzed by nickel 2,2′-bipyridine complex. Tetrahedron Lett. 41, 201–203 (2000).
137. Li, H. *et al.* Ni-Catalyzed Electrochemical Decarboxylative C–C Couplings in Batch and Continuous Flow. *Org. Lett. 20*, 1338–1341 (2018).
138. Harwood, S. J. *et al.* Modular terpene synthesis enabled by mild electrochemical couplings. *Science 375*, 745–752 (2022).
139. Gallo, R. D. C. *et al.* Silica-supported $HClO_4$ promotes catalytic solvent- and metal-free O-H insertion reactions with diazo compounds. *Green Chem. 20*, 4547–4556 (2018).
140. Best, D. *et al.* Diastereo- and enantioselective Pd(II)-catalyzed additions of 2-alkylazaarenes to N-boc imines and nitroalkenes. *J. Am. Chem. Soc. 134*, 18193–18196 (2012).
141. Breipohl, G. *et al.* Facile SPS of peptides having C-terminal Asn and Gln. *Int. J. Pept. Protein Res. 35*, 281–283 (1990).
142. Klussmann, M. *et al*. Synthesis of TRIP and Analysis of Phosphate Salt Impurities. *Synlett 2010*, 2189–2192 (2010).
143. Li, S. *et al.* Phosphoric Acid-Catalyzed Asymmetric Synthesis of SPINOL Derivatives. *J. Am. Chem. Soc. 138*, 16561–16566 (2016).
144. Yin, L. *et al.* Enantioselective Synthesis of 3,3′-Diaryl-SPINOLs: Rhodium-Catalyzed Asymmetric Arylation/BF_3-Promoted Spirocyclization Sequence. *Angew. Chem. Int. Ed. 58*, 2474–2478 (2019).
145. Zhang, Y. L. *et al.* Vinyl Sulfonium Salts as the Radical Acceptor for Metal-Free Decarboxylative Alkenylation. *Org. Lett. 22*, 7768–7772 (2020).
146. Hu, X. *et al*. Ir-catalyzed Asymmetric Hydrogenation of *α*-Imino Esters with Chiral Ferrocenylphosphine-Phosphoramidite Ligands. *Adv. Synth. Catal. 361*, 5063–5068 (2019).
147. Xu, B. *et al.* Asymmetric N-H Insertion Reaction Cooperatively Catalyzed by Rhodium and Chiral Spiro Phosphoric Acids. *Angew. Chem. Int. Ed. 50*, 11483–11486 (2011).
148. Teegardin, K. A. *et al.* Formation of Non-Natural *α*,*α*-Disubstituted Amino Esters via Catalytic Michael Addition. *Org. Lett. 20*, 7239–7244 (2018).
149. Chen, J. *et al.* Visible light-driven photocatalytic generation of sulfonamidyl radicals for alkene hydroamination of unsaturated sulfonamides. *Chem. Commun. 54*, 6780–6783 (2018).
150. Gualandi, A. *et al*. Allylation of aldehydes by dual photoredox and nickel catalysis. *Chem. Commun. 55*, 6838–6841 (2019).
151. Dey, P. *et al.* [bmim][Br] as an Inexpensive and Efficient Medium for the Barbier-Type Allylation Reaction Using a Catalytic Amount of Indium: Mechanistic

Studies. *European J. Org. Chem. 2018*, 1333–1341 (2018).
152. Zhang, Q. *et al.* Separation of 'light fluorous' reagents and catalysts by fluorous solid-phase extraction: Synthesis and study of a family of triarylphosphines bearing linear and branched fluorous tags. *J. Org. Chem. 65*, 8866–8873 (2000).
153. Pogula, J. *et al.* Copper-Impregnated Magnesium-Lanthanum Mixed Oxide: A Reusable Heterogeneous Catalyst for Allylation of Aldehydes and Ketones. *Adv. Synth. Catal. 362*, 1176–1183 (2020).
154. Vasylyev, M. *et al.* Rhodium-catalyzed reductive allylation of conjugated aldehydes with allyl acetate. *J. Org. Chem. 75*, 2710–2713 (2010).
155. Shi, C. *et al.* Photocatalytic Umpolung Synthesis of Nucleophilic π-Allylcobalt Complexes for Allylation of Aldehydes. *ACS Catal. 11*, 2992–2998 (2021).
156. Felpin, F. X. *et al.* Enantioselective reduction of heteroaromatic *β*,*γ*-unsaturated ketones as an alternative to allylboration of aldehydes.: Application: asymmetric synthesis of SIB-1508Y. *Tetrahedron 58*, 7381–7389 (2002).
157. Kamei, K. *et al*. Copper-Catalyzed Allylation of Carbonyl Derivatives Using Allyl(2-pyridyl)silanes. *Org. Lett. 7*, 4725–4728 (2005).
158. Cui, Y. *et al.* Facile preparation of allylzinc species from allylboronates and zinc amide via a boron-to-zinc exchange process and their reactions with carbonyl compounds, imines and hydrazones. *Chem. Commun. 48*, 10319–10321 (2012).
159. Matsuoka, H. *et al.* General and convenient TsOH-induced allylboration of ketones. *Tetrahedron Lett. 50*, 2320–2321 (2009).
160. Sun, K. *et al.* Efficient iron single-atom catalysts for selective ammoxidation of alcohols to nitriles. *Nat. Commun. 13*, 1–9 (2022).
161. Zhang, Y. *et al.* Rational Fabrication of Low-Coordinate Single-Atom Ni Electrocatalysts by MOFs for Highly Selective CO_2 Reduction. *Angew. Chem. Int. Ed. 60*, 7607–7611 (2021).
162. Li, Z. *et al.* Copper-Catalyzed Umpolung of Imines through Carbon-to-Nitrogen Boryl Migration. *ACS Catal. 9*, 4388–4393 (2019).
163. Kim, B. H. *et al*. SmI_2 mediated allylation of aldimines with allyl bromide. *Synth. Commun. 31*, 2297–2303 (2001).
164. Wang, J. *et al.* A silver triflate-catalyzed cascade of in situ-oxidation and allylation of arylbenzylamines. *Tetrahedron Lett. 57*, 3444–3448 (2016).
165. Zhang, Y. *et al.* Solvent-free allylation and benzylation of aldimines mediated by zinc powder. *Tetrahedron Lett. 50*, 2925–2928 (2009).
166. Yadav, J. S. *et al*. Sulphamic acid: An efficient, cost-effective and recyclable solid acid catalyst for three-component synthesis of homoallylic amines. *Catal. Commun. 7*, 797–801 (2006).
167. Yuan, Y. *et al.* Iron-catalyzed efficient three-component allylation of imine in aqueous media. *Appl. Organomet. Chem. 23*, 485–491 (2009).
168. Fan, R. *et al.* Efficient three-component one-pot benzylation and allylation of aldehydes and amines for synthesis of homobenzylamines and homoallylamines. *J. Org.*

Chem. 72, 3149–3151 (2007).
169. Shen, K. H. *et al.* Novel and efficient method for the allylation of carbonyl compounds and imines using triallylaluminum. *J. Org. Chem. 71*, 3980–3983 (2006).
170. Shibata, I. *et al.* Allylic Tantalums as Highly Imine-Selective Reagents. *J. Org. Chem. 69*, 2185–2187 (2004).
171. Li, J. *et al.* Sn-mediated one-pot four-component allylation of aldimines. *Appl. Organomet. Chem. 28*, 286–289 (2014).
172. Gadde, K. *et al.* HFIP-mediated 2-aza-Cope rearrangement: metal-free synthesis of α-substituted homoallylamines at ambient temperature. *Org. Biomol. Chem. 19*, 4067–4075 (2021).
173. Ghosh, D. *et al.* Phosphotungstic Acid as an Efficient Catalyst for Allylation of Isatins and N-*tert*-Butyloxycarbonylamido Sulfones Under Solvent-Free Conditions. *Asian J. Org. Chem. 3*, 1173–1181 (2014).
174. Alvaro, G. *et al.* Diastereoselective addition of allylmetal compounds to imines derived from (*S*)-1-phenylethanamine. *J. Chem. Soc. - Perkin Trans. 1*, 875–882 (1996).
175. Cicco, L. *et al.* Addition of Highly Polarized Organometallic Compounds to N-*tert*-Butanesulfinyl Imines in Deep Eutectic Solvents under Air: Preparation of Chiral Amines of Pharmaceutical Interest. *ChemSusChem 13*, 3583–3588 (2020).
176. Sato, K. *et al.* Csp^3-Csp^3 homocoupling reaction of benzyl halides catalyzed by rhodium. *Org. Lett*. *16*, 3756–3759 (2014).